



HAL
open science

Glacial oscillations during the Bølling–Allerød Interstadial–Younger Dryas transition in the Ruda Valley, Central Pyrenees

M. Fernandes, M. Oliva, G. Vieira, D. Palacios, J. Fernández-fernández, J.
García-oteyza, Irene Schimmelpfennig, D. Antoniades

► **To cite this version:**

M. Fernandes, M. Oliva, G. Vieira, D. Palacios, J. Fernández-fernández, et al.. Glacial oscillations during the Bølling–Allerød Interstadial–Younger Dryas transition in the Ruda Valley, Central Pyrenees. *Journal of Quaternary Science*, 2021, 37 (1), pp.42-58. 10.1002/jqs.3379 . hal-03389538

HAL Id: hal-03389538

<https://hal.science/hal-03389538>

Submitted on 13 May 2022

HAL is a multi-disciplinary open access archive for the deposit and dissemination of scientific research documents, whether they are published or not. The documents may come from teaching and research institutions in France or abroad, or from public or private research centers.

L'archive ouverte pluridisciplinaire **HAL**, est destinée au dépôt et à la diffusion de documents scientifiques de niveau recherche, publiés ou non, émanant des établissements d'enseignement et de recherche français ou étrangers, des laboratoires publics ou privés.

1
2 1 **Glacial oscillations during the Bølling-Allerød Interstadial-Younger Dryas**
3 2 **transition in the Ruda Valley, Central Pyrenees**
4 3
5 4
6 5

7 5 M. Fernandes¹, M. Oliva², G. Vieira¹, D. Palacios³, J.M. Fernández-Fernández¹, J. Garcia-Oteyza², I.
8 6 Schimmelpennig⁴, ASTER Team^{4,5} & D. Antoniades⁶
9 7
10 8

11 9 ¹Centre for Geographical Studies, IGOT, Universidade de Lisboa, Lisbon, Portugal

12 10 ²Department of Geography, Universitat de Barcelona, Catalonia, Spain

13 11 ³Department of Geography, Universidad Complutense de Madrid, Madrid, Spain

14 12 ⁴Aix-Marseille Université, CNRS, IRD, INRAE, Coll. France, UM 34 CEREGE, Aix-en-Provence, France

15 13 ⁵Consortium: Georges Aumaître, Karim Keddadouche

16 14 ⁶Department of Geography & Centre for Northern Studies, Université Laval, Quebec, Canada
17 15
18 16

19 17 **Corresponding author**

20 18 Marcelo Fernandes, marcelo.fernandes@live.com

21 19 Centre for Geographical Studies – IGOT, Universidade de Lisboa

22 20 Rua Branca Edmée Marques, 1600-276 Lisbon, Portugal

23 21 Tel: +351962277913
24 22
25 23
26 24
27 25
28 26
29 27
30 28
31 29
32 30
33 31
34 32
35 33
36 34
37 35
38 36
39 37
40 38
41 39
42 40
43 41
44
45
46
47
48
49
50
51
52
53
54
55
56
57
58
59
60

Abstract

The Upper Garonne Basin included the largest glacial system in the Pyrenees during the last glacial cycle. Within the long-term glacial retreat during Termination-1 (T-1), glacier fluctuations left geomorphic evidence in the area. However, the chronology of T-1 glacial oscillations on the northern slope of the Central Pyrenees is still poorly constrained. Here, we introduce new geomorphological observations and a 12-sample dataset of ^{10}Be Cosmic-Ray Exposure (CRE) ages from the Ruda Valley. This U-shaped valley, surrounded by peaks exceeding 2800 m a.s.l., includes a sequence of moraines and polished surfaces that enabled to reconstruct the chronology of the last deglaciation. Following the maximum ice extent, warmer conditions prevailing at ~15-14 ka, during the Bølling-Allerød (B-A) Interstadial, favoured glacial retreat in the Ruda Valley. Within the B-A, glaciers experienced two phases of advance/stillstand with moraine formation at 13.5 and 13.0 ka. During the early YD, glacial retreat exposed the highest surfaces of the Saboredo Cirque (~2300-2350 m) at 12.7 ka. Small glaciers persisted only inside the highest cirques (~2470 m), such as in Sendrosa Cirque, with moraines stabilizing at 12.6 ka. The results of this work present the most complete chronology for Pyrenean glacial oscillations from the B-A to the YD.

Key words: Central Pyrenees, Bølling-Allerød, Younger Dryas, Cosmic-Ray Exposure dating, deglaciation

1. Introduction

The present-day landscape of the highest mid-latitude mountain environments is dominated by the effects of glacial dynamics that prevailed during the last glacial cycle and of post-glacial processes that reshaped glacial landforms during the subsequent deglaciation. Following the end of the Last Glacial Maximum (LGM) at 19-20 ka (Clark et al., 2009), most glaciated mountain regions underwent a rapid deglaciation only interrupted by brief periods of glacial growth. Glacial disappearance favoured paraglacial readjustment and intense periglacial and slope processes, which reshaped the already deglaciated valleys and cirques (Ballantyne, 2008). The current spatial distribution of glacial and periglacial features in the high elevations of most mid-latitude ice-free mountain ranges – such as the Pyrenees, where this research focuses on – results from the climatic shifts during Termination-1 (hereafter T-1), the period spanning from 20-19 to 11.7 ka (Denton et al., 2014).

At present, mid-latitude mountains such as those of the Mediterranean region are only sparsely glaciated, with small glaciers located in sheltered cirques (Hughes, 2014). However, there are several other mountain ranges located between 30 and 50° latitude North, such as the Alps or the Himalaya, which are still heavily glaciated and record recent dramatic glacial recession trends (Huss et al., 2021). An accurate comprehension of the climatic sensitivity of current glaciated mountain landscapes can help to understand the timing and magnitude of glacial change during the rapid climate shifts of T-1. The alternation of millennial-scale cold/warm periods during T-1 promoted a temporal pattern of glacial advances and retreats across the Northern Hemisphere (Allard et al., 2021; Rea et al., 2020). Ice core records from the Greenland interior show the following succession of climatic phases in the North Atlantic region during T-1: a cold climate regime during the Oldest Dryas (OD; GS-2.1a: 17.5-14.6 ka), followed by the general warm Bølling-Allerød (B-A) Interstadial (GI-1: 14.6-12.9 ka), with a subsequent intensification of cold conditions during the Younger Dryas (YD; GS-1: 12.9-11.7 ka) (Rasmussen et al., 2014).

In the Iberian mountains, recent advances in constraining the chronology of glacial activity during T-1 using Cosmic-Ray Exposure (CRE) dating have revealed contrasting spatio-temporal patterns (García-Ruiz et al., 2016b; Oliva et al., 2019; Palacios et al., 2017a). Whereas the maximum ice extent occurred asynchronously, glacial oscillations during T-1 show a more synchronous response: colder phases favoured glacial growth, whereas warm periods promoted glacial recession (Oliva et al., 2019) and the evolution from debris-free glaciers to rock glaciers such as those in the Iberian Range (García-Ruiz et al., 2020), Cantabrian Mountains (Rodríguez-Rodríguez et al., 2016) and Central (Palacios et al., 2017a, b) and Eastern Pyrenees (Andrés et al., 2018). To date, there is geomorphic evidence of glacial advances during the OD and YD, as well as of glacial retreat during the B-A and following the YD in the Cantabrian Mountains (Rodríguez-Rodríguez et al., 2017), Central Range (Carrasco et al., 2015; Palacios et al., 2012b), and Sierra Nevada (Gómez-Ortiz et al., 2012; Palacios et al., 2016). However, CRE ages require a careful interpretation and support of geomorphological criteria, as their uncertainty ranges may be greater than the time spanning the T-1 phases (Oliva et al., 2021a).

1
2 93 The Pyrenees were the most extensively glaciated mountain system during the maximum ice extent of the last
3 94 glaciation in Iberia, hosting ~50% of the peninsula's glacial surface (Oliva et al., 2021b). The chronology of
4 95 glacier fluctuations during T-1 seems to have followed a similar temporal pattern, although available data is
5 96 principally derived from the range's southern slope (Andrés et al., 2018; Palacios et al., 2015b, 2017b, 2017a).
6 97 Pyrenean glaciers readvanced to the valley bottoms during the OD, with ice tongues > 15 km long. During the
7 98 B-A, by 15-14 ka, high temperatures favoured rapid deglaciation and glaciers disappeared from relatively low
8 99 cirques shaped under peaks of ~2600 m a.s.l. (Oliva et al., 2021a). A subsequent readvance occurred during
9 100 the YD, with smaller glaciers of only ~4 km length confined within the cirques of the highest massifs above
10 101 2200 m (Crest et al., 2017; García-Ruiz et al., 2016a; Jomelli et al., 2020; Palacios et al., 2017b, 2015a; Pallàs
11 102 et al., 2006). Following both cold periods, glacial retreat triggered intense paraglacial dynamics at ~15-14 ka
12 103 and ~11-10.5 ka, respectively, which led to the formation of rock glaciers and debris-covered glaciers,
13 104 particularly in cirques below 2800 m (Andrés et al., 2018; Palacios et al., 2017b).

15 105 The timing of glacial oscillations is still poorly constrained on the northern slope of the Pyrenees, such as in
16 106 the Upper Garonne Basin where this work focuses on. Recently, Reixach et al. (2021) have summarized the
17 107 glacial evolution from 19 to 12 ka in the northern Pyrenees, reporting a spatial and temporal pattern for T-1
18 108 glacial oscillations similar to that on the southern slopes of the range. Jomelli et al. (2020) confirmed glacial
19 109 growth during the YD in the Ariège Valley, where glaciers persisted in the highest cirques until the early
20 110 Holocene. Another recent study that focused on the Bacivèr Cirque, near our study area, revealed a rapid
21 111 deglaciation during the B-A, followed by glacial readvance and the formation of the highest moraines at the
22 112 B-A/YD transition at ~12.9 ka; subsequently, intense paraglacial readjustment favoured the formation of
23 113 debris-covered glaciers and rock glaciers inside these moraine systems (Oliva et al., 2021a).

25 114 In order to complement our understanding of the glacial history of the Pyrenees, this study uses new data to
26 115 improve the deglaciation chronology of the Upper Garonne Basin, the largest glacial system in this mountain
27 116 range, during the local last glacial maximum (ILGM; Fernandes et al., 2017). Glacial retreat in the Ruda Valley,
28 117 where this work focuses on, left widespread geomorphic evidence of glacial and paraglacial origin that can be
29 118 used to reconstruct the last stages of long-term deglaciation in the Central Pyrenees.

31 119 Our study, therefore, has the following objectives:

- 32 120 - To date the glacial landforms of the Upper Garonne Basin.
- 33 121 - To discuss the T-1 deglaciation in the Upper Garonne Basin and its geomorphological implications in
34 122 the context of the known chronologies from the Pyrenees southern slope and from other Iberian and
35 123 European mountain ranges.
- 36 124 - To examine the paleoclimatic and paleoenvironmental significance of the glacial response of the
37 125 northern slope of the Pyrenees and compare it with the paleoclimatic evolution inferred from other
38 126 records in the North Atlantic region.

42 128 2. Study area

43 129 The Pyrenees stretch E-W over 400 km across north Iberia, with the highest peaks (> 3000 m) in the central
44 130 part of the range. This study focuses on the Ruda Valley, located between latitudes 42°40' N - 42°42' N and
45 131 longitudes 0°57' E - 1°00' E (Fig. 1), that constitutes the headwaters of the Upper Garonne Basin. The area is
46 132 included in the peripheral protection area of the National Park of Aigüestortes and Sant Maurici Lake.

49 133 Figure 1

50
51 134 The Upper Garonne Valley shows the typical U-shaped cross-section of glacial valleys, and the Garonne River
52 135 flows to the N-NW through the central axis of the Pyrenees. Several tributary rivers drain the glacial valleys
53 136 descending from glacial cirques carved below peaks from 2800 to 3000 m. Glacial cirques are prevalingly
54 137 NE-oriented, with floors generally between 2200 and 2400 m (Lopes et al., 2018).

56 138 The U-shaped Ruda Valley, drained by the Ruda River that runs 12 km northwards, constitutes the headwaters
57 139 of the Upper Garonne Basin. Its catchment encompasses 34 km², with an elevation range of ~1300 m between
58 140 Saboredo Peak (2827 m) and the village of Baqueira (~1500 m). The Saboredo Cirque is located in the
59 141 headwaters of the Ruda Valley; the cirque is N-exposed, extending over 5.7 km², with its floor at ~2250-2400

1
2 142 m. Saboredo (2827 m), Sendrosa (2702 m) and Locampo (2658 m) peaks are the highest elevations of the
3 143 cirque, while its toe is located at ~2250 m.

4
5 144 The present-day mean annual air temperature (MAAT) at Port de la Bonaigua station (2266 m) is 3 °C, with
6 145 the regional 0 °C isotherm in the Central Pyrenees estimated to be at 2950 m (López-Moreno et al., 2019).
7 146 Annual precipitation reaches 1227 mm and falls mostly as snow (average depth of 1 m) from October to May,
8 147 with a snow duration of 7-8 months in the cirque floor. The combination of low temperatures and abundant
9 148 snowfall determines the scarce vegetation cover above the treeline (2200-2300 m), where barren rocky terrain
10 149 is widespread, together with small alpine meadows.

11 149
12
13 150 The landscape of the Ruda Valley resulted from the interaction of tectonics and vertical incision, both during
14 151 Quaternary glaciations and interglacial periods, the latter dominated by alluvial and mass-wasting processes
15 152 (Fernandes et al., 2017). Glacial and periglacial landforms are preserved on different lithologies across the
16 153 valley, composed of Carboniferous granodiorites and granites in the highest sections, with Cambrian-Devonian
17 154 metamorphic (hornfels, marbles, slates, quartzites, schists) and sedimentary rocks (limestones, sandstones,
18 155 conglomerates and lutites) in the lowest parts of the valley (ICGC, 2017; Quesada and Oliveira, 2019).
19 155 However, despite abundant geomorphic evidence revealing that the Garonne Valley presented the longest
20 156 glacier in the Pyrenees during the ILGM (ca. 80 km; Fernandes et al., 2017), the chronological framework of
21 157 glacial activity in the entire Upper Garonne Basin is still unknown. The headwaters of the Ruda Valley include
22 158 a rich sequence of moraine systems and polished bedrock surfaces – as well as relict rock glaciers and protalus
23 159 lobes (Fernandes et al., 2018) – that can be used to improve the temporal resolution for the chronosequence of
24 160 the final deglaciation of the upper Garonne Valley.
25 161
26 161
27
28 162

29 163 3. Methodology

30
31 164 We reconstructed the last deglaciation chronology of the Ruda Valley in the Upper Garonne Basin by
32 165 integrating geomorphological and chronological techniques. Field work was conducted during the summer of
33 166 2019, when snow cover was limited to the concave and sheltered areas at the highest elevations (>2500 m),
34 166 which enabled better identification of the glacial landforms, as well as sampling for CRE dating.
35 167

36 168 3.1 Geomorphological mapping

37
38 169 We produced a geomorphological map focusing on glacial and periglacial landforms based on recent general
39 170 geomorphological maps from the area (Fernandes et al., 2017; Fernandes et al., 2021). Here we used the same
40 171 approach based on the combination of aerial orthophotographs (0.25 m cell size) and high-resolution LIDAR
41 171 digital elevation models (point density of 0.5-2 m⁻²) from the “Institut Cartogràfic i Geològic de Catalunya”
42 172 (<http://www.icc.cat/appdownloads>). The symbology of geomorphological landforms followed Joly (1997).
43 173
44

45 174 3.2 Field strategy and sampling

46 175 We collected 12 granite and granodiorite samples for CRE dating, using a hammer and chisel, from elevations
47 176 spanning from 1862 to 2470 m (Table 1). To ensure that samples were intact since glacial retreat, we targeted
48 176 at well-anchored moraine boulders and glacially polished bedrock that stood out within their surroundings,
49 177 which minimizes the risk of having been buried under sediments (Fig. 2). To ensure the best cosmic-ray flux
50 178 reception of the sampling sites, we restricted sample extraction to flat-topped and gentle surfaces, and sampled
51 179 a thickness of up to 3-5 cm. Corrections for partial shielding due to the surrounding topography were
52 180 implemented using the ArcGIS toolbox by Li (2018), which applies equations describing the effects of
53 181 geometric shielding on the sampling sites and a model to predict the nuclide production rate at depth in sloped
54 182 surfaces (Dunne et al. 1999); it required only a point shapefile of the sampling sites including strike/dip of the
55 183 sampling surfaces and a digital elevation model of 5 m spatial resolution.
56 183
57 184
58

59 185 Table 1

60 186 Figure 2

1

2 187 **3.3 Laboratory procedures and exposure age calculation**

3
4 188 Samples were crushed and sieved (>200 g) at the Physical Geography Laboratory of the Universidad
5 189 Complutense de Madrid (Spain) to the 125-500 μm fraction, which was subsequently processed at the
6 190 ‘Laboratoire National des Nucléides Cosmogéniques’ (LN₂C) of the ‘Centre Européen de Recherche et
7 191 d’Enseignement des Géosciences de l’Environnement’ (CEREGE; Aix-en-Provence, France). In accordance
8 192 with the quartz-rich lithology of the samples, they were treated for the extraction of the *in-situ*-produced
9 193 cosmogenic nuclide ¹⁰Be.

11
12 194 First, magnetic minerals were discarded through magnetic separation conducted in a “Frantz LB-1” magnetic
13 195 separator. Once the non-magnetic fraction was isolated, it underwent several rounds of chemical attacks with
14 196 a 1:2 mixture of concentrated hydrochloric (HCl) and hexafluorosilicic (H₂SiF₆, 2/3) acids to dissolve and
15 197 discard the non-quartz minerals. The remaining minerals (i.e. non-dissolved feldspar minerals) were
16 198 subsequently attacked with 4-6 successive partial dissolutions with HF to remove the atmospheric ¹⁰Be and
17 199 discard the remaining impurities. In order to be sure that the quartz was pure, samples were examined under a
18 200 binocular microscope. As a result, ~20 g of pure quartz per sample was used to extract the ¹⁰Be (Table 2). After
19 201 adding ~150 μL of an in-house manufactured (from a phenakite crystal) ⁹Be carrier solution (spike,
20 202 concentration: $3025 \pm 9 \mu\text{g g}^{-1}$; Merchel et al., 2008), the purified quartz was dissolved with 48% concentrated
21 203 HF (3.5 mL per g of quartz + 30 mL in excess). Following total dissolution, the resulting solution was
22 204 evaporated until dryness, and the residue was recovered with HCl (7.1 molar). Be was then precipitated at
23 205 pH=8 to beryllium hydroxide (Be(OH)₂) by means of ammonia (NH₃), and separated from other elements in
24 206 resin columns: a Dowex 1x8 anionic exchange column to remove elements such as Fe, Mn and Ti, and a
25 207 Dowex 50W x8 cationic exchange column to discard B and separate Be from Al (Merchel and Herpers, 1999).
26 208 The final eluted Be was again precipitated, dried and oxidized to BeO at 700 °C. Finally, the targets for the
27 209 accelerator mass spectrometer (AMS) measurements were prepared by mixing with niobium powder at an
28 210 approximate 1:1 proportion and pressing the mixture into copper cathodes.

29
30 211 The targets were analysed at the ‘Accelerator pour les Sciences de la Terre, Environnement et Risques’
31 212 (ASTER) national AMS facility at CEREGE in order to measure the ¹⁰Be/⁹Be ratio from which the ¹⁰Be
32 213 concentration was later inferred (Table 2). AMS measurements were calibrated against the in-house standard
33 214 STD-11 with an assigned ¹⁰Be/⁹Be ratio of $(1.191 \pm 0.013) \times 10^{-11}$ (Braucher et al., 2015). Based on calibration
34 215 with the previous ASTER AMS standard NIST-27900 (SRM4325), the new STD-11 is fully compatible with
35 216 07KNSTD. The analytical 1 σ uncertainties include uncertainties in the AMS counting statistics, an external
36 217 0.5% AMS error (Arnold et al., 2010) and the uncertainty related to the chemical blank correction. The ¹⁰Be
37 218 half-life considered was $(1.3870 \pm 0.0012) \times 10^6$ years (Chmeleff et al., 2010; Korschinek et al., 2010).

38 219 **Table 2**

39 220 We calculated ¹⁰Be exposure ages by using the CREP online calculator (Martin et al., 2017; available online
40 221 at: <http://crep.cirp.cnr.fr/#/>), where we selected the following settings: LSD (Lifton-Sato-Dunai)
41 222 elevation/latitude scaling scheme (Lifton et al., 2014), ERA40 atmospheric model (Uppala et al., 2005) and
42 223 geomagnetic database based on the LSD framework (Lifton et al., 2014). These settings yielded a world-wide
43 224 mean sea level high latitude (SLHL) ¹⁰Be production rate of $3.98 \pm 0.22 \text{ atoms g}^{-1} \text{ yr}^{-1}$. Exposure ages of the
44 225 samples with their 1 σ full and analytical uncertainties are shown in Table 2. The uncertainties discussed
45 226 throughout the text include analytical and production rate error unless otherwise stated.

46 227 In order to evaluate the potential impact of erosion on the exposure ages, we assumed a steady erosion rate (1
47 228 mm ka⁻¹) following a conservative maximum value in such a lithological setting according to André (2002).
48 229 The impact of snow cover was explored assuming that snow currently remains in the area an annual average
49 230 of 7.5 months at 2200-2300 m with a mean thickness of 100 cm – and assuming a snow density of 0.2 g cm⁻³
50 231 (Styllas et al., 2018) – (Table 3), based on the available data from the Bonaigua weather station (Fig. 1)
51 232 available since 1997-1998 (Servei Meteorològic de Catalunya; http://www.igc.cat/web/ca/allaus_gruix_neu_v2.php?e=bonaigua&t=totes). Erosion and snow corrections, as
52 233

a whole, resulted in ages that were ~9% older (~1% erosion; ~8% snow cover). However, to enable comparisons with other areas, we use the non-corrected ages throughout the text. Moreover, both the thickness and duration of snow cover must have varied significantly since the cirque's deglaciation, given the alternation of cold/warm periods and their associated moisture supplies. Finally, the chi-squared test according to Ward and Wilson (1978) was applied to the samples belonging to each geomorphological unit established in the geomorphological map (Table 1) in order to detect potential exposure age outliers (i.e. "too old" or "too young"; Heyman et al., 2011). No outliers were detected (Table 3).

Table 3

3.4 Glacier reconstruction and Equilibrium-Line Altitude (ELA) calculation

A three-dimensional paleoglacier reconstruction was performed for the different glacial phases using the 'GLaRe' ArcGIS toolbox devised by Pellitero et al. (2016). Former ice thickness was estimated by applying a perfect-plasticity physical-based rheological model along flowlines from the termini to the headwall (Van der Veen, 1999; Benn and Hulton, 2010). Such a toolbox requires only a flowline, a tentative paleoglacier geometry - approximated from lateral or frontal moraines - and a digital elevation model. Ice thickness was modelled by using a constant shear stress of 100 kPa (Paterson, 1994; Benn and Hulton, 2010). The effect of lateral side drag was corrected by integrating shape factors (F-factor) obtained from cross-sections (Schilling and Hollin, 1981).

ELAs were calculated by using the automatic toolbox 'ELA calculation' developed by Pellitero et al. (2015). The selected methods were the Accumulation Area Ratio (Porter, 1975; AARs: 0.6 ± 0.05) and the Area Altitude Balance Ratio (AABR; Osmaston, 2005). We considered two balance ratios for the AABR method: 1.75 ± 0.71 (global) and 1.9 ± 0.81 (mid-latitude marine glaciers) (Rea, 2009). The average ELAs were used to discuss the paleoclimatic implications of the identified glacier advance/stillstand phases.

4. Results

The Ruda Valley preserves glacial and periglacial landforms indicative of glacial evolution during the last deglaciation in the Upper Garonne Basin. The chronological framework of this evolution is unveiled by a dataset of 12 ^{10}Be CRE ages obtained from glacial landforms.

4.1 Geomorphological evidence

The wide range of glacial features from the highest sectors to the Ruda Valley floor shows evidence that the entire valley was heavily glaciated during the ILGM and recorded several advances or stillstands within the long-term deglaciation trend. The Ruda Valley is divided into two main geomorphological units (Fig. 3):

- (i) The valley floor and mountain slopes follow the typical U-shaped morphology of a glacial valley. The steep slopes, descending from ~2200 to 1800 m, connect the lateral cirques with the valley floor. The hillslopes of the valley start at the upper edge of hanging glacial cirques that define the glacial trimline, marking the uppermost extent of recent glaciations. Hillslopes are concave to rectilinear 300-400 m-long sections steeper than 30° that are mostly colonized by forest (i.e. *Pinus nigra*). The upper part of the valley is defined by two staggered, overdeepened basins filled with peatlands at average elevations of 2150 and 2070 m. At their margins, two moraine systems occur at 2190 and 2080 m. Two samples were collected from boulders from the external frontal moraine (ARAN-38 and ARAN-37) and the other two were obtained from the internal moraine unit: one from a boulder on the moraine ridge (ARAN-27), and the other from a polished surface with glacial striae (ARAN-28) and moraine boulders (Fig. 4). The lowest part of the valley floor, with a relatively flat slope characteristic of U-shaped glacial valleys and descending from ~1800 to 1500 m, is colonized by alpine meadows and coniferous forests. Isolated *roches moutonnées* are found in the highest section of the valley bottom where granites prevail ($> \sim 1800$ m), while they are absent in lower areas, where slates and marbles are the dominant lithology. Two samples were collected from polished surfaces at 1900 and 1860 m (ARAN-39 and ARAN-40).

(ii) The highest peaks of the Ruda Valley surrounding the Saboredo Cirque range from 2700-2800 m (Sendrosa and Saboredo peaks) to 2525 m in the mountain divide that may have functioned as a glacial diffluence pass between the Saboredo (Garonne basin) and the Ratera cirques (Noguera Pallaresa basin) (Fig. 3). Saboredo is a complex cirque (Barr and Spagnolo, 2015) that includes several minor hollows carved out on the marginal flanks of the peaks. They are separated by truncated spurs with polished surfaces, where one sample (ARAN-31) was collected to examine the timing of glacial thinning at the cirque level. The highest moraines in the Ruda Valley are located at ~2400-2500 m, at the foot of the highest peaks. A prominent cirque moraine at an altitude of 2470 m is located on the eastern slope of Sendrosa Peak; here, we collected two samples (ARAN-33 and ARAN-32). Above the upper moraines, fed by abundant debris supply from the cirque rock walls, rock glaciers and protalus lobes are found. The cirque floors extend between 2200 and 2400 m and preserve features indicative of intense glacial erosion (e.g. overdeepened basins or glacial thresholds) and glacial deposits (e.g. moraines or erratic boulders). In the Saboredo Cirque, glacial abrasion and periglacial processes shaped a large amphitheatre with several overdeepened basins. They are surrounded by polished surfaces and occupied by peatlands and lakes. Three samples were collected from polished surfaces from 2360 to 2270 m (Fig. 3) (ARAN-36; ARAN-35; ARAN-34; Fig. 2; Table 1). Glacial retreat left scattered boulders and till across the area.

Figure 3

Figure 4

4.2 Geochronological data

The 12 CRE samples collected from the Ruda Valley returned a chronology spanning from $\sim 15 \pm 0.9$ to 11.8 ± 0.7 ka, with all ages being consistent with the geomorphological distribution of the dated surfaces (Fig. 4).

Polished surfaces from the highest parts of the Ruda Valley located ~200-250 m below the cirques provided CRE ages of 15.0 ± 0.9 (ARAN-40) and 13.8 ± 0.8 ka (ARAN-39, Fig. 4A) (average: 14.4 ± 1.2 ka). A similar age was obtained from a sample collected from a truncated spur dividing the Sendrosa and Saboredo cirques, which yielded 14.8 ± 0.9 ka (ARAN-31). A sample collected from a polished surface at the edge of the Saboredo cirque floor (Fig. 3) reported an age of 14.0 ± 0.8 ka (ARAN-34, Fig. 4D).

Moraine boulders from the external moraine located in the lower overdeepened basin yielded ages of 13.3 ± 0.8 (ARAN-38) and 13.7 ± 1.0 ka (ARAN-37) (average: 13.5 ± 0.9 ka). A boulder from the internal moraine ridge located 110 m above the former moraine provided an age of 13.1 ± 0.8 ka (ARAN-27); this age was compared with a sample from a polished surface which correlates with the internal moraine (Fig. 4C) that returned an age of 13.0 ± 0.8 ka (ARAN-28), which agrees with the latter.

Two samples from polished surfaces of the Saboredo Cirque above 2300 m yielded ages of 12.8 ± 0.8 (ARAN-35) and 12.7 ± 0.8 ka (ARAN-36) (12.7 ± 0.8 ka). The highest moraines are located inside the highest cirque hollows, such as the Sendrosa hollow. Here, two moraine boulders yielded ages of 11.8 ± 0.7 (ARAN-33) and 13.3 ± 1.0 ka (ARAN-32) (12.6 ± 1.3 ka).

4.3 Reconstructed paleoglaciers and ELAs

The ELAs of the three reconstructed paleoglacier extents were calculated for the Ruda catchment. The paleoglacier existing at 13.5 ± 0.9 ka deposited a moraine system at 2080 m, with an average ELA located at 2461 m (Table 4). The paleoglacier at 13.0 ± 0.8 ka formed a moraine at 2190 m, with an average ELA at 2505 m. Finally, the Sendrosa Cirque moraine located at 2470 m was dated at 12.6 ± 1.3 ka, with an ELA of 2571 m (Table 4).

Table 4

5. Discussion

5.1 Interpretation of the geomorphological observations and CRE results

The geomorphological analysis supported by ^{10}Be dating of glacial landforms show the spatial and temporal patterns of the deglaciation between the B-A and the early YD in the Ruda Valley (Fig. 5). Although the CRE dataset is consistent with sequence of glacial landforms, uncertainty remains in assigning ages either to the late B-A or to the early YD.

The ages of samples from polished surfaces at the valley at 1860-1900 m (ARAN-40 and ARAN-39; 14.4 ± 1.2 ka) suggest that the beginning of glacial retreat in the Ruda Valley took place during the B-A. As glaciers retreated, they became confined within their respective cirques, as revealed by the age of 14.8 ± 0.9 ka (ARAN-31) of a polished surface on the ridge dividing the Sendrosa and Saboredo cirques (Fig. 3). The sample from an outcrop on the lower edge of the cirque (ARAN-34; 14.0 ± 0.8 ka) indicates that ice covered the entire Saboredo cirque floor until ~ 14 ka.

The sampled boulders of the external moraine system (ARAN-38 and ARAN-37) showed statistical coherence based on the chi-squared test following Ward and Wilson (1978) and suggested a glacier advance or stillstand at 13.5 ± 0.9 ka. The age of 13.0 ± 0.8 ka from a moraine boulder (ARAN-27) and an adjacent polished surface (ARAN-28) of the internal moraine system indicate another short advance or stillstand, which is also consistent with the geochronological sequence. These results from staggered moraine systems at ~ 2080 and ~ 2190 m provided chronologically consistent mean ages within the B-A. But is based on their distinct relative position that they have been ascribed to two different stages. Nevertheless, during this period, glaciers flowed from the Saboredo and Sendrosa cirques and generated moraines on the lower overdeepened basins.

According to the ages of samples from the highest surfaces of the Saboredo Cirque floor at 2320-2360 m (ARAN-35 and ARAN-36; 12.7 ± 0.8 ka), the entire cirque floor was deglaciated at the onset of the YD. These ages are consistent with those of the samples from the highest dated moraine cirques in the Sendrosa Cirque at 2460-2470 m (ARAN-32 and ARAN-33), which was also abandoned by the ice by 12.6 ± 1.3 ka. No statistical inconsistency was detected in the exposure ages from this moraine.

Figure 5

5.2 The chronology of deglaciation

During the ILGM, the Garonne glacier flowed ~ 80 km reaching the Loures-Barousse-Barbazan basin, where it formed a terminal moraine system (Fernandes et al., 2017; Stange et al., 2014). Until the onset of deglaciation, 300-400 m thick ice sat in the Ruda Valley, as shown by the highest lateral moraines between the Ruda and Aiguamòg valleys. This ice thickness must have favoured the occurrence of warm-based glaciers, thus implying basal sliding evidenced by striations on the bedrock surface. Hence, no nuclide inheritance from previous exposure periods is expected at the sampled surfaces.

Samples from polished surfaces from the bottom of the Ruda Valley at 1860-1900 m indicate that by 14.4 ± 1.2 ka, i.e. during the B-A, the glacier was retreating towards the glacial cirque, and was already disconnected from the main Ruda glacier. Consequently, one third of the Ruda Valley was already deglaciated at that time, indicating that by the early B-A the Garonne glacier represented only $\sim 5\%$ of the length that it had during the ILGM (Fernandes et al., 2017).

As glaciers retreated and thinned during the B-A, ice masses became individualized within their respective cirques, and the valley glaciers flowing from Sendrosa and Saboredo cirques merged only in the lowest overdeepened basins (Fig. 3). As conditions were less favourable, glaciers receded to higher elevations and the Sendrosa and Saboredo paleoglaciers became isolated in their respective basins by 14.8 ± 0.9 ka (Fig. 3). The ice covered the entire Saboredo cirque floor until ~ 14 ka, as revealed by the sample collected from an outcrop on the edge of the cirque (14.0 ± 0.8 ka), indicating that glacial recession in the Ruda Valley was underway at ~ 15 -14 ka. Similarly, a rapid deglaciation was also recorded at ~ 15 -14 ka in the nearby Bacivèr Cirque, which favoured its complete deglaciation (Fig. 1; Oliva et al., 2021a).

The strong clustering of ages at between ~ 13.5 and 12.7 ka confirms the dynamic environmental response of the Ruda palaeoglaciers to the abrupt climate transition between the B-A and the early YD. However, our CRE

dataset cannot assess the magnitude and patterns of glacial recession during the early B-A in the Ruda Valley, or whether the entire cirque was deglaciated and glaciers reformed and subsequently advanced. Our results suggest, however, that the millennial-scale trend towards glacier recession during the B-A was interrupted by two glacial advances or stillstands with moraine development at 13.5 ± 0.9 and 13.0 ± 0.8 ka (Fig. 5). Samples from moraines located at average elevations of ~ 2080 and ~ 2190 m, respectively, indicated the existence of valley glaciers 3.5 and 2.5 km long during the middle of the B-A and during the transition from the B-A to the YD. Indeed, the reconstructed glacial surface for both bases was of 4.4 and 3.8 km², respectively, with a maximum ice thickness of 300 and 200 m for each of these phases (Fig. 6a, b).

Figure 6

Evidence of glacial recession during the middle of the B-A was also recorded on polished surfaces from the neighbouring Bacivèr Cirque at 13.5 ± 0.8 ka (Oliva et al., 2021a). Local topographical factors, such as the shape of the cirque floor (convex versus concave areas) determined the pattern of glacial flow of thin ice masses during the glacial advances/stillstands that occurred during the B-A. Glaciers flowed downwards from the cirque through concave areas across the western slope, favouring the development of the moraine arcs and crests in lower overdeepened basins (Fig. 3). It is likely that the topography played a major role in determining the process and timing of the deglaciation in both cirques: the accumulation area above 2400 m is larger in the Saboredo Cirque (552 ha) with respect to the Bacivèr Cirque (244 ha) and its prevailing aspect is also more favourable for ice persistence (N vs W).

The Saboredo Cirque floor became ice free at the beginning of the YD, as revealed by the samples from polished surfaces of the cirque floor at ~ 2350 m (average age = 12.7 ± 0.8 ka). The evidence of glacial striations on the rock surface make unlikely the possibility of nuclide inheritance at the sampling sites. Glaciers might thus also have persisted during the early YD in the highest hollows of the Saboredo Cirque, as was the case in the northern cirque of Sendrosa Peak. Here, the cirque moraine at 2470 m, formed by a 0.4 km-long glacier (with a surface of 0.7 km² and a thickness of 90 m; Fig. 6c), was abandoned at 12.6 ± 1.3 ka. Inside the highest glacial cirques of the Ruda Valley, there are numerous relict rock glaciers and protalus lobes indicative of the past occurrence of permafrost during their formation (Fernandes et al., 2018). As in most of the Pyrenees, these are probably glacier-derived permafrost features associated with the paraglacial phase, when glacial shrinking favoured wall debuttrressing, a high debris supply and the subsequent burial of the residual ice masses (Andrés et al., 2018; Oliva et al., 2016).

In short, by the early B-A the Garonne Paleoglacier had receded $\sim 95\%$ of its ~ 80 km length of the ILGM (Fernandes et al., 2017; Stange et al., 2014). The Ruda Paleoglacier receded 4 km in only ~ 1.7 ka (~ 14.4 to ~ 12.7 ka) from an elevation of ~ 1800 to >2400 – 2500 m. This trend towards glacial shrinking before the final ice disappearance was interrupted by three phases of glacier advance or stillstands at 13.5 ± 0.9 , 13.0 ± 0.8 and 12.6 ± 1.3 ka, which generated moraines at ~ 2080 , 2190 and 2470 m, respectively.

5.3 Late Quaternary glacial dynamics in the Central Pyrenees and Iberian Peninsula in the context of European glacial evolution

The scientific knowledge on the chronology of the last deglaciation in the Pyrenees has experienced substantial advances over the last years in parallel to progress on glacial chronological constraints in other European and Iberian mountain ranges (García-Ruiz et al., 2010; Palacios and García-Ruiz, 2015). There is increasing evidence that the timing of glacial oscillations during T-1 across Europe followed a similar sequence (Palacios et al., 2021): a significant glacier advance took place during the OD followed by a rapid retreat during the B-A and a subsequent more limited glacier advance during the YD (Oliva et al., 2019).

Dated evidence of glacial responses in the Pyrenees to Northern Hemisphere cold events during T-1 have mostly focused on the southern slope (Oliva et al., 2019), although there is an increasing body of new data from the northern slope of the range that confirms glacial advances and stillstands there during the OD and YD, and glacial shrinking during the B-A (Reixach et al., 2021). The elevation of the peaks as well as the topography of the cirques played a major role in the duration and intensity of the glaciation during T-1 in the

high massifs of the Pyrenees. Cirques surrounded by peaks above 2800-2900 m likely included glaciers during most of T-1 until the onset of the Holocene (see e.g. [Jomelli et al., 2020](#); [Pallàs et al., 2006](#); [Reixach et al., 2021](#)), while those situated at the foot of lower peaks (i.e. 2500-2600 m) were completely deglaciated during the B-A ([Oliva et al., 2021a](#); [Palacios et al., 2017b](#)). Following ice retreat, the slopes were affected by intense readjustments (large, catastrophic rock slope failures, rock slope deformations, rockfalls, and rockslides), particularly in areas where the local lithostructure was prone to instability ([Fernandes et al., 2020](#)).

In the Central Pyrenees, a period of glacial growth occurred during the OD after the massive deglaciation that took place following the LGM. Moraines dated at 17-15 ka have been reported in the highest valleys of the main massifs, such as in the Ariège ([Delmas et al., 2011](#); [Jomelli et al., 2020](#); [Reixach et al., 2021](#)), Ésera ([Crest et al., 2017](#)), Gállego ([Palacios et al., 2015a](#)), Malniu ([Andrés et al., 2018](#); [Palacios et al., 2015b](#); [Pallàs et al., 2010](#)), Têt ([Delmas et al., 2008](#); [Tomkins et al., 2018](#)), Arànsér ([Andrés et al., 2018](#); [Palacios et al., 2015b](#)), and Bassiès ([Crest et al., 2017](#)). During that time, glaciers flowed downslope from the headwaters of the highest valleys, with valley glaciers often exceeding 10-15 km ([Oliva et al., 2019](#)). Consequently, it is likely that, by that time, most of the Ruda Valley was still glaciated, with the ice tongue probably merging with the main Garonne Paleoglacier that was also fed by neighbouring glacier tributaries, such as those descending from the Beret area ([Oliva et al., 2021a](#)). Some of the lateral moraine remnants distributed on the left side of the Garonne Valley, ca. 20 km from the highest parts of the Saboredo Cirque, formerly attributed to the OD ([Fernandes et al., 2021](#); [Fernandes et al., 2017](#)) may be also correlated with some of the highest moraines and erratic boulders distributed in the Ruda Valley ([Fig. 3](#)). Other Iberian mountain ranges include geomorphic evidence of glacial advances during the OD ([Palacios et al., 2017a](#)), such as in the Monasterio Valley in the Cantabrian Mountains ([Serrano et al., 2016](#)), Peña Negra Valley in the Iberian Range ([García-Ruiz et al., 2020](#)), Peñalara massif in the Central Range ([Palacios et al., 2012a](#)), San Juan Valley in the Sierra Nevada ([Palacios et al., 2016](#)), En Garcia Valley in the Eastern Pyrenees ([Reixach et al., 2021](#)), and Gállego and Ésera valleys in the Central Pyrenees ([Crest et al., 2017](#); [Palacios et al., 2017b](#)).

No moraine remnants have been found in the lowest and central sections of the Ruda Valley, and the prevailing lithology of slates and marbles in this area is not favourable for the preservation of glacially abraded surfaces. Indeed, the neighbouring Bacivèr Cirque was completely deglaciated also by ~15-14 ka ([Oliva et al., 2021a](#)). Thus, our data cannot confirm whether small glaciers persisted in the highest parts of the Ruda Valley during the B-A, although CRE ages support climatic conditions during the early B-A unfavourable for the maintenance of the OD ice masses ([Fig. 7](#)). In other valleys of the Pyrenees, glaciers also receded rapidly at ~14.6-14 ka as shown by CRE ages from polished surfaces and scattered erratic boulders in the Ariège (14.4 ± 1.1 , 14.1 ± 0.7 , 14.0 ± 0.8 ka; [Delmas et al., 2011](#)), Gállego (14.6 ± 2.3 ka; [Palacios et al., 2015a](#)) and Ésera valleys (14.3 ± 0.5 ka; [Crest et al., 2017](#)). Locally, some massifs of the Pyrenees were fully deglaciated during the B-A, with small glaciers persisting only in the highest cirques ([Delmas, 2015](#)). A similar pattern was detected in other Iberian ranges, such as in the Sierra Nevada ([Palacios et al., 2016](#)), Cantabrian Mountains ([Rodríguez-Rodríguez et al., 2017](#)) and the Iberian Range ([García-Ruiz et al., 2020](#)), where ice masses shrank significantly by ~15-14 ka. Glacial retreat in the Iberian Mountains was triggered by the sudden temperature increase of 3-5 °C at the onset of the B-A in western Europe, as inferred from climate models ([Renssen and Isarin, 2001](#)). In parallel, significant shifts occurred in the Atlantic Meridional Overturning Circulation ([Obase and Abe-Ouchi, 2019](#)). In north Iberia, a maximum increase of the mean annual temperature of 7.5°C at the onset of GI-1 has been estimated in northern Iberia, based on the Ostolo cave speleothem isotopic record ([Bernal-Wormull et al., 2021](#)). Marine records from the western Iberian margin also pointed to a 5-6°C of warming at the onset of the B-A ([Martrat et al., 2007](#)). These warmer conditions also favoured the recession of glaciers across most European mountain ranges, such as in the Alps at 15.9-14.3 cal ka BP ([Ivy-Ochs, 2015](#)), Tatra Mountains at 14.8-14.2 ka ([Zasadni et al., 2020](#)), Taurus Mountains at 14.6 ± 2.8 ka ([Ciner and Sarikaya, 2015](#)), as well as the Scandinavian Ice Sheet, which recorded a shrinking trend starting at 14.6 cal ka BP ([Mangerud et al., 2013](#)).

1
2 463 However, the B-A was a climatically unstable period characterised by an alternation of warm and cold
3 464 temperatures (Rasmussen et al., 2014). The gradual decrease of temperatures from the early to the late B-A
4 465 was depicted by periods of enhanced cold conditions in the high latitudes of the Northern Hemisphere, which
5 466 also favoured periods of glacial growth in the Pyrenees (Table 5). Indeed, CRE results indicate the formation
6 467 of moraines in the Ruda Valley at 13.5 ± 0.9 and 13.0 ± 0.8 ka (Fig. 7). These CRE ages are consistent with
7 468 the chronostratigraphic sequence but must be taken as approximate due to their uncertainty ranges and the low
8 469 number of dated samples at each moraine. At that time, small ice tongues ~ 3 km long flowed downslope from
9 470 the main Saboredo Cirque as well as from other neighbouring glacial hollows to overdeepened basins, forming
10 471 moraines at 2080 and 2190 m, respectively. Whereas evidence of phases of glacier advance or stillstands during
11 472 the transition from the late B-A to the early YD were already found in other cirques in the Central Pyrenees,
12 473 such as in the Bacivèr Cirque (Oliva et al., 2021a), and in the Cuerpo de Hombre Valley (Sierra de Gredos,
13 474 Central Range), with moraine stabilization at 13.1 ka (Carrasco et al., 2015), this is the first study that reports
14 475 geochronological evidence of a phase with glacial development in the second half of the B-A after the long-
15 476 term cooling initiated at ~ 14.5 ka (Fig. 7; Table 5). A few studies in Europe have also found evidence of glacier
16 477 advances or stillstands during the middle B-A, such as in the Tatra Mountains where moraines stabilized at
17 478 13.4 ± 0.5 ka (Engel et al., 2017). By contrast, geomorphic evidence of a period of glacial expansion during
18 479 the transition between the B-A to the early YD was detected in several regions, such as in the
19 480 Hardangerfjorden-Herdla area, western Norway, where a till deposit suggested a glacier advance of the
20 481 Scandinavian Ice sheet at 13.5-13.0 ka (Mangerud et al., 2016), and in the West Highland and Mull ice fields
21 482 of the Scottish Highlands, where 18 ^{14}C dates from organic fragments found in basal tills revealed a glacial
22 483 readvance from the end of the B-A or earliest YD (Bromley et al., 2018), although these results are considered
23 484 controversial (Small and Fabel, 2016).

29 485 Table 5

30
31 486 Based on the position of these two moraine ridges, the ELA in the Ruda Valley glacier must have been located
32 487 at 2461 and 2505 m during the glacial advances of the second part of the B-A and the late B-A or early YD,
33 488 respectively. Considering that the regional ELA in the Pyrenees currently lies at approximately 3100 m
34 489 (Jomelli et al., 2020; René, 2011), the ELA must have been located 639-595 m lower than present-day
35 490 conditions. Assuming an average lapse rate of $0.65 \text{ }^\circ\text{C } 100 \text{ m}^{-1}$ and no change in precipitation, we infer that
36 491 summer temperatures must have been 4.2 and 3.9 $^\circ\text{C}$ lower than present-day during these two phases (Table
37 492 4).

40 493 Figure 7

41
42 494 The temperature decrease during the early YD favoured the persistence of glaciers inside the highest hollows
43 495 in the Ruda Valley, depositing moraines at ~ 2400 -2500 m, which were later abandoned by the ice at $12.6 \pm$
44 496 1.3 ka (Fig 7). The existence of glaciers at high altitudes of the Saboredo Cirque is also confirmed by polished
45 497 surfaces at elevations of 2200-2300 m that were dated at 12.7 ± 0.8 ka. In the neighbouring Bacivèr Cirque,
46 498 moraines at 2400 m were abandoned by the ice at 12.8 ka (Oliva et al., 2021a). The elevation difference
47 499 between the ELA during the YD (2571 m) in the Ruda Valley and present-day values indicates that summer
48 500 temperatures were ~ 3.4 $^\circ\text{C}$ lower during that cold phase (Table 4), which is very similar to the ~ 3.0 $^\circ\text{C}$ inferred
49 501 for the Bacivèr Cirque (Oliva et al., 2021a). Indeed, topoclimatic factors must have played a key role
50 502 maintaining small glaciers during the YD at the foot of steep cirque walls, where shading and snow
51 503 accumulation allowed the longer persistence of reduced ice masses (Boston and Lukas, 2019). In the Pyrenees,
52 504 YD glacial advances have been detected in cirques of the Central (Delmas, 2009; Delmas et al., 2008; García-
53 505 Ruiz et al., 2016a) and Eastern sectors (Crest et al., 2017; Jomelli et al., 2020; Pallàs et al., 2010; Reixach et
54 506 al., 2021), where 2-3.5 km-long glaciers formed at 12.9-11.2 ka. Based on chronostratigraphic data from a
55 507 variety of sources, evidence of YD glacial advances was also recorded in the highest cirques of other Iberian
56 508 massifs, although no direct ages are yet available (García-Ruiz et al., 2016a). This is true for the NW ranges
57 509 (Cowton et al., 2009) and the Cantabrian Mountains (Pellitero et al., 2019; Serrano et al., 2015), where
58 510 moraines above 1800 and 2000 m, respectively, were associated with this cold phase. In the Sierra Nevada,

1
2 511 YD moraines dated at 13-12 ka are located in the highest cirques facing east from 2350 (north face) to 2800 m
3 512 (south face) (Oliva et al., 2014; Palacios et al., 2016). These glacial advances were driven by a temperature
4 513 cooling quantified at 2-4 °C in western Europe that was triggered by a slowdown of the overturning circulation
5 514 in the North Atlantic (Renssen et al., 2018). In the Pyrenees, the YD was the coldest period of the last
6 515 deglaciation recorded by a decrease of ^{18}O in the Ostolo and Seso speleothems that might reflect the
7 516 temperature decrease of $\sim 5^\circ\text{C}$ (Bartolomé et al., 2015; Bernal-Wormull et al., 2021). Colder conditions also
8 517 favoured glacial growth in other mountainous regions of Europe, with widespread advances across the Alps
9 518 between 13.5 and 12 ka (Ivy-Ochs, 2015; Ivy-Ochs et al., 2009), in the Tatra Mountains where moraines
10 519 stabilized at 11.9 ± 0.5 ka (Engel et al., 2017) and in Turkey where they formed at 12.6 ± 2.3 ka (Ciner and
11 520 Sarikaya, 2015).

12
13 521 The final deglaciation of the cirques favoured paraglacial dynamics and the formation of the numerous rock
14 522 glaciers existing today in the Saboredo and Sendrosa cirques, as well as in the lateral cirques distributed along
15 523 the Ruda Valley (Fig. 3). These features are currently inactive under the present-day climate regime (Fernandes
16 524 et al., 2018), with abundant lichen coverage and forest colonization, particularly on the lowest ridges. In the
17 525 Pyrenees, as well as in other Iberian ranges, cirque wall readjustment following deglaciation triggered different
18 526 landforms, such as debris-covered glaciers or rock glaciers, that remained active until the early Holocene
19 527 (Oliva et al., 2019). This is the case of the Bacivèr cirque, where the debris-covered glacier that formed inside
20 528 the highest YD moraines stabilized at 7.2 ± 0.5 ka (Oliva et al., 2021a), or of several other massifs in the
21 529 Central and Eastern Pyrenees where rock glaciers were active until well into the Holocene (Andrés et al., 2018;
22 530 García-Ruiz et al., 2016a). A similar pattern was also detected in other Iberian massifs, such as in the Iberian
23 531 Range (Aumaître et al., 2017) or Sierra Nevada (Palacios et al., 2016), where these paraglacial landforms
24 532 formed immediately after the deglaciation of the cirques, and remained active until the complete melting of
25 533 their relict ice during the Holocene Thermal Maximum.
26
27

28 534 6. Conclusions

29
30 535 The Central Pyrenees were extensively glaciated during Quaternary glacial phases and were only slightly
31 536 transformed by periglacial, nival and slope processes during subsequent interglacial periods such as the
32 537 Holocene. As a result, the landscape in the Central Pyrenees includes a wide range of geomorphological
33 538 features that constitutes a prominent natural heritage that contributed to the designation of most protected areas
34 539 in this mountain range. This is the case of the Ruda Valley, located on the periphery of the National Park of
35 540 Aigüestortes and Sant Maurici Lake. The valley is one of the most scenic glacial valleys of the Pyrenees, and
36 541 includes a wide variety of glacial and periglacial landforms, particularly above 1800 m. However, in contrast
37 542 to the southern slope of the Central Pyrenees where the timing of the glacial evolution has been widely studied,
38 543 on the northern side there are still temporal and spatial gaps in the chronology of glacial activity. In this work,
39 544 we determined the magnitude and timing of T-1 glacial oscillations in the Upper Garonne Basin by producing
40 545 12 new CRE ages of glacial landforms (moraine boulders and glacially polished surfaces) that provide evidence
41 546 of the spatio-temporal pattern of glacial oscillations from the B-A to the YD.
42

43 547 The Upper Garonne Basin hosted the largest glacial system of the Pyrenees during the last glacial cycle thanks
44 548 to its Atlantic-influenced climate and the high altitude of the peaks in the central part of this range. The long-
45 549 term post-LGM warming favoured glacial recession, particularly during the early B-A, and by 14.4 ± 1.2 ka
46 550 the Ruda Paleoglacier was already disconnected from the main Garonne Paleoglacier. At that time, the glacier
47 551 front was located at 1860-1900 m, and some areas of the Saboredo Cirque were already ice-free as a result of
48 552 ice thinning. The B-A was also a period of great climatic variability, and the small glaciers in the Ruda Valley
49 553 showed rapid response times with formation of moraines during the coldest B-A phases in north Iberia. Phases
50 554 of glacier advance or stillstands promoted the development of moraines at 13.5 ± 0.9 ka, as well as during the
51 555 transition between the late B-A and the onset of the YD at 13.0 ± 0.8 ka. The YD probably favoured the
52 556 persistence of small glaciers during an early stage of this cold phase; there is evidence of glacial retreat at the
53 557 uppermost part of the cirque floor at 12.7 ± 0.7 ka (~ 2300 -2350 m) and moraine abandonment of the highest

1
2 558 cirque moraines (2470 m) at 12.6 ± 1.3 ka. Subsequently, glacial disappearance must have promoted
3 559 paraglacial dynamics and the formation of the (currently relict) rock glaciers existing within these moraines.
4

5 560 Whereas the impact of the B-A deglaciation on the current landscape of the Pyrenean cirques was already
6 561 known, the sequence of glacial advances and retreats during the B-A and YD presented in this study provides
7 562 one of the most accurate deglacial histories in southern Europe. This opens new perspectives on the
8 563 paleoclimatic evolution in the Iberian Peninsula, in particular, and the Mediterranean region in general. The
9 564 period spanning from the B-A to the YD has been shown to be a major driver of transformation of the mountain
10 565 landscapes of the Pyrenees and a key phase to better frame Holocene environmental dynamics in the highest
11 566 lands of this mountain range. Future studies with new chronological data from other Pyrenean valleys and
12 567 Iberian mountains will help to better understand T-1 glacier advances and retreats as well as the climate
13 568 mechanisms behind millennial-scale glacial oscillations in southern Europe.

16 569 **Acknowledgements**

17
18 570 This work was funded by the Research Group ANTALP (Antarctic, Arctic, Alpine Environments; 2017-SGR-
19 571 1102), the Government of Catalonia and the Centro de Estudos Geográficos/IGOT - University of Lisbon (FCT
20 572 I.P. UIDB/00295/2020 and UIDP/00295/2020). The research topics complement those of the project
21 573 PALEOGREEN (CTM2017-87976-P) funded by the Spanish Ministry of Economy and Competitiveness and
22 574 the project NUNANTAR funded by the Fundação para a Ciência e Tecnologia of Portugal (02/SAICT/2017 -
23 575 32002). Marcelo Fernandes holds a PhD fellowship of the Fundação para a Ciência e Tecnologia of Portugal
24 576 (FCT - UIDB/00295/2020); Marc Oliva is supported by the Ramón y Cajal Program (RYC-2015-17597) and
25 577 José M. Fernández-Fernández is supported by a postdoctoral grant within the NUNANTAR project. ¹⁰Be
26 578 measurements were performed at the ASTER AMS national facility (CEREGE, Aix-en-Provence), which is
27 579 supported by the INSU/CNRS and the ANR through the “Projets thématiques d'excellence” program for the
28 580 “Equipements d'excellence” ASTER-CEREGE action and IRD. This research is also framed within the College
29 581 on Polar and Extreme Environments (Polar2E) of the University of Lisbon. We also thank the National Park
30 582 of Aigüestortes and Sant Maurici Lake for providing field access to the study sites and the reviewers for their
31 583 constructive comments that helped to improve the quality of an earlier version of the manuscript.
32
33
34
35

37 585 **7. References**

- 36 584
37 585
38
39 586
40
41 587 Allard, J.L., Hughes, P., Woodward, J.C., 2021. Heinrich Stadial aridity forced Mediterranean-wide glacier
42 588 retreat in the last cold stage. *Nat. Geosci.* <https://doi.org/10.1038/s41561-021-00703-6>
- 43 589 André, M.F., 2002. Rates of Postglacial rock weathering on glacially scoured outcrops (Abisko-Riksgränsen
44 590 area, 68°N). *Geogr. Ann. Ser. A Phys. Geogr.* 84, 139–150. <https://doi.org/10.1111/j.0435-3676.2002.00168.x>
- 45 591
46
47 592 Andrés, N., Gómez-Ortiz, A., Fernández-Fernández, J.M., Tanarro García, L.M., Salvador-Franch, F., Oliva,
48 593 M., Palacios, D., 2018. Timing of deglaciation and rock glacier origin in the southeastern Pyrenees: a
49 594 review and new data. *Boreas* 47, 1050–1071. <https://doi.org/10.1111/bor.12324>
- 50
51 595 Arnold, M., Merchel, S., Boulès, D.L., Braucher, R., Benedetti, L., Finkel, R.C., Aumaître, G., Gott dang,
52 596 A., Klein, M., 2010. The French accelerator mass spectrometry facility ASTER: Improved performance
53 597 and developments. *Nucl. Instruments Methods Phys. Res. Sect. B Beam Interact. with Mater. Atoms*
54 598 268, 1954–1959. <https://doi.org/10.1016/j.nimb.2010.02.107>
- 55 599 Aumaître, G., Boulès, D., Keddadouche, K., Schimmelpfennig, I., Léanni, L., Fernández-Fernández, J.M.,
56 600 Palacios, D., Andrés, N., Úbeda, J., García-Ruiz, J.M., Gómez-Villar, A., Santos-González, J., Álvarez-
57 601 Martínez, J., Arnáez, J., 2017. Chronological and geomorphological investigation of fossil debris-
58 602 covered glaciers in relation to deglaciation processes: A case study in the Sierra de La Demanda,
59 603 northern Spain. *Quat. Sci. Rev.* 170, 232–249. <https://doi.org/10.1016/j.quascirev.2017.06.034>
- 60
604 Ballantyne, C.K., 2008. After the ice: Holocene geomorphic activity in the Scottish Highlands, Scottish

- 1
2 605 Geographical Journal. <https://doi.org/10.1080/14702540802300167>
- 3
4 606 Barr, I., Spagnolo, M., 2015. Glacial cirques as palaeoenvironmental indicators: Their potential and
5 607 limitations. *Earth-Science Rev.* 151, 48–78. <https://doi.org/10.1016/j.earscirev.2015.10.004>
- 6 608 Bartolomé, M., Moreno, A., Sancho, C., Stoll, H.M., Cacho, I., Spötl, C., Belmonte, Á., Edwards, R.L.,
7 609 Cheng, H., Hellstrom, J.C., 2015. Hydrological change in Southern Europe responding to increasing
8 610 North Atlantic overturning during Greenland Stadial 1. *Proc. Natl. Acad. Sci.* 112, 6568–6572.
9 611 <https://doi.org/10.1073/pnas.1503990112>
- 10
11 612 Benn, D.I., Hulton, N.R.J., 2010. An Excel™ spreadsheet program for reconstructing the surface profile of
12 613 former mountain glaciers and ice caps. *Comput. Geosci.* 36, 605–610.
13 614 <https://doi.org/10.1016/j.cageo.2009.09.016>
- 14
15 615 Bernal-Wormull, J.L., Moreno, A., Bartolomé, M., Aranburu, A., Arriolabengoa, M., Iriarte, E., Cacho, I.,
16 616 Spötl, C., Edwards, R.L., Cheng, H., 2021. Immediate temperature response in northern Iberia to last
17 617 deglacial changes in the North Atlantic. *Geology* XX, 6–10.
18 618 <https://doi.org/10.1130/G48660.1/5304545/g48660.pdf>
- 19 619 Boston, C.M., Lukas, S., 2019. Topographic controls on plateau icefield recession: insights from the
20 620 Younger Dryas Monadhliath Icefield, Scotland. *J. Quat. Sci.* 34, 433–451.
21 621 <https://doi.org/10.1002/jqs.3111>
- 22
23 622 Braucher, R., Guillou, V., Bourlès, D.L., Arnold, M., Aumaître, G., Keddadouche, K., Nottoli, E., 2015.
24 623 Preparation of ASTER in-house 10Be/9Be standard solutions. *Nucl. Instruments Methods Phys. Res.*
25 624 *Sect. B Beam Interact. with Mater. Atoms* 361, 335–340.
26 625 <https://doi.org/https://doi.org/10.1016/j.nimb.2015.06.012>
- 27
28 626 Bromley, G., Putnam, A., Borns, H., Lowell, T., Sandford, T., Barrell, D., 2018. Interstadial Rise and
29 627 Younger Dryas Demise of Scotland's Last Ice Fields Paleooceanography and Paleoclimatology.
30 628 *Paleoceanogr. Paleoclimatology* 412–429. <https://doi.org/10.1002/2018PA003341>
- 31 629 Carrasco, R.M., Pedraza, J., Domínguez-Villar, D., Willenbring, J.K., Villa, J., 2015. Sequence and
32 630 chronology of the Cuerpo de Hombre paleoglacier (Iberian Central System) during the last glacial
33 631 cycle. *Quat. Sci. Rev.* 129, 163–177. <https://doi.org/10.1016/j.quascirev.2015.09.021>
- 34
35 632 Chmeleff, J., von Blanckenburg, F., Kossert, K., Jakob, D., 2010. Determination of the 10Be half-life by
36 633 multicollector ICP-MS and liquid scintillation counting. *Nucl. Instruments Methods Phys. Res. Sect. B*
37 634 *Beam Interact. with Mater. Atoms* 268, 192–199. <https://doi.org/10.1016/j.nimb.2009.09.012>
- 38
39 635 Ciner, A., Sarikaya, M.A., 2015. Cosmogenic 36 Cl geochronology of late Quaternary glaciers in the Bolkar
40 636 Mountains, south central Turkey, in: Hughes, P. D. & Woodward, J.C. (Ed.), *Quaternary Glaciation in*
41 637 *the Mediterranean Mountains*. <https://doi.org/http://doi.org/10.1144/SP433.3>
- 42 638 Clark, P.U., Dyke, A., Shakun, J., Carlson, A., Wohlfarth, B., Mitrovica, J., Hostetler, S., McCabe, A., 2009.
43 639 *The Last Glacial Maximum*. *Science* (80-.). 325, 710–714. <https://doi.org/10.1126/science.1172873>
- 44
45 640 Cowton, T., Hughes, P., Gibbard, P.L., 2009. Palaeoglaciation of Parque Natural Lago de Sanabria,
46 641 northwest Spain. *Geomorphology* 108, 282–291. <https://doi.org/10.1016/j.geomorph.2009.02.007>
- 47 642 Crest, Y., Delmas, M., Braucher, R., Gunnell, Y., Calvet, M., 2017. Cirques have growth spurts during
48 643 deglacial and interglacial periods: Evidence from 10Be and 26Al nuclide inventories in the central and
49 644 eastern Pyrenees. *Geomorphology* 278, 60–77. <https://doi.org/10.1016/j.geomorph.2016.10.035>
- 51 645 Delmas, M., 2015. The last maximum ice extent and subsequent deglaciation of the Pyrenees: an overview of
52 646 recent research. *Cuad. Investig. Geográfica* 41, 359. <https://doi.org/10.18172/cig.2708>
- 53
54 647 Delmas, M., 2009. Chronologie et impact géomorphologique des glaciations quaternaires dans l'est des
55 648 Pyrénées. *Lab. Rech. en géographie Phys. MEDI-TERRA, Univ. Perpignan. LGP Meudon, Univ. Paris*
56 649 *1 Panthéon Sorbonne Ph.D.*, 529.
- 57 650 Delmas, M., Calvet, M., Gunnell, Y., Braucher, R., Bourlès, D., 2011. Palaeogeography and 10Be exposure-
58 651 age chronology of Middle and Late Pleistocene glacier systems in the northern Pyrenees: Implications
59 652 for reconstructing regional palaeoclimates. *Palaeogeogr. Palaeoclimatol. Palaeoecol.* 305, 109–122.
60 653 <https://doi.org/10.1016/j.palaeo.2011.02.025>

- 1
2 654 Delmas, M., Gunnell, Y., Braucher, R., Calvet, M., Bourlès, D., 2008. Exposure age chronology of the last
3 655 glaciation in the eastern Pyrenees. *Quat. Res.* 69, 231–241. <https://doi.org/10.1016/j.yqres.2007.11.004>
- 4
5 656 Dunne, J., Elmore, D., Muzikar, P., 1999. Scaling factors for the rates of production of cosmogenic nuclides
6 657 for geometric shielding and attenuation at depth on sloped surfaces. *Geomorphology* 27, 3–11.
7 658 [https://doi.org/10.1016/S0169-555X\(98\)00086-5](https://doi.org/10.1016/S0169-555X(98)00086-5)
- 8 659 Fernandes, M., Oliva, M., Palma, P., Ruiz-Fernández, J., Lopes, L., 2017. Glacial stages and post-glacial
9 660 environmental evolution in the Upper Garonne valley, Central Pyrenees. *Sci. Total Environ.* 584–585,
10 661 1282–1299. <https://doi.org/10.1016/j.scitotenv.2017.01.209>
- 11
12 662 Fernandes, M., Oliva, M., Vieira, G., 2020. Paraglacial slope failures in the Aran valley (Central Pyrenees).
13 663 *Quat. Int.* 566–567, 24–38. <https://doi.org/10.1016/j.quaint.2020.07.045>
- 14
15 664 Fernandes, M., Oliva, M., Vieira, G., Lopes, L., 2021. Geomorphological map of the Aran valley (Upper
16 665 Garonne valley, Central Pyrenees). *J. Maps.*
- 17 666 Fernandes, M., Palma, P., Lopes, L., Ruiz-Fernández, J., Pereira, P., Oliva, M., 2018. Spatial distribution and
18 667 morphometry of permafrost-related landforms in the Central Pyrenees and associated paleoclimatic
19 668 implications. *Quat. Int.* 470. <https://doi.org/10.1016/j.quaint.2017.08.071>
- 20
21 669 García-Ruiz, J.M., Moreno, A., González-Sampériz, P., Valero-Garcés, B.L., Martí-Bono, C., 2010. La
22 670 cronología del último ciclo glaciar en las montañas del sur de Europa. Una revisión. *Cuaternario y*
23 671 *Geomorfol.* 24, 35–46. [https://doi.org/10.1016/S0034-7094\(11\)70016-2](https://doi.org/10.1016/S0034-7094(11)70016-2)
- 24
25 672 García-Ruiz, J.M., Palacios, D., Fernández-Fernández, J.M., Andrés, N., Arnáez, J., Gómez-Villar, A.,
26 673 Santos-González, J., Álvarez-Martínez, J., Lana-Renault, N., Léanni, L., 2020. Glacial stages in the
27 674 Peña Negra valley, Iberian Range, northern Iberian Peninsula: Assessing the importance of the glacial
28 675 record in small cirques in a marginal mountain area. *Geomorphology* 362, 107195.
29 676 <https://doi.org/10.1016/j.geomorph.2020.107195>
- 30 677 García-Ruiz, J.M., Palacios, D., González-Sampériz, P., De Andrés, N., Moreno, A., Valero-Garcés, B.,
31 678 Gómez-Villar, A., 2016a. Mountain glacier evolution in the Iberian Peninsula during the Younger
32 679 Dryas. *Quat. Sci. Rev.* 138, 16–30. <https://doi.org/10.1016/j.quascirev.2016.02.022>
- 33
34 680 García-Ruiz, J.M., Palacios, D., González-Sampériz, P., de Andrés, N., Moreno, A., Valero-Garcés, B.L.,
35 681 Gómez-Villar, A., 2016b. Evidencias de actividad glaciar durante el Dryas Reciente (12,9–11,7 ka BP)
36 682 en la Península Ibérica. *Cuaternario y Geomorfol.* 30, 9–21. [https://doi.org/10.17735/cyg.v30i1-](https://doi.org/10.17735/cyg.v30i1-2.39250)
37 683 [2.39250](https://doi.org/10.17735/cyg.v30i1-2.39250)
- 38
39 684 Gómez-Ortiz, A., Palacios, D., Palade, B., Vázquez-Selem, L., Salvador-Franch, F., 2012. The deglaciation
40 685 of the Sierra Nevada (Southern Spain). *Geomorphology* 159–160, 93–105.
41 686 <https://doi.org/10.1016/j.geomorph.2012.03.008>
- 42 687 González-Sampériz, P., Valero-Garcés, B.L., Moreno, A., Jalut, G., García-Ruiz, J.M., Martí-Bono, C.,
43 688 Delgado-Huertas, A., Navas, A., Otto, T., Dedoubat, J., 2006. Climate variability in the Spanish
44 689 Pyrenees during the last 30,000 yr revealed by the El Portalet sequence. *Quat. Res.* 66, 38–52.
- 45
46 690 Heyman, J., Stroeven, A.P., Harbor, J.M., Caffee, M.W., 2011. Too young or too old: evaluating cosmogenic
47 691 exposure dating based on an analysis of compiled boulder exposure ages. *Earth Planet. Sci. Lett.* 302,
48 692 71–80.
- 49
50 693 Hughes, P., 2014. Little Ice Age glaciers in the Mediterranean mountains. *Geophys. Res. Abstr.* 16, 2014.
- 51 694 Huss, M., Bauder, A., Linsbauer, A., Gabbi, J., Kappenberger, G., Steinegger, U., Farinotti, D., 2021. More
52 695 than a century of direct glacier mass-balance observations on Claridenfirn, Switzerland. *J. Glaciol.* 1–
53 696 17. <https://doi.org/10.1017/jog.2021.22>
- 54
55 697 ICGC, 2017. Base de dades geològiques de Catalunya 1:50.000 v1.0.
- 56 698 Ivy-Ochs, S., 2015. Variaciones glaciares en los Alpes europeos al final de la última glaciación. *Cuad.*
57 699 *Investig. Geogr.* 41, 295–315. <https://doi.org/10.18172/cig.2750>
- 58
59 700 Ivy-Ochs, S., Kerschner, H., Maisch, M., Christl, M., Kubik, P.W., Schlüchter, C., 2009. Latest Pleistocene
60 701 and Holocene glacier variations in the European Alps. *Quat. Sci. Rev.* 28, 2137–2149.
702 <https://doi.org/10.1016/j.quascirev.2009.03.009>

- 1
2 703 Joly, F., 1997. Glossaire de géomorphologie. Base de données sémiologiques pour la cartographie,
3 704 Masson/Arm. ed. Paris.
- 4
5 705 Jomelli, V., Chapron, E., Favier, V., Rinterknecht, V., Braucher, R., Tournier, N., Gascoïn, S., Marti, R.,
6 706 Galop, D., Binet, S., Deschamps, C., Tissoux, H., Aumaitre, G., Bourlès, D.L., Keddadouche, K., 2020.
7 707 Glacier fluctuations during the Late Glacial and Holocene on the Ariège valley, northern slope of the
8 708 Pyrenees and reconstructed climatic conditions. *Mediterr. Geosci. Rev.* [https://doi.org/10.1007/s42990-](https://doi.org/10.1007/s42990-020-00018-5)
9 709 020-00018-5
- 10 710 Korschinek, G., Bergmaier, A., Faestermann, T., Gerstmann, U.C., Knie, K., Rugel, G., Wallner, A.,
11 711 Dillmann, I., Dollinger, G., von Gostomski, C.L., Kossert, K., Maiti, M., Poutivtsev, M., Rimmert, A.,
12 712 2010. A new value for the half-life of ^{10}Be by Heavy-Ion Elastic Recoil Detection and liquid
13 713 scintillation counting. *Nucl. Instruments Methods Phys. Res. Sect. B Beam Interact. with Mater. Atoms*
14 714 268, 187–191. <https://doi.org/10.1016/j.nimb.2009.09.020>
- 15
16 715 Li, Y., 2018. Determining topographic shielding from digital elevation models for cosmogenic nuclide
17 716 analysis: a GIS model for discrete sample sites. *J. Mt. Sci.* 15, 939–947.
18 717 <https://doi.org/10.1007/s11629-018-4895-4>
- 19
20 718 Lifton, N., Sato, T., Dunai, T., 2014. Scaling in situ cosmogenic nuclide production rates using analytical
21 719 approximations to atmospheric cosmic-ray fluxes. *Earth Planet. Sci. Lett.* 386, 149–160.
22 720 <https://doi.org/10.1016/j.epsl.2013.10.052>
- 23
24 721 Lopes, L., Oliva, M., Fernandes, M., Pereira, P., Palma, P., Ruiz-Fernández, J., 2018. Spatial distribution of
25 722 morphometric parameters of glacial cirques in the Central Pyrenees (Aran and Boí valleys). *J. Mt. Sci.*
26 723 15. <https://doi.org/10.1007/s11629-018-4873-x>
- 27 724 López-Moreno, J.I., Alonso-González, E., Monserrat, O., Del Río, L.M., Otero, J., Lapazaran, J., Luzi, G.,
28 725 Dematteis, N., Serreta, A., Rico, I., Serrano, E., Bartolomé, M., Moreno, A., Buisan, S., Revuelto, J.,
29 726 2019. Ground-based remote-sensing techniques for diagnosis of the current state and recent evolution
30 727 of the Monte Perdido Glacier, Spanish Pyrenees. *J. Glaciol.* 65, 85–100.
31 728 <https://doi.org/10.1017/jog.2018.96>
- 32
33 729 Mangerud, J., Aarseth, I., Hughes, A.L.C., Lohne, Ø.S., Skår, K., Sønstegeard, E., Inge, J., 2016. A major re-
34 730 growth of the Scandinavian Ice Sheet in western Norway during Allerød-Younger Dryas. *Quat. Sci.*
35 731 *Rev.* 132, 175–205. <https://doi.org/10.1016/j.quascirev.2015.11.013>
- 36
37 732 Mangerud, J., Goehring, B.M., Lohne, Ø.S., Svendsen, J.I., Gyllencreutz, R., 2013. Collapse of marine-based
38 733 outlet glaciers from the Scandinavian Ice Sheet. *Quat. Sci. Rev.* 67, 8–16.
39 734 <https://doi.org/10.1016/j.quascirev.2013.01.024>
- 40 735 Martin, L.C.P., Blard, P.-H., Balco, G., Lavé, J., Delunel, R., Lifton, N., Laurent, V., 2017. The CREp
41 736 program and the ICE-D production rate calibration database: A fully parameterizable and updated
42 737 online tool to compute cosmic-ray exposure ages. *Quat. Geochronol.* 38, 25–49.
43 738 <https://doi.org/10.1016/J.QUAGEO.2016.11.006>
- 44
45 739 Martrat, B., Grimalt, J.O., Shackleton, N.J., De Abreu, L., Hutterli, M.A., Stocker, T.F., 2007. Four climate
46 740 cycles of recurring deep and surface water destabilizations on the Iberian margin. *Science (80-)*. 317,
47 741 502–507. <https://doi.org/10.1126/science.1139994>
- 48
49 742 Merchel, S., Arnold, M., Aumaitre, G., Benedetti, L., Bourlès, D.L., Braucher, R., Alfimov, V., Freeman,
50 743 S.P.H.T., Steier, P., Wallner, A., 2008. Nuclear Instruments and Methods in Physics Research B
51 744 Towards more precise ^{10}Be and ^{36}Cl data from measurements at the 10 Å 14 level : Influence of
52 745 sample preparation Be / B e. *Nucl. Inst. Methods Phys. Res. B* 266, 4921–4926.
53 746 <https://doi.org/10.1016/j.nimb.2008.07.031>
- 54 747 Merchel, S., Hergers, U., 1999. An Update on Radiochemical Separation Techniques for the Determination
55 748 of Long-Lived Radionuclides via Accelerator Mass Spectrometry. *Radiochim. Acta* 84, 215–219.
56 749 <https://doi.org/10.1524/ract.1999.84.4.215>
- 57
58 750 Moreno, A., Stoll, H., Jiménez-Sánchez, M., Cacho, I., Valero-Garcés, B., Ito, E., Edwards, R.L., 2010. A
59 751 speleothem record of glacial (25–11.6 kyr BP) rapid climatic changes from northern Iberian Peninsula.
60 752 *Glob. Planet. Change* 71, 218–231. <https://doi.org/10.1016/j.gloplacha.2009.10.002>

- 1
2 753 Obase, T., Abe-Ouchi, A., 2019. Abrupt Bølling-Allerød Warming Simulated under Gradual Forcing of the
3 754 Last Deglaciation. *Geophys. Res. Lett.* 46, 11397–11405. <https://doi.org/10.1029/2019GL084675>
- 4
5 755 Oliva, M., Fernandes, M., Palacios, D., Fernández-Fernández, J.M., Schimmelpfennig, I., Team, A.S.T.E.R.,
6 756 Antoniades, D., 2021a. Rapid deglaciation during the Bølling-Allerød Interstadial in the Central
7 757 Pyrenees and associated glacial and periglacial landforms. *Geomorphology* 107735.
8 758 <https://doi.org/10.1016/j.geomorph.2021.107735>
- 9 759 Oliva, M., Gómez Ortiz, A., Palacios, D., Salvador-Franch, F., Salvà-Catarineu, M., 2014. Environmental
10 760 evolution in Sierra Nevada (South Spain) since the Last Glaciation, based on multi-proxy records.
11 761 *Quat. Int.* 353, 195–209. <https://doi.org/10.1016/j.quaint.2014.02.009>
12
- 13 762 Oliva, M., Palacios, D., Fernández-Fernández, J.M., 2021b. Iberia, land of glaciers. Elsevier.
- 14 763 Oliva, M., Palacios, D., Fernández-Fernández, J.M., Rodríguez-Rodríguez, L., García-Ruiz, J.M., Andrés,
15 764 N., Carrasco, R.M., Pedraza, J., Pérez-Alberti, A., Valcárcel, M., Hughes, P., 2019. Late Quaternary
16 765 glacial phases in the Iberian Peninsula. *Earth-Science Rev.* 192, 564–600.
17 766 <https://doi.org/10.1016/j.earscirev.2019.03.015>
- 19 767 Oliva, M., Serrano, E., Gómez-Ortiz, A., González-Amuchastegui, M.J., Nieuwendam, A., Palacios, D.,
20 768 Pérez-Alberti, A., Pellitero, R., Ruiz-Fernández, J., Valcárcel, M., Vieira, G., Antoniades, D., 2016.
21 769 Spatial and temporal variability of periglaciation of the Iberian Peninsula. *Quat. Sci. Rev.* 137, 176–
22 770 199. <https://doi.org/10.1016/j.quascirev.2016.02.017>
23
- 24 771 Osmaston, H., 2005. Estimates of glacier equilibrium line altitudes by the Area×Altitude, the Area×Altitude
25 772 Balance Ratio and the Area×Altitude Balance Index methods and their validation. *Quat. Int.* 138–139,
26 773 22–31. <https://doi.org/10.1016/j.quaint.2005.02.004>
- 27
28 774 Palacios, D., Andrés, N., Marcos, J., Vázquez-Selem, L., 2012a. Maximum glacial advance and deglaciation
29 775 of the Pinar Valley (Sierra de Gredos, Central Spain) and its significance in the Mediterranean context.
30 776 *Geomorphology* 177–178, 51–61. <https://doi.org/10.1016/j.geomorph.2012.07.013>
- 31 777 Palacios, D., de Andrés, N., de Marcos, J., Vázquez-Selem, L., 2012b. Glacial landforms and their
32 778 paleoclimatic significance in Sierra de Guadarrama, Central Iberian Peninsula. *Geomorphology* 139–
33 779 140, 67–78. <https://doi.org/10.1016/j.geomorph.2011.10.003>
34
- 35 780 Palacios, D., de Andrés, N., Gómez-Ortiz, A., García-Ruiz, J.M., 2017a. Evidence of glacial activity during
36 781 the Oldest Dryas in the mountains of Spain. *Geol. Soc. London, Spec. Publ.* 433, 87–110.
37 782 <https://doi.org/10.1144/SP433.10>
- 38
39 783 Palacios, D., de Andrés, N., López-Moreno, J.I., García-Ruiz, J.M., 2015a. Late Pleistocene deglaciation in
40 784 the upper Gállego Valley, central Pyrenees. *Quat. Res. (United States)* 83, 397–414.
41 785 <https://doi.org/10.1016/j.yqres.2015.01.010>
- 42 786 Palacios, D., García-Ruiz, J.M., 2015. Foreword: Deglaciation in Europe. New insights and questions. *Cuad.*
43 787 *Investig. Geogr.* 41, 257–259. <https://doi.org/10.18172/cig.2808>
44
- 45 788 Palacios, D., García-Ruiz, J.M., Andrés, N., Schimmelpfennig, I., Campos, N., Léanni, L., Aumaître, G.,
46 789 Boulès, D.L., Keddadouche, K., 2017b. Deglaciation in the central Pyrenees during the Pleistocene–
47 790 Holocene transition: Timing and geomorphological significance. *Quat. Sci. Rev.* 162, 111–127.
48 791 <https://doi.org/10.1016/j.quascirev.2017.03.007>
- 49
50 792 Palacios, D., Gómez-Ortiz, A., Andrés, N., Salvador-Franch, F., Oliva, M., 2016. Timing and new
51 793 geomorphologic evidence of the last deglaciation stages in Sierra Nevada (southern Spain). *Quat. Sci.*
52 794 *Rev.* 150, 110–129. <https://doi.org/10.1016/j.quascirev.2016.08.012>
- 53 795 Palacios, D., Gómez-Ortiz, A., Andrés, N., Vázquez-Selem, L., Salvador-Franch, F., Oliva, M., 2015b.
54 796 Maximum extent of Late Pleistocene glaciers and last deglaciation of La Cerdanya mountains,
55 797 Southeastern Pyrenees. *Geomorphology* 231, 116–129. <https://doi.org/10.1016/j.geomorph.2014.10.037>
56
- 57 798 Palacios, D., Hughes, P., García-Ruiz, J.M., Andrés, N., 2021. European Glacial Landscapes. Elsevier.
- 58 799 Pallàs, R., Rodés, Á., Braucher, R., Boulès, D., Delmas, M., Calvet, M., Gunnell, Y., 2010. Small, isolated
59 800 glacial catchments as priority targets for cosmogenic surface exposure dating of Pleistocene climate
60 801 fluctuations, southeastern Pyrenees. *Geology* 38, 891–894. <https://doi.org/10.1130/G31164.1>

- 1
2 802 Pallàs, R., Rodés, Á., Braucher, R., Carcaillet, J., Ortuño, M., Bordonau, J., Bourlès, D., Vilaplana, J.M.,
3 803 Masana, E., Santanach, P., 2006. Late Pleistocene and Holocene glaciation in the Pyrenees: a critical
4 804 review and new evidence from ^{10}Be exposure ages, south-central Pyrenees. *Quat. Sci. Rev.* 25, 2937–
5 805 2963. <https://doi.org/10.1016/j.quascirev.2006.04.004>
- 6
7 806 Paterson, W.S.B., 1994. *The Physics of Glaciers*, 3rd Editio. ed. Elsevier, London.
8 807 <https://doi.org/10.1016/C2009-0-14802-X>
- 9 808 Pellitero, R., Fernández-Fernández, J.M., Campos, N., Serrano, E., Pisabarro, A., 2019. Late Pleistocene
10 809 climate of the northern Iberian Peninsula: New insights from palaeoglaciers at Fuentes Carrionas
11 810 (Cantabrian Mountains). *J. Quat. Sci.* 34, 342–354. <https://doi.org/10.1002/jqs.3106>
- 12
13 811 Pellitero, R., Rea, B.R., Spagnolo, M., Bakke, J., Hughes, P., Ivy-Ochs, S., Lukas, S., Ribolini, A., 2015. A
14 812 GIS tool for automatic calculation of glacier equilibrium-line altitudes. *Comput. Geosci.* 82, 55–62.
15 813 <https://doi.org/10.1016/j.cageo.2015.05.005>
- 16
17 814 Pellitero, R., Rea, B.R., Spagnolo, M., Bakke, J., Ivy-Ochs, S., Frew, C.R., Hughes, P., Ribolini, A., Lukas,
18 815 S., Renssen, H., 2016. GlaRe, a GIS tool to reconstruct the 3D surface of palaeoglaciers. *Comput.*
19 816 *Geosci.* 94, 77–85. <https://doi.org/10.1016/j.cageo.2016.06.008>
- 20 817 Quesada, C., Oliveira, J., 2019. *The Geology of Iberia: A Geodynamic Approach: The Variscan Cycle*.
- 21
22 818 Rasmussen, S.O., Bigler, M., Blockley, S.P., Blunier, T., Buchardt, S.L., Clausen, H.B., Cvijanovic, I., Dahl-
23 819 Jensen, D., Johnsen, S., Fischer, H., Gkinis, V., Guillevic, M., Hoek, W.Z., Lowe, J.J., Pedro, J.B.,
24 820 Popp, T., Seierstad, I.K., Steffensen, J.P., Svensson, A.M., Vallelonga, P., Vinther, B.M., Walker,
25 821 M.J.C., Wheatley, J.J., Winstrup, M., 2014. A stratigraphic framework for abrupt climatic changes
26 822 during the Last Glacial period based on three synchronized Greenland ice-core records: Refining and
27 823 extending the INTIMATE event stratigraphy. *Quat. Sci. Rev.* 106, 14–28.
28 824 <https://doi.org/10.1016/j.quascirev.2014.09.007>
- 29
30 825 Rea, B.R., 2009. Defining modern day Area-Altitude Balance Ratios (AABRs) and their use in glacier-
31 826 climate reconstructions. *Quat. Sci. Rev.* 28, 237–248. <https://doi.org/10.1016/j.quascirev.2008.10.011>
- 32 827 Rea, B.R., Pellitero, R., Spagnolo, M., Hughes, P., Ivy-Ochs, S., Renssen, H., Ribolini, A., Bakke, J., Lukas,
33 828 S., Braithwaite, R.J., 2020. Atmospheric circulation over Europe during the Younger Dryas. *Sci. Adv.*
34 829 6.
- 35
36 830 Reixach, T., Delmas, M., Calvet, M., 2021. Climatic conditions between 19 and 12 ka in the eastern
37 831 Pyrenees, and wider implications for atmospheric circulation patterns in Europe. *Quat. Sci. Rev.* 260.
38 832 <https://doi.org/10.1016/j.quascirev.2021.106923>
- 39
40 833 René, P., 2011. Régression des glaciers pyrénéens et transformation du paysage depuis le Petit Âge
41 834 Glaciaire. *Sud-Ouest Eur.* 5–19. <https://doi.org/10.4000/soe.639>
- 42 835 Renssen, H., Goosse, H., Roche, M., Sepp, H., 2018. The global hydroclimate response during the Younger
43 836 Dryas event. <https://doi.org/10.1016/j.quascirev.2018.05.033>
- 44
45 837 Renssen, H., Isarin, R.F.B., 2001. The two major warming phases of the last deglaciation at 14.7 and 11.5 ka
46 838 cal BP in Europe. *Glob. Planet. Change* 30, 117–153.
- 47 839 Rodríguez-Rodríguez, L., Jiménez-Sánchez, M., Domínguez-Cuesta, M.J., Rinterknecht, V., Pallàs, R., 2017.
48 840 Timing of last deglaciation in the Cantabrian Mountains (Iberian Peninsula; North Atlantic Region)
49 841 based on in situ-produced ^{10}Be exposure dating. *Quat. Sci. Rev.* 171, 166–181.
50 842 <https://doi.org/10.1016/j.quascirev.2017.07.012>
- 51
52 843 Rodríguez-Rodríguez, L., Jiménez-Sánchez, M., Domínguez-Cuesta, M.J., Rinterknecht, V., Pallàs, R.,
53 844 Bourlès, D., 2016. Chronology of glaciations in the Cantabrian Mountains (NW Iberia) during the Last
54 845 Glacial Cycle based on in situ-produced ^{10}Be . *Quat. Sci. Rev.* 138, 31–48.
55 846 <https://doi.org/10.1016/j.quascirev.2016.02.027>
- 56
57 847 Schilling, D.H., Hollin, J.T., 1981. Numerical reconstructions of valley glaciers and small ice caps, in:
58 848 Denton, G.H., Hughes, T.J. (Eds.), *The Last Great Ice Sheets*. Wiley, New York, pp. 207–220.
- 59 849 Serrano, E., Gómez-Lende, M., Pellitero, R., González-Trueba, J.J., 2015. Deglaciación en la Cordillera
60 850 Cantábrica: Modelo y evolución. *Cuad. Investig. Geogr.* 41, 389–408.
851 <https://doi.org/10.18172/cig.2716>

- 1
2 852 Serrano, E., González-Trueba, J.J., Pellitero, R., Gómez-Lende, M., 2016. Quaternary glacial history of the
3 853 Cantabrian Mountains of northern Spain: a new synthesis. *Geol. Soc. London, Spec. Publ.* 433, 55–85.
4 854 <https://doi.org/10.1144/sp433.8>
5
6 855 Small, D., Fabel, D., 2016. Was Scotland deglaciated during the Younger Dryas ? *Quat. Sci. Rev.* 145, 259–
7 856 263. <https://doi.org/10.1016/j.quascirev.2016.05.031>
8 857 Stange, K.M., van Balen, R.T., Kasse, C., Vandenberghe, J., Carcaillet, J., 2014. Linking morphology across
9 858 the glaciofluvial interface: A ^{10}Be supported chronology of glacier advances and terrace formation in
10 859 the Garonne River, northern Pyrenees, France. *Geomorphology* 207, 71–95.
11 860 <https://doi.org/10.1016/j.geomorph.2013.10.028>
12
13 861 Styllas, M.N., Schimmelpfennig, I., Benedetti, L., Ghilardi, M., Aumaître, G., Bourlès, D., Keddadouche, K.,
14 862 2018. Late-glacial and Holocene history of the northeast Mediterranean mountains - New insights from
15 863 in situ-produced ^{36}Cl -based cosmic ray exposure dating of paleo-glacier deposits on Mount Olympus,
16 864 Greece. *Quat. Sci. Rev.* 193, 244–265. <https://doi.org/10.1016/j.quascirev.2018.06.020>
17
18 865 Tomkins, M.D., Dortch, J.M., Hughes, P., Huck, J.J., Stimson, A.G., Delmas, M., Calvet, M., Pallàs, R.,
19 866 2018. Rapid age assessment of glacial landforms in the Pyrenees using Schmidt hammer exposure
20 867 dating (SHED). *Quat. Res.* 90, 26–37. <https://doi.org/10.1017/qua.2018.12>
21 868 Uppala, S.M., Kållberg, P.W., Simmons, A.J., Andrae, U., da Costa Bechtold, V., Fiorino, M., Gibson, J.K.,
22 869 Haseler, J., Hernandez, A., Kelly, M.A., Li, X., Onogi, K., Saarinen, S., Sokka, N., Allan, R.P.,
23 870 Andersson, E., Arpe, K., Balmaseda, M.A., Beljaars, A.C.M., van de Berg, L., Bidlot, J., Bormann, N.,
24 871 Caires, S., Chevallier, F., Dethof, A., Dragosavac, M., Fisher, M., Fuentes, M., Hagemann, S., Hólm,
25 872 E., Hoskins, B.J., Isaksen, L., Janssen, P.A.E.M., Jenne, R., McNally, A.P., Mahfouf, J.F., Morcrette,
26 873 J.J., Rayner, N.A., Saunders, R.W., Simon, P., Sterl, A., Trenberth, K.E., Untch, A., Vasiljevic, D.,
27 874 Viterbo, P., Woollen, J., 2005. The ERA-40 re-analysis. *Q. J. R. Meteorol. Soc.* 131, 2961–3012.
28 875 <https://doi.org/10.1256/qj.04.176>
29
30 876 Ward, G.K., Wilson, S.R., 1978. Procedures for Comparing and Combining Radiocarbon Age
31 877 Determinations: a Critique. *Archaeometry* 20, 19–31. <https://doi.org/10.1111/j.1475->
32 878 [4754.1978.tb00208.x](https://doi.org/10.1111/j.1475-4754.1978.tb00208.x)
33
34 879 Zasadni, J., Piotr, K., Bro, E., Ivy-ochs, S., Andrzej, Ś., Christl, M., Balá, L., 2020. Latest Pleistocene glacier
35 880 advances and post-Younger Dryas rock glacier stabilization in the Mt. Kriváň group, High Tatra
36 881 Mountains, Slovakia. *Geomorphology* 358. <https://doi.org/10.1016/j.geomorph.2020.107093>
37
38 882
39 883
40
41
42
43
44
45
46
47
48
49
50
51
52
53
54
55
56
57
58
59
60

List of figures

Figure 1. Geographical setting of the Ruda Valley. (A) Location in Europe. (B) Location in the Pyrenees with the distribution of the studies mentioned in the discussion (green stars). (C) Limits and topography of the valley with the distribution and view direction of the photos in Figure 2.

Figure 2. Examples of the main geomorphological landforms of glacial origin in the Ruda Valley, together with the location and typology of the dated samples: (A) terminal moraine damming a paleolake at 2080 m; (B) N-S perspective of the Saboredo Cirque floor showing several lakes distributed in staggered overdeepened basins; (C) polished bedrock surface including striations that reveal the former glacial flow; and (D) *roches moutonnées* located in the forested valley bottom of the valley at 1860 m.

Figure 3. (A) Geomorphological map of the study area, with the location of the CRE samples; and (B) enlargement of the highest parts of the cirque including the location of the ^{10}Be ages.

Figure 4. Examples of sampled moraines and polished bedrock surfaces, together with CRE ages (ka).

Figure 5. Reconstruction of the glacial extent during the different time stages: (A) Extensive glaciers occupying the entire Upper Garonne Basin during the ILGM based on the reconstruction of [Fernandes et al. \(2017\)](#); (B) Glacial extent during the mid B-A at ~13.5 ka in the Ruda Valley; (C) Glacier flowing from the Saboredo Cirque during the transition between the late B-A and the early YD at ~13 ka; and (D) Small glaciers confined within the highest hollows next to the Sendrosa (D) and Saboredo (E) peaks during the early YD at ~12.7/12.6 ka.

Figure 6. Schematic evolution of the glacial phases recorded in the Ruda Valley during the last glacial cycle: (A) extensive and thick glaciers inundated the valley and only few nunataks protruded the ice during the ILGM; (B) warm temperatures in the early B-A favoured glacial recession, and subsequently the lowest areas of the valley as well as some rock outcrops of the cirque became exposed; (C) glacial advances/stillstands formed moraines during the B-A and at the transition to the YD; (D) small glaciers persisted during the early YD in the highest north-facing cirques; and (E) subsequent temperature increases favoured complete deglaciation and triggered paraglacial dynamics, which promoted the formation of rock glaciers in the recently deglaciated ice-free cirques.

Figure 7. Normalized probability distribution functions (PDF) of surface exposure ages vs. temperature evolution from the OD to the early Holocene based on the $\delta^{18}\text{O}$ record from the NGRIP ice core from Greenland and the $\delta^{18}\text{O}$ record from the speleothem of the Ostolo cave in north Iberia (time periods are defined after [Rasmussen et al. \(2014\)](#)). The plots of the units result from the sum of the individual PDF of the samples belonging to them; cold (warm) phases are represented by the blue (red) bands.

1 **List of tables**

2 **Table 1. Geographic location of samples, topographic shielding factor and sample thickness.**

3

4

5

6

Sample name	Landform	Latitude (DD)	Longitude (DD)	Elevation (m a.s.l.) ^a	Topographic shielding factor	Thickness (cm)	Lithology	Size of the boulders largest axis (m)
<i>Valley polished surfaces</i>								
ARAN-40	Polished surface	42.6416	0.9713	1862	0.9630	3.7	Granodiorite	
ARAN-39	Polished surface	42.6393	0.9701	1900	0.9640	5.0	Granodiorite	
<i>Valley external moraines</i>								
ARAN-38	Moraine boulder	42.6296	0.9624	2079	0.9759	4.2	Granite	3.5
ARAN-37	Moraine boulder	42.6299	0.9620	2075	0.9752	3.0	Granite	3
<i>Valley internal moraines</i>								
ARAN-28	Polished surface	42.6263	0.9593	2188	1.0000	3.5	Granite	
ARAN-27	Moraine boulder	42.6257	0.9599	2184	0.9852	5.0	Granite	4
<i>Cirque polished surfaces</i>								
ARAN-36	Polished surface	42.6111	0.9681	2360	0.9806	3.5	Granite	
ARAN-35	Polished surface	42.6152	0.9630	2316	0.9875	3.2	Granite	
ARAN-34	Polished surface	42.6224	0.9596	2266	0.9901	5.0	Granite	
ARAN-31	Polished surface	42.6274	0.9536	2378	1.0000	3.0	Granite	
<i>Cirque moraines</i>								
ARAN-33	Moraine boulder	42.6275	0.9487	2470	0.9841	3.0	Granite	5
ARAN-32	Moraine boulder	42.6277	0.9480	2467	0.9789	4.0	Granite	6

7

8

9

10

11

12

13

14

15

16

17

18

19

20

21

22

23

24

25

26

27

28

29

30

31

32 ^a Elevations are derived from the 5 m Digital Elevation Model of the Spanish "Instituto Geográfico Nacional" and are subjected to a vertical accuracy of ± 5 m.

33

34

35

36

37

38

39

40

41

42

43

44

45

46

Table 2. AMS analytical data and calculated exposure ages. $^{10}\text{Be}/^{9}\text{Be}$ ratios were inferred from measurements at the ASTER AMS facility. Chemistry blank correction was done by subtracting the number of ^{10}Be atoms in the blank from that in the sample. Individual ages are shown with their full uncertainties (including analytical AMS uncertainty and production rate uncertainty) and analytical uncertainty only within brackets. Arithmetic mean ages are given with their full uncertainties (including standard deviation and production rate uncertainty) and standard deviations only in brackets.

^{10}Be samples analytical AMS data								
Sample name	Quartz weight (g)	Mass of carrier (^9Be mg)	ASTER AMS cathode number	$^{10}\text{Be}/^9\text{Be}$ (10^{-14})	Blank correction (%)	$[^{10}\text{Be}]$ (10^4 atoms g^{-1})	Age (ka)	Mean age (ka)
<i>Valley polished surfaces</i>								
ARAN-40	20.44	0.46	CHBL	16.34 ± 0.56	2.11	23.85 ± 0.83	15.0 ± 0.9 (0.5)	14.4 ± 1.2 (0.8)
ARAN-39	21.32	0.45	CHBK	15.92 ± 0.49	2.18	22.15 ± 0.70	13.8 ± 0.8 (0.4)	
<i>Valley external moraines</i>								
ARAN-38	21.11	0.46	CHBJ	17.56 ± 0.54	1.95	24.99 ± 0.79	13.3 ± 0.8 (0.4)	13.5 ± 0.9 (0.2)
ARAN-37	21.38	0.46	CHBI	18.08 ± 0.87	1.09	25.74 ± 1.25	13.7 ± 1.0 (0.6)	
<i>Valley internal moraines</i>								
ARAN-28	20.97	0.46	CHBB	18.79 ± 0.62	1.05	27.13 ± 0.91	13.0 ± 0.8 (0.4)	13.0 ± 0.8 (0.1)
ARAN-27	20.89	0.45	CHBA	18.64 ± 0.58	1.85	26.61 ± 0.84	13.1 ± 0.8 (0.4)	
<i>Cirque polished surfaces</i>								
ARAN-36	21.51	0.46	CHBH	21.24 ± 0.65	1.62	29.53 ± 0.92	12.7 ± 0.8 (0.4)	12.7 ± 0.8 (0.0)
ARAN-35	21.43	0.47	CHBG	20.18 ± 0.62	1.65	29.05 ± 0.91	12.8 ± 0.8 (0.4)	
ARAN-34	20.85	0.46	CHBF	21.13 ± 0.66	1.63	30.35 ± 0.96	14.0 ± 0.8 (0.4)	
ARAN-31	21.40	0.44	CHBC	26.54 ± 0.72	1.35	35.74 ± 0.98	14.8 ± 0.9 (0.4)	
<i>Cirque moraines</i>								
ARAN-33	20.26	0.45	CHBE	20.30 ± 0.68	1.70	29.92 ± 1.02	11.8 ± 0.7 (0.4)	12.6 ± 1.3 (1.0)
ARAN-32	21.63	0.45	CHBD	24.19 ± 1.26	0.85	33.15 ± 1.75	13.3 ± 1.0 (0.7)	
Chemistry blank details								
Blank name	Processed with	mass of carrier (^9Be mg)	ASTER AMS cathode number	$^{10}\text{Be}/^9\text{Be}$ (10^{-14})	$[^{10}\text{Be}]$ (10^4 atoms)			
BK-1	ARAN-27, 31, 33, 34, 35, 36, 38, 39, 40	0.46	CHAT	0.34 ± 0.04	10.30 ± 1.24	-	-	
BK-2	ARAN-32	0.46	CHBM	0.20 ± 0.03	6.13 ± 0.80	-	-	
BK-3	ARAN-28, 37	0.46	IGHI	0.20 ± 0.03	5.98 ± 0.93	-	-	

Table 3. Exposure ages according to erosion and snow cover corrections.

Sample name	Exposure ages (arithmetic mean, in ka)			
	No correction	Erosion correction	Snow correction	Erosion + snow correction
<i>Valley - polished surfaces</i>	14.4 ± 1.2	14.6 ± 1.2	15.5 ± 1.3	15.7 ± 1.3
ARAN-40	$15.0 \pm 0.9 (0.5)$	$15.2 \pm 0.9 (0.5)$	$16.1 \pm 1.0 (0.5)$	$16.4 \pm 1.0 (0.6)$
ARAN-39	$13.8 \pm 0.8 (0.4)$	$14.0 \pm 0.8 (0.4)$	$14.8 \pm 0.9 (0.4)$	$15.0 \pm 0.9 (0.5)$
<i>Valley - external moraines</i>	13.5 ± 0.9	13.7 ± 0.9	14.5 ± 1.0	14.7 ± 1.0
ARAN-38	$13.3 \pm 0.8 (0.4)$	$13.5 \pm 0.8 (0.4)$	$14.4 \pm 0.9 (0.4)$	$14.6 \pm 0.9 (0.4)$
ARAN-37	$13.7 \pm 1.0 (0.6)$	$13.8 \pm 1.0 (0.7)$	$14.7 \pm 1.0 (0.7)$	$14.9 \pm 1.0 (0.7)$
<i>Valley - internal moraines</i>	13.0 ± 0.8	13.2 ± 0.8	14.1 ± 0.9	14.2 ± 0.9
ARAN-28	$13.0 \pm 0.8 (0.4)$	$13.1 \pm 0.8 (0.4)$	$14.0 \pm 0.9 (0.5)$	$14.2 \pm 0.9 (0.5)$
ARAN-27	$13.1 \pm 0.8 (0.4)$	$13.3 \pm 0.8 (0.4)$	$14.1 \pm 0.8 (0.4)$	$14.3 \pm 0.9 (0.4)$
<i>Cirque - polished surfaces</i>	12.7 ± 0.7	12.9 ± 0.8	13.7 ± 0.8	13.9 ± 0.8
ARAN-36	$12.7 \pm 0.8 (0.4)$	$12.9 \pm 0.8 (0.4)$	$13.7 \pm 0.8 (0.4)$	$13.9 \pm 0.8 (0.4)$
ARAN-35	$12.8 \pm 0.8 (0.4)$	$12.9 \pm 0.8 (0.4)$	$13.8 \pm 0.8 (0.4)$	$14.0 \pm 0.8 (0.4)$
ARAN-34	$14.0 \pm 0.8 (0.4)$	$14.2 \pm 0.9 (0.4)$	$15.1 \pm 0.9 (0.5)$	$15.3 \pm 0.9 (0.5)$
ARAN-31	$14.8 \pm 0.9 (0.4)$	$15.1 \pm 0.9 (0.4)$	$16.0 \pm 0.9 (0.4)$	$16.2 \pm 0.9 (0.4)$
<i>Cirque - moraines</i>	12.6 ± 1.3	12.7 ± 1.4	13.5 ± 1.4	13.7 ± 1.5
ARAN-33	$11.8 \pm 0.7 (0.4)$	$12.0 \pm 0.8 (0.4)$	$12.7 \pm 0.8 (0.4)$	$12.9 \pm 0.8 (0.4)$
ARAN-32	$13.3 \pm 1.0 (0.7)$	$13.5 \pm 1.0 (0.7)$	$14.3 \pm 1.0 (0.7)$	$14.5 \pm 1.0 (0.7)$

Table 4. Reconstructed ELAs (m a.s.l.) for the middle, late B-A and YD moraines using the AAR and AABR methods.

Phase	Glacier	AAR (0.6±0.2)	AABR (1.9±0.81)	AABR (1.75±0.71)	Average ELA
Valley external moraines (middle B-A; GI-1c)	Ruda	2481 ± 20	2449 -30/+20	2454 -30/+15	2461
Valley internal moraines (transition B-A/YD; GI-1b)	Ruda	2515 -15/+10	2498 -25/+15	2503 -25/+20	2505
Cirque moraines (early YD)	Sendrosa	2568 -10/+5	2571 -15/+5	2576 ± 10	2571

Table 5. Glacial response in the Ruda Valley during the B-A Interstidal according to the reconstructed climate in Greenland and in Iberian Peninsula.

Phase (ages in ka)	Climate trend in Greenland based on ice core records (Rasmussen et al., 2014)	Glacier response in the Ruda Valley	Climate in the Iberian Peninsula based on other independent proxies
GI-1e (14.7-14.1)	Abrupt warming (3-5°C)	Rapid recession at ~15-14 ka	Gradual warming in the northern Iberia at 15.4-13.4 cal ka BP (Moreno et al., 2010). Warming conditions in the Pyrenees at 14.7-14.0 cal ka BP (González-Sampérez et al., 2006).
GI-1d (14.1-14.0)	Short cold reversal (1-2°C)		
GI-1c (14.0-13.3)	Significant warming at the beginning (2-4°C) followed by a gradual cooling at (~2°C). Intense cold conditions at 13.7-13.6 ka	Glacier advance or stillstand with moraine formation at 13.5 ka	Colder conditions starting at 13.5 cal ka BP in northern Iberia (Moreno et al., 2010). Cold climate in the Pyrenees at 14-13.4 cal ka BP (González-Sampérez et al., 2006).
GI-1b (13.3-13.1)	Short cold reversal (1-2°C)	-	Short periods of colder and drier conditions (Moreno et al., 2010). Expansion of cold-climate forest species in the Pyrenees at 13.4-13.1 cal ka BP (González-Sampérez et al., 2006).
GI-1a (13.1-12.9)	Early warming followed by a general cooling	Glacier advance or stillstand with moraine formation at 13.0 ka	Cold and dry conditions in the Pyrenees starting at 13.1 cal ka BP (González-Sampérez et al., 2006).

1
2 1 **Glacial oscillations during the Bølling-Allerød Interstadial-Younger Dryas**
3 2 **transition in the Ruda Valley, Central Pyrenees**
4 3
5 4
6 5

7 5 M. Fernandes¹, M. Oliva², G. Vieira¹, D. Palacios³, J.M. Fernández-Fernández¹, J. Garcia-Oteyza², I.
8 6 Schimmelpennig⁴, ASTER Team^{4,5} & D. Antoniades⁶
9 7
10 8

11 9 ¹Centre for Geographical Studies, IGOT, Universidade de Lisboa, Lisbon, Portugal

12 10 ²Department of Geography, Universitat de Barcelona, Catalonia, Spain

13 11 ³Department of Geography, Universidad Complutense de Madrid, Madrid, Spain

14 12 ⁴Aix-Marseille Université, CNRS, IRD, INRAE, Coll. France, UM 34 CEREGE, Aix-en-Provence, France

15 13 ⁵Consortium: Georges Aumaître, Karim Keddadouche

16 14 ⁶Department of Geography & Centre for Northern Studies, Université Laval, Quebec, Canada
17 15
18 16

19 17 **Corresponding author**

20 18 Marcelo Fernandes, marcelo.fernandes@live.com

21 19 Centre for Geographical Studies – IGOT, Universidade de Lisboa

22 20 Rua Branca Edmée Marques, 1600-276 Lisbon, Portugal

23 21 Tel: +351962277913
24 22
25 23
26 24
27 25
28 26
29 27
30 28
31 29
32 30
33 31
34 32
35 33
36 34
37 35
38 36
39 37
40 38
41 39
42 40
43 41
44
45
46
47
48
49
50
51
52
53
54
55
56
57
58
59
60

Abstract

The Upper Garonne Basin included the largest glacial system in the Pyrenees during the last glacial cycle. Within the long-term glacial retreat during Termination-1 (T-1), glacier fluctuations left geomorphic evidence in the area. However, the chronology of T-1 glacial oscillations on the northern slope of the Central Pyrenees is still poorly constrained. Here, we introduce new geomorphological observations and a 12-sample dataset of ^{10}Be Cosmic-Ray Exposure (CRE) ages from the Ruda Valley. This U-shaped valley, surrounded by peaks exceeding 2800 m a.s.l., includes a sequence of moraines and polished surfaces that enabled to reconstruct the chronology of the last deglaciation. Following the maximum ice extent, warmer conditions prevailing at ~15-14 ka, during the Bølling-Allerød (B-A) Interstadial, favoured glacial retreat in the Ruda Valley. Within the B-A, glaciers experienced two phases of advance/stillstand with moraine formation at 13.5 and 13.0 ka. During the early YD, glacial retreat exposed the highest surfaces of the Saboredo Cirque (~2300-2350 m) at 12.7 ka. Small glaciers persisted only inside the highest cirques (~2470 m), such as in Sendrosa Cirque, with moraines stabilizing at 12.6 ka. The results of this work present the most complete chronology for Pyrenean glacial oscillations from the B-A to the YD.

Key words: Central Pyrenees, Bølling-Allerød, Younger Dryas, Cosmic-Ray Exposure dating, deglaciation

1. Introduction

The present-day landscape of the highest mid-latitude mountain environments is dominated by the effects of glacial dynamics that prevailed during the last glacial cycle and of post-glacial processes that reshaped glacial landforms during the subsequent deglaciation. Following the end of the Last Glacial Maximum (LGM) at 19-20 ka (Clark et al., 2009), most glaciated mountain regions underwent a rapid deglaciation only interrupted by brief periods of glacial growth. Glacial disappearance favoured paraglacial readjustment and intense periglacial and slope processes, which reshaped the already deglaciated valleys and cirques (Ballantyne, 2008). The current spatial distribution of glacial and periglacial features in the high elevations of most mid-latitude ice-free mountain ranges – such as the Pyrenees, where this research focuses on – results from the climatic shifts during Termination-1 (hereafter T-1), the period spanning from 20-19 to 11.7 ka (Denton et al., 2014).

At present, mid-latitude mountains such as those of the Mediterranean region are only sparsely glaciated, with small glaciers located in sheltered cirques (Hughes, 2014). However, there are several other mountain ranges located between 30 and 50° latitude North, such as the Alps or the Himalaya, which are still heavily glaciated and record recent dramatic glacial recession trends (Huss et al., 2021). An accurate comprehension of the climatic sensitivity of current glaciated mountain landscapes can help to understand the timing and magnitude of glacial change during the rapid climate shifts of T-1. The alternation of millennial-scale cold/warm periods during T-1 promoted a temporal pattern of glacial advances and retreats across the Northern Hemisphere (Allard et al., 2021; Rea et al., 2020). Ice core records from the Greenland interior show the following succession of climatic phases in the North Atlantic region during T-1: a cold climate regime during the Oldest Dryas (OD; GS-2.1a: 17.5-14.6 ka), followed by the general warm Bølling-Allerød (B-A) Interstadial (GI-1: 14.6-12.9 ka), with a subsequent intensification of cold conditions during the Younger Dryas (YD; GS-1: 12.9-11.7 ka) (Rasmussen et al., 2014).

In the Iberian mountains, recent advances in constraining the chronology of glacial activity during T-1 using Cosmic-Ray Exposure (CRE) dating have revealed contrasting spatio-temporal patterns (García-Ruiz et al., 2016b; Oliva et al., 2019; Palacios et al., 2017a). Whereas the maximum ice extent occurred asynchronously, glacial oscillations during T-1 show a more synchronous response: colder phases favoured glacial growth, whereas warm periods promoted glacial recession (Oliva et al., 2019) and the evolution from debris-free glaciers to rock glaciers such as those in the Iberian Range (García-Ruiz et al., 2020), Cantabrian Mountains (Rodríguez-Rodríguez et al., 2016) and Central (Palacios et al., 2017a, b) and Eastern Pyrenees (Andrés et al., 2018). To date, there is geomorphic evidence of glacial advances during the OD and YD, as well as of glacial retreat during the B-A and following the YD in the Cantabrian Mountains (Rodríguez-Rodríguez et al., 2017), Central Range (Carrasco et al., 2015; Palacios et al., 2012b), and Sierra Nevada (Gómez-Ortiz et al., 2012; Palacios et al., 2016). However, CRE ages require a careful interpretation and support of geomorphological criteria, as their uncertainty ranges may be greater than the time spanning the T-1 phases (Oliva et al., 2021a).

1
2 93 The Pyrenees were the most extensively glaciated mountain system during the maximum ice extent of the last
3 94 glaciation in Iberia, hosting ~50% of the peninsula's glacial surface (Oliva et al., 2021b). The chronology of
4 95 glacier fluctuations during T-1 seems to have followed a similar temporal pattern, although available data is
5 96 principally derived from the range's southern slope (Andrés et al., 2018; Palacios et al., 2015b, 2017b, 2017a).
6 97 Pyrenean glaciers readvanced to the valley bottoms during the OD, with ice tongues > 15 km long. During the
7 98 B-A, by 15-14 ka, high temperatures favoured rapid deglaciation and glaciers disappeared from relatively low
8 99 cirques shaped under peaks of ~2600 m a.s.l. (Oliva et al., 2021a). A subsequent readvance occurred during
9 100 the YD, with smaller glaciers of only ~4 km length confined within the cirques of the highest massifs above
10 101 2200 m (Crest et al., 2017; García-Ruiz et al., 2016a; Jomelli et al., 2020; Palacios et al., 2017b, 2015a; Pallàs
11 102 et al., 2006). Following both cold periods, glacial retreat triggered intense paraglacial dynamics at ~15-14 ka
12 103 and ~11-10.5 ka, respectively, which led to the formation of rock glaciers and debris-covered glaciers,
13 104 particularly in cirques below 2800 m (Andrés et al., 2018; Palacios et al., 2017b).

15 105 The timing of glacial oscillations is still poorly constrained on the northern slope of the Pyrenees, such as in
16 106 the Upper Garonne Basin where this work focuses on. Recently, Reixach et al. (2021) have summarized the
17 107 glacial evolution from 19 to 12 ka in the northern Pyrenees, reporting a spatial and temporal pattern for T-1
18 108 glacial oscillations similar to that on the southern slopes of the range. Jomelli et al. (2020) confirmed glacial
19 109 growth during the YD in the Ariège Valley, where glaciers persisted in the highest cirques until the early
20 110 Holocene. Another recent study that focused on the Bacivèr Cirque, near our study area, revealed a rapid
21 111 deglaciation during the B-A, followed by glacial readvance and the formation of the highest moraines at the
22 112 B-A/YD transition at ~12.9 ka; subsequently, intense paraglacial readjustment favoured the formation of
23 113 debris-covered glaciers and rock glaciers inside these moraine systems (Oliva et al., 2021a).

25 114 In order to complement our understanding of the glacial history of the Pyrenees, this study uses new data to
26 115 improve the deglaciation chronology of the Upper Garonne Basin, the largest glacial system in this mountain
27 116 range, during the local last glacial maximum (ILGM; Fernandes et al., 2017). Glacial retreat in the Ruda Valley,
28 117 where this work focuses on, left widespread geomorphic evidence of glacial and paraglacial origin that can be
29 118 used to reconstruct the last stages of long-term deglaciation in the Central Pyrenees.

31 119 Our study, therefore, has the following objectives:

- 32 120 - To date the glacial landforms of the Upper Garonne Basin.
- 33 121 - To discuss the T-1 deglaciation in the Upper Garonne Basin and its geomorphological implications in
34 122 the context of the known chronologies from the Pyrenees southern slope and from other Iberian and
35 123 European mountain ranges.
- 36 124 - To examine the paleoclimatic and paleoenvironmental significance of the glacial response of the
37 125 northern slope of the Pyrenees and compare it with the paleoclimatic evolution inferred from other
38 126 records in the North Atlantic region.

42 128 2. Study area

43 129 The Pyrenees stretch E-W over 400 km across north Iberia, with the highest peaks (> 3000 m) in the central
44 130 part of the range. This study focuses on the Ruda Valley, located between latitudes 42°40' N - 42°42' N and
45 131 longitudes 0°57' E - 1°00' E (Fig. 1), that constitutes the headwaters of the Upper Garonne Basin. The area is
46 132 included in the peripheral protection area of the National Park of Aigüestortes and Sant Maurici Lake.

49 133 Figure 1

50
51 134 The Upper Garonne Valley shows the typical U-shaped cross-section of glacial valleys, and the Garonne River
52 135 flows to the N-NW through the central axis of the Pyrenees. Several tributary rivers drain the glacial valleys
53 136 descending from glacial cirques carved below peaks from 2800 to 3000 m. Glacial cirques are prevalingly
54 137 NE-oriented, with floors generally between 2200 and 2400 m (Lopes et al., 2018).

56 138 The U-shaped Ruda Valley, drained by the Ruda River that runs 12 km northwards, constitutes the headwaters
57 139 of the Upper Garonne Basin. Its catchment encompasses 34 km², with an elevation range of ~1300 m between
58 140 Saboredo Peak (2827 m) and the village of Baqueira (~1500 m). The Saboredo Cirque is located in the
59 141 headwaters of the Ruda Valley; the cirque is N-exposed, extending over 5.7 km², with its floor at ~2250-2400

1
2 142 m. Saboredo (2827 m), Sendrosa (2702 m) and Locampo (2658 m) peaks are the highest elevations of the
3 143 cirque, while its toe is located at ~2250 m.

4
5 144 The present-day mean annual air temperature (MAAT) at Port de la Bonaigua station (2266 m) is 3 °C, with
6 145 the regional 0 °C isotherm in the Central Pyrenees estimated to be at 2950 m (López-Moreno et al., 2019).
7 146 Annual precipitation reaches 1227 mm and falls mostly as snow (average depth of 1 m) from October to May,
8 147 with a snow duration of 7-8 months in the cirque floor. The combination of low temperatures and abundant
9 148 snowfall determines the scarce vegetation cover above the treeline (2200-2300 m), where barren rocky terrain
10 149 is widespread, together with small alpine meadows.

11 149
12
13 150 The landscape of the Ruda Valley resulted from the interaction of tectonics and vertical incision, both during
14 151 Quaternary glaciations and interglacial periods, the latter dominated by alluvial and mass-wasting processes
15 152 (Fernandes et al., 2017). Glacial and periglacial landforms are preserved on different lithologies across the
16 153 valley, composed of Carboniferous granodiorites and granites in the highest sections, with Cambrian-Devonian
17 154 metamorphic (hornfels, marbles, slates, quartzites, schists) and sedimentary rocks (limestones, sandstones,
18 155 conglomerates and lutites) in the lowest parts of the valley (ICGC, 2017; Quesada and Oliveira, 2019).
19 156 However, despite abundant geomorphic evidence revealing that the Garonne Valley presented the longest
20 157 glacier in the Pyrenees during the ILGM (ca. 80 km; Fernandes et al., 2017), the chronological framework of
21 158 glacial activity in the entire Upper Garonne Basin is still unknown. The headwaters of the Ruda Valley include
22 159 a rich sequence of moraine systems and polished bedrock surfaces – as well as relict rock glaciers and protalus
23 160 lobes (Fernandes et al., 2018) – that can be used to improve the temporal resolution for the chronosequence of
24 161 the final deglaciation of the upper Garonne Valley.
25 161
26 161
27
28 162

29 163 3. Methodology

30
31 164 We reconstructed the last deglaciation chronology of the Ruda Valley in the Upper Garonne Basin by
32 165 integrating geomorphological and chronological techniques. Field work was conducted during the summer of
33 166 2019, when snow cover was limited to the concave and sheltered areas at the highest elevations (>2500 m),
34 167 which enabled better identification of the glacial landforms, as well as sampling for CRE dating.

35 167 3.1 Geomorphological mapping

36 168
37 168
38 169 We produced a geomorphological map focusing on glacial and periglacial landforms based on recent general
39 170 geomorphological maps from the area (Fernandes et al., 2017; Fernandes et al., 2021). Here we used the same
40 171 approach based on the combination of aerial orthophotographs (0.25 m cell size) and high-resolution LIDAR
41 172 digital elevation models (point density of 0.5-2 m⁻²) from the “Institut Cartogràfic i Geològic de Catalunya”
42 173 (<http://www.icc.cat/appdownloads>). The symbology of geomorphological landforms followed Joly (1997).
43 174
44

45 174 3.2 Field strategy and sampling

46 175 We collected 12 granite and granodiorite samples for CRE dating, using a hammer and chisel, from elevations
47 176 spanning from 1862 to 2470 m (Table 1). To ensure that samples were intact since glacial retreat, we targeted
48 177 at well-anchored moraine boulders and glacially polished bedrock that stood out within their surroundings,
49 178 which minimizes the risk of having been buried under sediments (Fig. 2). To ensure the best cosmic-ray flux
50 179 reception of the sampling sites, we restricted sample extraction to flat-topped and gentle surfaces, and sampled
51 179 a thickness of up to 3-5 cm. Corrections for partial shielding due to the surrounding topography were
52 180 implemented using the ArcGIS toolbox by Li (2018), which applies equations describing the effects of
53 181 geometric shielding on the sampling sites and a model to predict the nuclide production rate at depth in sloped
54 182 surfaces (Dunne et al. 1999); it required only a point shapefile of the sampling sites including strike/dip of the
55 183 sampling surfaces and a digital elevation model of 5 m spatial resolution.
56 183
57 184
58

59 185 Table 1

60 186 Figure 2

3.3 Laboratory procedures and exposure age calculation

Samples were crushed and sieved (>200 g) at the Physical Geography Laboratory of the Universidad Complutense de Madrid (Spain) to the 125-500 μm fraction, which was subsequently processed at the ‘Laboratoire National des Nucléides Cosmogéniques’ (LN₂C) of the ‘Centre Européen de Recherche et d’Enseignement des Géosciences de l’Environnement’ (CEREGE; Aix-en-Provence, France). In accordance with the quartz-rich lithology of the samples, they were treated for the extraction of the *in-situ*-produced cosmogenic nuclide ¹⁰Be.

First, magnetic minerals were discarded through magnetic separation conducted in a “Frantz LB-1” magnetic separator. Once the non-magnetic fraction was isolated, it underwent several rounds of chemical attacks with a 1:2 mixture of concentrated hydrochloric (HCl) and hexafluorosilicic (H₂SiF₆, 2/3) acids to dissolve and discard the non-quartz minerals. The remaining minerals (i.e. non-dissolved feldspar minerals) were subsequently attacked with 4-6 successive partial dissolutions with HF to remove the atmospheric ¹⁰Be and discard the remaining impurities. In order to be sure that the quartz was pure, samples were examined under a binocular microscope. As a result, ~20 g of pure quartz per sample was used to extract the ¹⁰Be (Table 2). After adding ~150 μL of an in-house manufactured (from a phenakite crystal) ⁹Be carrier solution (spike, concentration: $3025 \pm 9 \mu\text{g g}^{-1}$; Merchel et al., 2008), the purified quartz was dissolved with 48% concentrated HF (3.5 mL per g of quartz + 30 mL in excess). Following total dissolution, the resulting solution was evaporated until dryness, and the residue was recovered with HCl (7.1 molar). Be was then precipitated at pH=8 to beryllium hydroxide (Be(OH)₂) by means of ammonia (NH₃), and separated from other elements in resin columns: a Dowex 1x8 anionic exchange column to remove elements such as Fe, Mn and Ti, and a Dowex 50W x8 cationic exchange column to discard B and separate Be from Al (Merchel and Herpers, 1999). The final eluted Be was again precipitated, dried and oxidized to BeO at 700 °C. Finally, the targets for the accelerator mass spectrometer (AMS) measurements were prepared by mixing with niobium powder at an approximate 1:1 proportion and pressing the mixture into copper cathodes.

The targets were analysed at the ‘Accelerator pour les Sciences de la Terre, Environnement et Risques’ (ASTER) national AMS facility at CEREGE in order to measure the ¹⁰Be/⁹Be ratio from which the ¹⁰Be concentration was later inferred (Table 2). AMS measurements were calibrated against the in-house standard STD-11 with an assigned ¹⁰Be/⁹Be ratio of $(1.191 \pm 0.013) \times 10^{-11}$ (Braucher et al., 2015). Based on calibration with the previous ASTER AMS standard NIST-27900 (SRM4325), the new STD-11 is fully compatible with 07KNSTD. The analytical 1 σ uncertainties include uncertainties in the AMS counting statistics, an external 0.5% AMS error (Arnold et al., 2010) and the uncertainty related to the chemical blank correction. The ¹⁰Be half-life considered was $(1.3870 \pm 0.0012) \times 10^6$ years (Chmeleff et al., 2010; Korschinek et al., 2010).

Table 2

We calculated ¹⁰Be exposure ages by using the CREP online calculator (Martin et al., 2017; available online at: <http://crep.cirp.cnr.fr/#/>), where we selected the following settings: LSD (Lifton-Sato-Dunai) elevation/latitude scaling scheme (Lifton et al., 2014), ERA40 atmospheric model (Uppala et al., 2005) and geomagnetic database based on the LSD framework (Lifton et al., 2014). These settings yielded a world-wide mean sea level high latitude (SLHL) ¹⁰Be production rate of $3.98 \pm 0.22 \text{ atoms g}^{-1} \text{ yr}^{-1}$. Exposure ages of the samples with their 1 σ full and analytical uncertainties are shown in Table 2. The uncertainties discussed throughout the text include analytical and production rate error unless otherwise stated.

In order to evaluate the potential impact of erosion on the exposure ages, we assumed a steady erosion rate (1 mm ka⁻¹) following a conservative maximum value in such a lithological setting according to André (2002). The impact of snow cover was explored assuming that snow currently remains in the area an annual average of 7.5 months at 2200-2300 m with a mean thickness of 100 cm – and assuming a snow density of 0.2 g cm⁻³ (Styllas et al., 2018) – (Table 3), based on the available data from the Bonaigua weather station (Fig. 1) available since 1997-1998 (Servei Meteorològic de Catalunya; http://www.igc.cat/web/ca/allaus_gruix_neu_v2.php?e=bonaigua&t=totes). Erosion and snow corrections, as

a whole, resulted in ages that were ~9% older (~1% erosion; ~8% snow cover). However, to enable comparisons with other areas, we use the non-corrected ages throughout the text. Moreover, both the thickness and duration of snow cover must have varied significantly since the cirque's deglaciation, given the alternation of cold/warm periods and their associated moisture supplies. Finally, the chi-squared test according to Ward and Wilson (1978) was applied to the samples belonging to each geomorphological unit established in the geomorphological map (Table 1) in order to detect potential exposure age outliers (i.e. "too old" or "too young"; Heyman et al., 2011). No outliers were detected (Table 3).

Table 3

3.4 Glacier reconstruction and Equilibrium-Line Altitude (ELA) calculation

A three-dimensional paleoglacier reconstruction was performed for the different glacial phases using the 'GLaRe' ArcGIS toolbox devised by Pellitero et al. (2016). Former ice thickness was estimated by applying a perfect-plasticity physical-based rheological model along flowlines from the termini to the headwall (Van der Veen, 1999; Benn and Hulton, 2010). Such a toolbox requires only a flowline, a tentative paleoglacier geometry - approximated from lateral or frontal moraines - and a digital elevation model. Ice thickness was modelled by using a constant shear stress of 100 kPa (Paterson, 1994; Benn and Hulton, 2010). The effect of lateral side drag was corrected by integrating shape factors (F-factor) obtained from cross-sections (Schilling and Hollin, 1981).

ELAs were calculated by using the automatic toolbox 'ELA calculation' developed by Pellitero et al. (2015). The selected methods were the Accumulation Area Ratio (Porter, 1975; AARs: 0.6 ± 0.05) and the Area Altitude Balance Ratio (AABR; Osmaston, 2005). We considered two balance ratios for the AABR method: 1.75 ± 0.71 (global) and 1.9 ± 0.81 (mid-latitude marine glaciers) (Rea, 2009). The average ELAs were used to discuss the paleoclimatic implications of the identified glacier advance/stillstand phases.

4. Results

The Ruda Valley preserves glacial and periglacial landforms indicative of glacial evolution during the last deglaciation in the Upper Garonne Basin. The chronological framework of this evolution is unveiled by a dataset of 12 ^{10}Be CRE ages obtained from glacial landforms.

4.1 Geomorphological evidence

The wide range of glacial features from the highest sectors to the Ruda Valley floor shows evidence that the entire valley was heavily glaciated during the ILGM and recorded several advances or stillstands within the long-term deglaciation trend. The Ruda Valley is divided into two main geomorphological units (Fig. 3):

- (i) The valley floor and mountain slopes follow the typical U-shaped morphology of a glacial valley. The steep slopes, descending from ~2200 to 1800 m, connect the lateral cirques with the valley floor. The hillslopes of the valley start at the upper edge of hanging glacial cirques that define the glacial trimline, marking the uppermost extent of recent glaciations. Hillslopes are concave to rectilinear 300-400 m-long sections steeper than 30° that are mostly colonized by forest (i.e. *Pinus nigra*). The upper part of the valley is defined by two staggered, overdeepened basins filled with peatlands at average elevations of 2150 and 2070 m. At their margins, two moraine systems occur at 2190 and 2080 m. Two samples were collected from boulders from the external frontal moraine (ARAN-38 and ARAN-37) and the other two were obtained from the internal moraine unit: one from a boulder on the moraine ridge (ARAN-27), and the other from a polished surface with glacial striae (ARAN-28) and moraine boulders (Fig. 4). The lowest part of the valley floor, with a relatively flat slope characteristic of U-shaped glacial valleys and descending from ~1800 to 1500 m, is colonized by alpine meadows and coniferous forests. Isolated *roches moutonnées* are found in the highest section of the valley bottom where granites prevail ($> \sim 1800$ m), while they are absent in lower areas, where slates and marbles are the dominant lithology. Two samples were collected from polished surfaces at 1900 and 1860 m (ARAN-39 and ARAN-40).

(ii) The highest peaks of the Ruda Valley surrounding the Saboredo Cirque range from 2700-2800 m (Sendrosa and Saboredo peaks) to 2525 m in the mountain divide that may have functioned as a glacial diffluence pass between the Saboredo (Garonne basin) and the Ratera cirques (Noguera Pallaresa basin) (Fig. 3). Saboredo is a complex cirque (Barr and Spagnolo, 2015) that includes several minor hollows carved out on the marginal flanks of the peaks. They are separated by truncated spurs with polished surfaces, where one sample (ARAN-31) was collected to examine the timing of glacial thinning at the cirque level. The highest moraines in the Ruda Valley are located at ~2400-2500 m, at the foot of the highest peaks. A prominent cirque moraine at an altitude of 2470 m is located on the eastern slope of Sendrosa Peak; here, we collected two samples (ARAN-33 and ARAN-32). Above the upper moraines, fed by abundant debris supply from the cirque rock walls, rock glaciers and protalus lobes are found. The cirque floors extend between 2200 and 2400 m and preserve features indicative of intense glacial erosion (e.g. overdeepened basins or glacial thresholds) and glacial deposits (e.g. moraines or erratic boulders). In the Saboredo Cirque, glacial abrasion and periglacial processes shaped a large amphitheatre with several overdeepened basins. They are surrounded by polished surfaces and occupied by peatlands and lakes. Three samples were collected from polished surfaces from 2360 to 2270 m (Fig. 3) (ARAN-36; ARAN-35; ARAN-34; Fig. 2; Table 1). Glacial retreat left scattered boulders and till across the area.

Figure 3

Figure 4

4.2 Geochronological data

The 12 CRE samples collected from the Ruda Valley returned a chronology spanning from $\sim 15 \pm 0.9$ to 11.8 ± 0.7 ka, with all ages being consistent with the geomorphological distribution of the dated surfaces (Fig. 4).

Polished surfaces from the highest parts of the Ruda Valley located ~200-250 m below the cirques provided CRE ages of 15.0 ± 0.9 (ARAN-40) and 13.8 ± 0.8 ka (ARAN-39, Fig. 4A) (average: 14.4 ± 1.2 ka). A similar age was obtained from a sample collected from a truncated spur dividing the Sendrosa and Saboredo cirques, which yielded 14.8 ± 0.9 ka (ARAN-31). A sample collected from a polished surface at the edge of the Saboredo cirque floor (Fig. 3) reported an age of 14.0 ± 0.8 ka (ARAN-34, Fig. 4D).

Moraine boulders from the external moraine located in the lower overdeepened basin yielded ages of 13.3 ± 0.8 (ARAN-38) and 13.7 ± 1.0 ka (ARAN-37) (average: 13.5 ± 0.9 ka). A boulder from the internal moraine ridge located 110 m above the former moraine provided an age of 13.1 ± 0.8 ka (ARAN-27); this age was compared with a sample from a polished surface which correlates with the internal moraine (Fig. 4C) that returned an age of 13.0 ± 0.8 ka (ARAN-28), which agrees with the latter.

Two samples from polished surfaces of the Saboredo Cirque above 2300 m yielded ages of 12.8 ± 0.8 (ARAN-35) and 12.7 ± 0.8 ka (ARAN-36) (12.7 ± 0.8 ka). The highest moraines are located inside the highest cirque hollows, such as the Sendrosa hollow. Here, two moraine boulders yielded ages of 11.8 ± 0.7 (ARAN-33) and 13.3 ± 1.0 ka (ARAN-32) (12.6 ± 1.3 ka).

4.3 Reconstructed paleoglaciers and ELAs

The ELAs of the three reconstructed paleoglacier extents were calculated for the Ruda catchment. The paleoglacier existing at 13.5 ± 0.9 ka deposited a moraine system at 2080 m, with an average ELA located at 2461 m (Table 4). The paleoglacier at 13.0 ± 0.8 ka formed a moraine at 2190 m, with an average ELA at 2505 m. Finally, the Sendrosa Cirque moraine located at 2470 m was dated at 12.6 ± 1.3 ka, with an ELA of 2571 m (Table 4).

Table 4

5. Discussion

5.1 Interpretation of the geomorphological observations and CRE results

The geomorphological analysis supported by ^{10}Be dating of glacial landforms show the spatial and temporal patterns of the deglaciation between the B-A and the early YD in the Ruda Valley (Fig. 5). Although the CRE dataset is consistent with sequence of glacial landforms, uncertainty remains in assigning ages either to the late B-A or to the early YD.

The ages of samples from polished surfaces at the valley at 1860-1900 m (ARAN-40 and ARAN-39; 14.4 ± 1.2 ka) suggest that the beginning of glacial retreat in the Ruda Valley took place during the B-A. As glaciers retreated, they became confined within their respective cirques, as revealed by the age of 14.8 ± 0.9 ka (ARAN-31) of a polished surface on the ridge dividing the Sendrosa and Saboredo cirques (Fig. 3). The sample from an outcrop on the lower edge of the cirque (ARAN-34; 14.0 ± 0.8 ka) indicates that ice covered the entire Saboredo cirque floor until ~ 14 ka.

The sampled boulders of the external moraine system (ARAN-38 and ARAN-37) showed statistical coherence based on the chi-squared test following Ward and Wilson (1978) and suggested a glacier advance or stillstand at 13.5 ± 0.9 ka. The age of 13.0 ± 0.8 ka from a moraine boulder (ARAN-27) and an adjacent polished surface (ARAN-28) of the internal moraine system indicate another short advance or stillstand, which is also consistent with the geochronological sequence. These results from staggered moraine systems at ~ 2080 and ~ 2190 m provided chronologically consistent mean ages within the B-A. But is based on their distinct relative position that they have been ascribed to two different stages. Nevertheless, during this period, glaciers flowed from the Saboredo and Sendrosa cirques and generated moraines on the lower overdeepened basins.

According to the ages of samples from the highest surfaces of the Saboredo Cirque floor at 2320-2360 m (ARAN-35 and ARAN-36; 12.7 ± 0.8 ka), the entire cirque floor was deglaciated at the onset of the YD. These ages are consistent with those of the samples from the highest dated moraine cirques in the Sendrosa Cirque at 2460-2470 m (ARAN-32 and ARAN-33), which was also abandoned by the ice by 12.6 ± 1.3 ka. No statistical inconsistency was detected in the exposure ages from this moraine.

Figure 5

5.2 The chronology of deglaciation

During the ILGM, the Garonne glacier flowed ~ 80 km reaching the Loures-Barousse-Barbazan basin, where it formed a terminal moraine system (Fernandes et al., 2017; Stange et al., 2014). Until the onset of deglaciation, 300-400 m thick ice sat in the Ruda Valley, as shown by the highest lateral moraines between the Ruda and Aiguamòg valleys. This ice thickness must have favoured the occurrence of warm-based glaciers, thus implying basal sliding evidenced by striations on the bedrock surface. Hence, no nuclide inheritance from previous exposure periods is expected at the sampled surfaces.

Samples from polished surfaces from the bottom of the Ruda Valley at 1860-1900 m indicate that by 14.4 ± 1.2 ka, i.e. during the B-A, the glacier was retreating towards the glacial cirque, and was already disconnected from the main Ruda glacier. Consequently, one third of the Ruda Valley was already deglaciated at that time, indicating that by the early B-A the Garonne glacier represented only $\sim 5\%$ of the length that it had during the ILGM (Fernandes et al., 2017).

As glaciers retreated and thinned during the B-A, ice masses became individualized within their respective cirques, and the valley glaciers flowing from Sendrosa and Saboredo cirques merged only in the lowest overdeepened basins (Fig. 3). As conditions were less favourable, glaciers receded to higher elevations and the Sendrosa and Saboredo paleoglaciers became isolated in their respective basins by 14.8 ± 0.9 ka (Fig. 3). The ice covered the entire Saboredo cirque floor until ~ 14 ka, as revealed by the sample collected from an outcrop on the edge of the cirque (14.0 ± 0.8 ka), indicating that glacial recession in the Ruda Valley was underway at ~ 15 -14 ka. Similarly, a rapid deglaciation was also recorded at ~ 15 -14 ka in the nearby Bacivèr Cirque, which favoured its complete deglaciation (Fig. 1; Oliva et al., 2021a).

The strong clustering of ages at between ~ 13.5 and 12.7 ka confirms the dynamic environmental response of the Ruda palaeoglaciers to the abrupt climate transition between the B-A and the early YD. However, our CRE

dataset cannot assess the magnitude and patterns of glacial recession during the early B-A in the Ruda Valley, or whether the entire cirque was deglaciated and glaciers reformed and subsequently advanced. Our results suggest, however, that the millennial-scale trend towards glacier recession during the B-A was interrupted by two glacial advances or stillstands with moraine development at 13.5 ± 0.9 and 13.0 ± 0.8 ka (Fig. 5). Samples from moraines located at average elevations of ~ 2080 and ~ 2190 m, respectively, indicated the existence of valley glaciers 3.5 and 2.5 km long during the middle of the B-A and during the transition from the B-A to the YD. Indeed, the reconstructed glacial surface for both bases was of 4.4 and 3.8 km², respectively, with a maximum ice thickness of 300 and 200 m for each of these phases (Fig. 6a, b).

Figure 6

Evidence of glacial recession during the middle of the B-A was also recorded on polished surfaces from the neighbouring Bacivèr Cirque at 13.5 ± 0.8 ka (Oliva et al., 2021a). Local topographical factors, such as the shape of the cirque floor (convex versus concave areas) determined the pattern of glacial flow of thin ice masses during the glacial advances/stillstands that occurred during the B-A. Glaciers flowed downwards from the cirque through concave areas across the western slope, favouring the development of the moraine arcs and crests in lower overdeepened basins (Fig. 3). It is likely that the topography played a major role in determining the process and timing of the deglaciation in both cirques: the accumulation area above 2400 m is larger in the Saboredo Cirque (552 ha) with respect to the Bacivèr Cirque (244 ha) and its prevailing aspect is also more favourable for ice persistence (N vs W).

The Saboredo Cirque floor became ice free at the beginning of the YD, as revealed by the samples from polished surfaces of the cirque floor at ~ 2350 m (average age = 12.7 ± 0.8 ka). The evidence of glacial striations on the rock surface make unlikely the possibility of nuclide inheritance at the sampling sites. Glaciers might thus also have persisted during the early YD in the highest hollows of the Saboredo Cirque, as was the case in the northern cirque of Sendrosa Peak. Here, the cirque moraine at 2470 m, formed by a 0.4 km-long glacier (with a surface of 0.7 km² and a thickness of 90 m; Fig. 6c), was abandoned at 12.6 ± 1.3 ka. Inside the highest glacial cirques of the Ruda Valley, there are numerous relict rock glaciers and protalus lobes indicative of the past occurrence of permafrost during their formation (Fernandes et al., 2018). As in most of the Pyrenees, these are probably glacier-derived permafrost features associated with the paraglacial phase, when glacial shrinking favoured wall debuttrressing, a high debris supply and the subsequent burial of the residual ice masses (Andrés et al., 2018; Oliva et al., 2016).

In short, by the early B-A the Garonne Paleoglacier had receded $\sim 95\%$ of its ~ 80 km length of the ILGM (Fernandes et al., 2017; Stange et al., 2014). The Ruda Paleoglacier receded 4 km in only ~ 1.7 ka (~ 14.4 to ~ 12.7 ka) from an elevation of ~ 1800 to >2400 - 2500 m. This trend towards glacial shrinking before the final ice disappearance was interrupted by three phases of glacier advance or stillstands at 13.5 ± 0.9 , 13.0 ± 0.8 and 12.6 ± 1.3 ka, which generated moraines at ~ 2080 , 2190 and 2470 m, respectively.

5.3 Late Quaternary glacial dynamics in the Central Pyrenees and Iberian Peninsula in the context of European glacial evolution

The scientific knowledge on the chronology of the last deglaciation in the Pyrenees has experienced substantial advances over the last years in parallel to progress on glacial chronological constraints in other European and Iberian mountain ranges (García-Ruiz et al., 2010; Palacios and García-Ruiz, 2015). There is increasing evidence that the timing of glacial oscillations during T-1 across Europe followed a similar sequence (Palacios et al., 2021): a significant glacier advance took place during the OD followed by a rapid retreat during the B-A and a subsequent more limited glacier advance during the YD (Oliva et al., 2019).

Dated evidence of glacial responses in the Pyrenees to Northern Hemisphere cold events during T-1 have mostly focused on the southern slope (Oliva et al., 2019), although there is an increasing body of new data from the northern slope of the range that confirms glacial advances and stillstands there during the OD and YD, and glacial shrinking during the B-A (Reixach et al., 2021). The elevation of the peaks as well as the topography of the cirques played a major role in the duration and intensity of the glaciation during T-1 in the

high massifs of the Pyrenees. Cirques surrounded by peaks above 2800-2900 m likely included glaciers during most of T-1 until the onset of the Holocene (see e.g. Jomelli et al., 2020; Pallàs et al., 2006; Reixach et al., 2021), while those situated at the foot of lower peaks (i.e. 2500-2600 m) were completely deglaciated during the B-A (Oliva et al., 2021a; Palacios et al., 2017b). Following ice retreat, the slopes were affected by intense readjustments (large, catastrophic rock slope failures, rock slope deformations, rockfalls, and rockslides), particularly in areas where the local lithostructure was prone to instability (Fernandes et al., 2020).

In the Central Pyrenees, a period of glacial growth occurred during the OD after the massive deglaciation that took place following the LGM. Moraines dated at 17-15 ka have been reported in the highest valleys of the main massifs, such as in the Ariège (Delmas et al., 2011; Jomelli et al., 2020; Reixach et al., 2021), Ésera (Crest et al., 2017), Gállego (Palacios et al., 2015a), Malniu (Andrés et al., 2018; Palacios et al., 2015b; Pallàs et al., 2010), Têt (Delmas et al., 2008; Tomkins et al., 2018), Arànsér (Andrés et al., 2018; Palacios et al., 2015b), and Bassiès (Crest et al., 2017). During that time, glaciers flowed downslope from the headwaters of the highest valleys, with valley glaciers often exceeding 10-15 km (Oliva et al., 2019). Consequently, it is likely that, by that time, most of the Ruda Valley was still glaciated, with the ice tongue probably merging with the main Garonne Paleoglacier that was also fed by neighbouring glacier tributaries, such as those descending from the Beret area (Oliva et al., 2021a). Some of the lateral moraine remnants distributed on the left side of the Garonne Valley, ca. 20 km from the highest parts of the Saboredo Cirque, formerly attributed to the OD (Fernandes et al., 2021; Fernandes et al., 2017) may be also correlated with some of the highest moraines and erratic boulders distributed in the Ruda Valley (Fig. 3). Other Iberian mountain ranges include geomorphic evidence of glacial advances during the OD (Palacios et al., 2017a), such as in the Monasterio Valley in the Cantabrian Mountains (Serrano et al., 2016), Peña Negra Valley in the Iberian Range (García-Ruiz et al., 2020), Peñalara massif in the Central Range (Palacios et al., 2012a), San Juan Valley in the Sierra Nevada (Palacios et al., 2016), En Garcia Valley in the Eastern Pyrenees (Reixach et al., 2021), and Gállego and Ésera valleys in the Central Pyrenees (Crest et al., 2017; Palacios et al., 2017b).

No moraine remnants have been found in the lowest and central sections of the Ruda Valley, and the prevailing lithology of slates and marbles in this area is not favourable for the preservation of glacially abraded surfaces. Indeed, the neighbouring Bacivèr Cirque was completely deglaciated also by ~15-14 ka (Oliva et al., 2021a). Thus, our data cannot confirm whether small glaciers persisted in the highest parts of the Ruda Valley during the B-A, although CRE ages support climatic conditions during the early B-A unfavourable for the maintenance of the OD ice masses (Fig. 7). In other valleys of the Pyrenees, glaciers also receded rapidly at ~14.6-14 ka as shown by CRE ages from polished surfaces and scattered erratic boulders in the Ariège (14.4 ± 1.1 , 14.1 ± 0.7 , 14.0 ± 0.8 ka; Delmas et al., 2011), Gállego (14.6 ± 2.3 ka; Palacios et al., 2015a) and Ésera valleys (14.3 ± 0.5 ka; Crest et al., 2017). Locally, some massifs of the Pyrenees were fully deglaciated during the B-A, with small glaciers persisting only in the highest cirques (Delmas, 2015). A similar pattern was detected in other Iberian ranges, such as in the Sierra Nevada (Palacios et al., 2016), Cantabrian Mountains (Rodríguez-Rodríguez et al., 2017) and the Iberian Range (García-Ruiz et al., 2020), where ice masses shrank significantly by ~15-14 ka. Glacial retreat in the Iberian Mountains was triggered by the sudden temperature increase of 3-5 °C at the onset of the B-A in western Europe, as inferred from climate models (Renssen and Isarin, 2001). In parallel, significant shifts occurred in the Atlantic Meridional Overturning Circulation (Obase and Abe-Ouchi, 2019). In north Iberia, a maximum increase of the mean annual temperature of 7.5°C at the onset of GI-1 has been estimated in northern Iberia, based on the Ostolo cave speleothem isotopic record (Bernal-Wormull et al., 2021). Marine records from the western Iberian margin also pointed to a 5-6°C of warming at the onset of the B-A (Martrat et al., 2007). These warmer conditions also favoured the recession of glaciers across most European mountain ranges, such as in the Alps at 15.9-14.3 cal ka BP (Ivy-Ochs, 2015), Tatra Mountains at 14.8-14.2 ka (Zasadni et al., 2020), Taurus Mountains at 14.6 ± 2.8 ka (Ciner and Sarikaya, 2015), as well as the Scandinavian Ice Sheet, which recorded a shrinking trend starting at 14.6 cal ka BP (Mangerud et al., 2013).

1
2 463 However, the B-A was a climatically unstable period characterised by an alternation of warm and cold
3 464 temperatures (Rasmussen et al., 2014). The gradual decrease of temperatures from the early to the late B-A
4 465 was depicted by periods of enhanced cold conditions in the high latitudes of the Northern Hemisphere, which
5 466 also favoured periods of glacial growth in the Pyrenees (Table 5). Indeed, CRE results indicate the formation
6 467 of moraines in the Ruda Valley at 13.5 ± 0.9 and 13.0 ± 0.8 ka (Fig. 7). These CRE ages are consistent with
7 468 the chronostratigraphic sequence but must be taken as approximate due to their uncertainty ranges and the low
8 469 number of dated samples at each moraine. At that time, small ice tongues ~ 3 km long flowed downslope from
9 470 the main Saboredo Cirque as well as from other neighbouring glacial hollows to overdeepened basins, forming
10 471 moraines at 2080 and 2190 m, respectively. Whereas evidence of phases of glacier advance or stillstands during
11 472 the transition from the late B-A to the early YD were already found in other cirques in the Central Pyrenees,
12 473 such as in the Bacivèr Cirque (Oliva et al., 2021a), and in the Cuerpo de Hombre Valley (Sierra de Gredos,
13 474 Central Range), with moraine stabilization at 13.1 ka (Carrasco et al., 2015), this is the first study that reports
14 475 geochronological evidence of a phase with glacial development in the second half of the B-A after the long-
15 476 term cooling initiated at ~ 14.5 ka (Fig. 7; Table 5). A few studies in Europe have also found evidence of glacier
16 477 advances or stillstands during the middle B-A, such as in the Tatra Mountains where moraines stabilized at
17 478 13.4 ± 0.5 ka (Engel et al., 2017). By contrast, geomorphic evidence of a period of glacial expansion during
18 479 the transition between the B-A to the early YD was detected in several regions, such as in the
19 480 Hardangerfjorden-Herdla area, western Norway, where a till deposit suggested a glacier advance of the
20 481 Scandinavian Ice sheet at 13.5-13.0 ka (Mangerud et al., 2016), and in the West Highland and Mull ice fields
21 482 of the Scottish Highlands, where 18 ^{14}C dates from organic fragments found in basal tills revealed a glacial
22 483 readvance from the end of the B-A or earliest YD (Bromley et al., 2018), although these results are considered
23 484 controversial (Small and Fabel, 2016).

29 485 Table 5

30
31 486 Based on the position of these two moraine ridges, the ELA in the Ruda Valley glacier must have been located
32 487 at 2461 and 2505 m during the glacial advances of the second part of the B-A and the late B-A or early YD,
33 488 respectively. Considering that the regional ELA in the Pyrenees currently lies at approximately 3100 m
34 489 (Jomelli et al., 2020; René, 2011), the ELA must have been located 639-595 m lower than present-day
35 490 conditions. Assuming an average lapse rate of 0.65 $^{\circ}\text{C}$ 100 m^{-1} and no change in precipitation, we infer that
36 491 summer temperatures must have been 4.2 and 3.9 $^{\circ}\text{C}$ lower than present-day during these two phases (Table
37 492 4).

40 493 Figure 7

41
42 494 The temperature decrease during the early YD favoured the persistence of glaciers inside the highest hollows
43 495 in the Ruda Valley, depositing moraines at ~ 2400 - 2500 m, which were later abandoned by the ice at $12.6 \pm$
44 496 1.3 ka (Fig 7). The existence of glaciers at high altitudes of the Saboredo Cirque is also confirmed by polished
45 497 surfaces at elevations of 2200-2300 m that were dated at 12.7 ± 0.8 ka. In the neighbouring Bacivèr Cirque,
46 498 moraines at 2400 m were abandoned by the ice at 12.8 ka (Oliva et al., 2021a). The elevation difference
47 499 between the ELA during the YD (2571 m) in the Ruda Valley and present-day values indicates that summer
48 500 temperatures were ~ 3.4 $^{\circ}\text{C}$ lower during that cold phase (Table 4), which is very similar to the ~ 3.0 $^{\circ}\text{C}$ inferred
49 501 for the Bacivèr Cirque (Oliva et al., 2021a). Indeed, topoclimatic factors must have played a key role
50 502 maintaining small glaciers during the YD at the foot of steep cirque walls, where shading and snow
51 503 accumulation allowed the longer persistence of reduced ice masses (Boston and Lukas, 2019). In the Pyrenees,
52 504 YD glacial advances have been detected in cirques of the Central (Delmas, 2009; Delmas et al., 2008; García-
53 505 Ruiz et al., 2016a) and Eastern sectors (Crest et al., 2017; Jomelli et al., 2020; Pallàs et al., 2010; Reixach et
54 506 al., 2021), where 2-3.5 km-long glaciers formed at 12.9-11.2 ka. Based on chronostratigraphic data from a
55 507 variety of sources, evidence of YD glacial advances was also recorded in the highest cirques of other Iberian
56 508 massifs, although no direct ages are yet available (García-Ruiz et al., 2016a). This is true for the NW ranges
57 509 (Cowton et al., 2009) and the Cantabrian Mountains (Pellitero et al., 2019; Serrano et al., 2015), where
58 510 moraines above 1800 and 2000 m, respectively, were associated with this cold phase. In the Sierra Nevada,

1
2 511 YD moraines dated at 13-12 ka are located in the highest cirques facing east from 2350 (north face) to 2800 m
3 512 (south face) (Oliva et al., 2014; Palacios et al., 2016). These glacial advances were driven by a temperature
4 513 cooling quantified at 2-4 °C in western Europe that was triggered by a slowdown of the overturning circulation
5 514 in the North Atlantic (Renssen et al., 2018). In the Pyrenees, the YD was the coldest period of the last
6 515 deglaciation recorded by a decrease of ^{18}O in the Ostolo and Seso speleothems that might reflect the
7 516 temperature decrease of $\sim 5^\circ\text{C}$ (Bartolomé et al., 2015; Bernal-Wormull et al., 2021). Colder conditions also
8 517 favoured glacial growth in other mountainous regions of Europe, with widespread advances across the Alps
9 518 between 13.5 and 12 ka (Ivy-Ochs, 2015; Ivy-Ochs et al., 2009), in the Tatra Mountains where moraines
10 519 stabilized at 11.9 ± 0.5 ka (Engel et al., 2017) and in Turkey where they formed at 12.6 ± 2.3 ka (Ciner and
11 520 Sarikaya, 2015).

12
13 521 The final deglaciation of the cirques favoured paraglacial dynamics and the formation of the numerous rock
14 522 glaciers existing today in the Saboredo and Sendrosa cirques, as well as in the lateral cirques distributed along
15 523 the Ruda Valley (Fig. 3). These features are currently inactive under the present-day climate regime (Fernandes
16 524 et al., 2018), with abundant lichen coverage and forest colonization, particularly on the lowest ridges. In the
17 525 Pyrenees, as well as in other Iberian ranges, cirque wall readjustment following deglaciation triggered different
18 526 landforms, such as debris-covered glaciers or rock glaciers, that remained active until the early Holocene
19 527 (Oliva et al., 2019). This is the case of the Bacivèr cirque, where the debris-covered glacier that formed inside
20 528 the highest YD moraines stabilized at 7.2 ± 0.5 ka (Oliva et al., 2021a), or of several other massifs in the
21 529 Central and Eastern Pyrenees where rock glaciers were active until well into the Holocene (Andrés et al., 2018;
22 530 García-Ruiz et al., 2016a). A similar pattern was also detected in other Iberian massifs, such as in the Iberian
23 531 Range (Aumaître et al., 2017) or Sierra Nevada (Palacios et al., 2016), where these paraglacial landforms
24 532 formed immediately after the deglaciation of the cirques, and remained active until the complete melting of
25 533 their relict ice during the Holocene Thermal Maximum.

30 31 534 6. Conclusions

32
33 535 The Central Pyrenees were extensively glaciated during Quaternary glacial phases and were only slightly
34 536 transformed by periglacial, nival and slope processes during subsequent interglacial periods such as the
35 537 Holocene. As a result, the landscape in the Central Pyrenees includes a wide range of geomorphological
36 538 features that constitutes a prominent natural heritage that contributed to the designation of most protected areas
37 539 in this mountain range. This is the case of the Ruda Valley, located on the periphery of the National Park of
38 540 Aigüestortes and Sant Maurici Lake. The valley is one of the most scenic glacial valleys of the Pyrenees, and
39 541 includes a wide variety of glacial and periglacial landforms, particularly above 1800 m. However, in contrast
40 542 to the southern slope of the Central Pyrenees where the timing of the glacial evolution has been widely studied,
41 543 on the northern side there are still temporal and spatial gaps in the chronology of glacial activity. In this work,
42 544 we determined the magnitude and timing of T-1 glacial oscillations in the Upper Garonne Basin by producing
43 545 12 new CRE ages of glacial landforms (moraine boulders and glacially polished surfaces) that provide evidence
44 546 of the spatio-temporal pattern of glacial oscillations from the B-A to the YD.

45
46 547 The Upper Garonne Basin hosted the largest glacial system of the Pyrenees during the last glacial cycle thanks
47 548 to its Atlantic-influenced climate and the high altitude of the peaks in the central part of this range. The long-
48 549 term post-LGM warming favoured glacial recession, particularly during the early B-A, and by 14.4 ± 1.2 ka
49 550 the Ruda Paleoglacier was already disconnected from the main Garonne Paleoglacier. At that time, the glacier
50 551 front was located at 1860-1900 m, and some areas of the Saboredo Cirque were already ice-free as a result of
51 552 ice thinning. The B-A was also a period of great climatic variability, and the small glaciers in the Ruda Valley
52 553 showed rapid response times with formation of moraines during the coldest B-A phases in north Iberia. Phases
53 554 of glacier advance or stillstands promoted the development of moraines at 13.5 ± 0.9 ka, as well as during the
54 555 transition between the late B-A and the onset of the YD at 13.0 ± 0.8 ka. The YD probably favoured the
55 556 persistence of small glaciers during an early stage of this cold phase; there is evidence of glacial retreat at the
56 557 uppermost part of the cirque floor at 12.7 ± 0.7 ka (~ 2300 -2350 m) and moraine abandonment of the highest

1
2 558 cirque moraines (2470 m) at 12.6 ± 1.3 ka. Subsequently, glacial disappearance must have promoted
3 559 paraglacial dynamics and the formation of the (currently relict) rock glaciers existing within these moraines.
4

5 560 Whereas the impact of the B-A deglaciation on the current landscape of the Pyrenean cirques was already
6 561 known, the sequence of glacial advances and retreats during the B-A and YD presented in this study provides
7 562 one of the most accurate deglacial histories in southern Europe. This opens new perspectives on the
8 563 paleoclimatic evolution in the Iberian Peninsula, in particular, and the Mediterranean region in general. The
9 564 period spanning from the B-A to the YD has been shown to be a major driver of transformation of the mountain
10 565 landscapes of the Pyrenees and a key phase to better frame Holocene environmental dynamics in the highest
11 566 lands of this mountain range. Future studies with new chronological data from other Pyrenean valleys and
12 567 Iberian mountains will help to better understand T-1 glacier advances and retreats as well as the climate
13 568 mechanisms behind millennial-scale glacial oscillations in southern Europe.

16 569 Acknowledgements

17
18 570 This work was funded by the Research Group ANTALP (Antarctic, Arctic, Alpine Environments; 2017-SGR-
19 571 1102), the Government of Catalonia and the Centro de Estudos Geográficos/IGOT - University of Lisbon (FCT
20 572 I.P. UIDB/00295/2020 and UIDP/00295/2020). The research topics complement those of the project
21 573 PALEOGREEN (CTM2017-87976-P) funded by the Spanish Ministry of Economy and Competitiveness and
22 574 the project NUNANTAR funded by the Fundação para a Ciência e Tecnologia of Portugal (02/SAICT/2017 -
23 575 32002). Marcelo Fernandes holds a PhD fellowship of the Fundação para a Ciência e Tecnologia of Portugal
24 576 (FCT - UIDB/00295/2020); Marc Oliva is supported by the Ramón y Cajal Program (RYC-2015-17597) and
25 577 José M. Fernández-Fernández is supported by a postdoctoral grant within the NUNANTAR project. ¹⁰Be
26 578 measurements were performed at the ASTER AMS national facility (CEREGE, Aix-en-Provence), which is
27 579 supported by the INSU/CNRS and the ANR through the “Projets thématiques d'excellence” program for the
28 580 “Equipements d'excellence” ASTER-CEREGE action and IRD. This research is also framed within the College
29 581 on Polar and Extreme Environments (Polar2E) of the University of Lisbon. We also thank the National Park
30 582 of Aigüestortes and Sant Maurici Lake for providing field access to the study sites and the reviewers for their
31 583 constructive comments that helped to improve the quality of an earlier version of the manuscript.
32
33
34
35

37 585 7. References

- 36 584
37 585
38
39 586
40
41 587 Allard, J.L., Hughes, P., Woodward, J.C., 2021. Heinrich Stadial aridity forced Mediterranean-wide glacier
42 588 retreat in the last cold stage. *Nat. Geosci.* <https://doi.org/10.1038/s41561-021-00703-6>
- 43 589 André, M.F., 2002. Rates of Postglacial rock weathering on glacially scoured outcrops (Abisko-Riksgränsen
44 590 area, 68°N). *Geogr. Ann. Ser. A Phys. Geogr.* 84, 139–150. <https://doi.org/10.1111/j.0435-3676.2002.00168.x>
- 45 591
46
47 592 Andrés, N., Gómez-Ortiz, A., Fernández-Fernández, J.M., Tanarro García, L.M., Salvador-Franch, F., Oliva,
48 593 M., Palacios, D., 2018. Timing of deglaciation and rock glacier origin in the southeastern Pyrenees: a
49 594 review and new data. *Boreas* 47, 1050–1071. <https://doi.org/10.1111/bor.12324>
- 50
51 595 Arnold, M., Merchel, S., Boulès, D.L., Braucher, R., Benedetti, L., Finkel, R.C., Aumaître, G., Gott dang,
52 596 A., Klein, M., 2010. The French accelerator mass spectrometry facility ASTER: Improved performance
53 597 and developments. *Nucl. Instruments Methods Phys. Res. Sect. B Beam Interact. with Mater. Atoms*
54 598 268, 1954–1959. <https://doi.org/10.1016/j.nimb.2010.02.107>
- 55 599 Aumaître, G., Boulès, D., Keddadouche, K., Schimmelpennig, I., Léanni, L., Fernández-Fernández, J.M.,
56 600 Palacios, D., Andrés, N., Úbeda, J., García-Ruiz, J.M., Gómez-Villar, A., Santos-González, J., Álvarez-
57 601 Martínez, J., Arnáez, J., 2017. Chronological and geomorphological investigation of fossil debris-
58 602 covered glaciers in relation to deglaciation processes: A case study in the Sierra de La Demanda,
59 603 northern Spain. *Quat. Sci. Rev.* 170, 232–249. <https://doi.org/10.1016/j.quascirev.2017.06.034>
- 60
604 Ballantyne, C.K., 2008. After the ice: Holocene geomorphic activity in the Scottish Highlands, Scottish

- 1
2 605 Geographical Journal. <https://doi.org/10.1080/14702540802300167>
- 3
4 606 Barr, I., Spagnolo, M., 2015. Glacial cirques as palaeoenvironmental indicators: Their potential and
5 607 limitations. *Earth-Science Rev.* 151, 48–78. <https://doi.org/10.1016/j.earscirev.2015.10.004>
- 6 608 Bartolomé, M., Moreno, A., Sancho, C., Stoll, H.M., Cacho, I., Spötl, C., Belmonte, Á., Edwards, R.L.,
7 609 Cheng, H., Hellstrom, J.C., 2015. Hydrological change in Southern Europe responding to increasing
8 610 North Atlantic overturning during Greenland Stadial 1. *Proc. Natl. Acad. Sci.* 112, 6568–6572.
9 611 <https://doi.org/10.1073/pnas.1503990112>
- 10
11 612 Benn, D.I., Hulton, N.R.J., 2010. An Excel™ spreadsheet program for reconstructing the surface profile of
12 613 former mountain glaciers and ice caps. *Comput. Geosci.* 36, 605–610.
13 614 <https://doi.org/10.1016/j.cageo.2009.09.016>
- 14
15 615 Bernal-Wormull, J.L., Moreno, A., Bartolomé, M., Aranburu, A., Arriolabengoa, M., Iriarte, E., Cacho, I.,
16 616 Spötl, C., Edwards, R.L., Cheng, H., 2021. Immediate temperature response in northern Iberia to last
17 617 deglacial changes in the North Atlantic. *Geology* XX, 6–10.
18 618 <https://doi.org/10.1130/G48660.1/5304545/g48660.pdf>
- 19 619 Boston, C.M., Lukas, S., 2019. Topographic controls on plateau icefield recession: insights from the
20 620 Younger Dryas Monadhliath Icefield, Scotland. *J. Quat. Sci.* 34, 433–451.
21 621 <https://doi.org/10.1002/jqs.3111>
- 22
23 622 Braucher, R., Guillou, V., Bourlès, D.L., Arnold, M., Aumaître, G., Keddadouche, K., Nottoli, E., 2015.
24 623 Preparation of ASTER in-house 10Be/9Be standard solutions. *Nucl. Instruments Methods Phys. Res.*
25 624 *Sect. B Beam Interact. with Mater. Atoms* 361, 335–340.
26 625 <https://doi.org/https://doi.org/10.1016/j.nimb.2015.06.012>
- 27
28 626 Bromley, G., Putnam, A., Borns, H., Lowell, T., Sandford, T., Barrell, D., 2018. Interstadial Rise and
29 627 Younger Dryas Demise of Scotland’s Last Ice Fields Paleooceanography and Paleoclimatology.
30 628 *Paleoceanogr. Paleoclimatology* 412–429. <https://doi.org/10.1002/2018PA003341>
- 31 629 Carrasco, R.M., Pedraza, J., Domínguez-Villar, D., Willenbring, J.K., Villa, J., 2015. Sequence and
32 630 chronology of the Cuerpo de Hombre paleoglacier (Iberian Central System) during the last glacial
33 631 cycle. *Quat. Sci. Rev.* 129, 163–177. <https://doi.org/10.1016/j.quascirev.2015.09.021>
- 34
35 632 Chmeleff, J., von Blanckenburg, F., Kossert, K., Jakob, D., 2010. Determination of the 10Be half-life by
36 633 multicollector ICP-MS and liquid scintillation counting. *Nucl. Instruments Methods Phys. Res. Sect. B*
37 634 *Beam Interact. with Mater. Atoms* 268, 192–199. <https://doi.org/10.1016/j.nimb.2009.09.012>
- 38
39 635 Ciner, A., Sarikaya, M.A., 2015. Cosmogenic 36 Cl geochronology of late Quaternary glaciers in the Bolkar
40 636 Mountains, south central Turkey, in: Hughes, P. D. & Woodward, J.C. (Ed.), *Quaternary Glaciation in*
41 637 *the Mediterranean Mountains*. <https://doi.org/http://doi.org/10.1144/SP433.3>
- 42 638 Clark, P.U., Dyke, A., Shakun, J., Carlson, A., Wohlfarth, B., Mitrovica, J., Hostetler, S., McCabe, A., 2009.
43 639 *The Last Glacial Maximum*. *Science* (80-.). 325, 710–714. <https://doi.org/10.1126/science.1172873>
- 44
45 640 Cowton, T., Hughes, P., Gibbard, P.L., 2009. Palaeoglaciation of Parque Natural Lago de Sanabria,
46 641 northwest Spain. *Geomorphology* 108, 282–291. <https://doi.org/10.1016/j.geomorph.2009.02.007>
- 47 642 Crest, Y., Delmas, M., Braucher, R., Gunnell, Y., Calvet, M., 2017. Cirques have growth spurts during
48 643 deglacial and interglacial periods: Evidence from 10Be and 26Al nuclide inventories in the central and
49 644 eastern Pyrenees. *Geomorphology* 278, 60–77. <https://doi.org/10.1016/j.geomorph.2016.10.035>
- 51 645 Delmas, M., 2015. The last maximum ice extent and subsequent deglaciation of the Pyrenees: an overview of
52 646 recent research. *Cuad. Investig. Geográfica* 41, 359. <https://doi.org/10.18172/cig.2708>
- 53
54 647 Delmas, M., 2009. Chronologie et impact géomorphologique des glaciations quaternaires dans l’est des
55 648 Pyrénées. *Lab. Rech. en géographie Phys. MEDI-TERRA, Univ. Perpignan. LGP Meudon, Univ. Paris*
56 649 *1 Panthéon Sorbonne Ph.D.*, 529.
- 57 650 Delmas, M., Calvet, M., Gunnell, Y., Braucher, R., Bourlès, D., 2011. Palaeogeography and 10Be exposure-
58 651 age chronology of Middle and Late Pleistocene glacier systems in the northern Pyrenees: Implications
59 652 for reconstructing regional palaeoclimates. *Palaeogeogr. Palaeoclimatol. Palaeoecol.* 305, 109–122.
60 653 <https://doi.org/10.1016/j.palaeo.2011.02.025>

- 1
2 654 Delmas, M., Gunnell, Y., Braucher, R., Calvet, M., Bourlès, D., 2008. Exposure age chronology of the last
3 655 glaciation in the eastern Pyrenees. *Quat. Res.* 69, 231–241. <https://doi.org/10.1016/j.yqres.2007.11.004>
- 4
5 656 Dunne, J., Elmore, D., Muzikar, P., 1999. Scaling factors for the rates of production of cosmogenic nuclides
6 657 for geometric shielding and attenuation at depth on sloped surfaces. *Geomorphology* 27, 3–11.
7 658 [https://doi.org/10.1016/S0169-555X\(98\)00086-5](https://doi.org/10.1016/S0169-555X(98)00086-5)
- 8 659 Fernandes, M., Oliva, M., Palma, P., Ruiz-Fernández, J., Lopes, L., 2017. Glacial stages and post-glacial
9 660 environmental evolution in the Upper Garonne valley, Central Pyrenees. *Sci. Total Environ.* 584–585,
10 661 1282–1299. <https://doi.org/10.1016/j.scitotenv.2017.01.209>
- 11
12 662 Fernandes, M., Oliva, M., Vieira, G., 2020. Paraglacial slope failures in the Aran valley (Central Pyrenees).
13 663 *Quat. Int.* 566–567, 24–38. <https://doi.org/10.1016/j.quaint.2020.07.045>
- 14
15 664 Fernandes, M., Oliva, M., Vieira, G., Lopes, L., 2021. Geomorphological map of the Aran valley (Upper
16 665 Garonne valley, Central Pyrenees). *J. Maps.*
- 17 666 Fernandes, M., Palma, P., Lopes, L., Ruiz-Fernández, J., Pereira, P., Oliva, M., 2018. Spatial distribution and
18 667 morphometry of permafrost-related landforms in the Central Pyrenees and associated paleoclimatic
19 668 implications. *Quat. Int.* 470. <https://doi.org/10.1016/j.quaint.2017.08.071>
- 20
21 669 García-Ruiz, J.M., Moreno, A., González-Sampériz, P., Valero-Garcés, B.L., Martí-Bono, C., 2010. La
22 670 cronología del último ciclo glaciar en las montañas del sur de Europa. Una revisión. *Cuaternario y*
23 671 *Geomorfol.* 24, 35–46. [https://doi.org/10.1016/S0034-7094\(11\)70016-2](https://doi.org/10.1016/S0034-7094(11)70016-2)
- 24
25 672 García-Ruiz, J.M., Palacios, D., Fernández-Fernández, J.M., Andrés, N., Arnáez, J., Gómez-Villar, A.,
26 673 Santos-González, J., Álvarez-Martínez, J., Lana-Renault, N., Léanni, L., 2020. Glacial stages in the
27 674 Peña Negra valley, Iberian Range, northern Iberian Peninsula: Assessing the importance of the glacial
28 675 record in small cirques in a marginal mountain area. *Geomorphology* 362, 107195.
29 676 <https://doi.org/10.1016/j.geomorph.2020.107195>
- 30 677 García-Ruiz, J.M., Palacios, D., González-Sampériz, P., De Andrés, N., Moreno, A., Valero-Garcés, B.,
31 678 Gómez-Villar, A., 2016a. Mountain glacier evolution in the Iberian Peninsula during the Younger
32 679 Dryas. *Quat. Sci. Rev.* 138, 16–30. <https://doi.org/10.1016/j.quascirev.2016.02.022>
- 33
34 680 García-Ruiz, J.M., Palacios, D., González-Sampériz, P., de Andrés, N., Moreno, A., Valero-Garcés, B.L.,
35 681 Gómez-Villar, A., 2016b. Evidencias de actividad glaciar durante el Dryas Reciente (12,9-11,7 ka BP)
36 682 en la Península Ibérica. *Cuaternario y Geomorfol.* 30, 9–21. [https://doi.org/10.17735/cyg.v30i1-](https://doi.org/10.17735/cyg.v30i1-2.39250)
37 683 [2.39250](https://doi.org/10.17735/cyg.v30i1-2.39250)
- 38
39 684 Gómez-Ortiz, A., Palacios, D., Palade, B., Vázquez-Selem, L., Salvador-Franch, F., 2012. The deglaciation
40 685 of the Sierra Nevada (Southern Spain). *Geomorphology* 159–160, 93–105.
41 686 <https://doi.org/10.1016/j.geomorph.2012.03.008>
- 42 687 González-Sampériz, P., Valero-Garcés, B.L., Moreno, A., Jalut, G., García-Ruiz, J.M., Martí-Bono, C.,
43 688 Delgado-Huertas, A., Navas, A., Otto, T., Dedoubat, J., 2006. Climate variability in the Spanish
44 689 Pyrenees during the last 30,000 yr revealed by the El Portalet sequence. *Quat. Res.* 66, 38–52.
- 45
46 690 Heyman, J., Stroeven, A.P., Harbor, J.M., Caffee, M.W., 2011. Too young or too old: evaluating cosmogenic
47 691 exposure dating based on an analysis of compiled boulder exposure ages. *Earth Planet. Sci. Lett.* 302,
48 692 71–80.
- 49
50 693 Hughes, P., 2014. Little Ice Age glaciers in the Mediterranean mountains. *Geophys. Res. Abstr.* 16, 2014.
- 51 694 Huss, M., Bauder, A., Linsbauer, A., Gabbi, J., Kappenberger, G., Steinegger, U., Farinotti, D., 2021. More
52 695 than a century of direct glacier mass-balance observations on Claridenfirn, Switzerland. *J. Glaciol.* 1–
53 696 17. <https://doi.org/10.1017/jog.2021.22>
- 54
55 697 ICGC, 2017. Base de dades geològiques de Catalunya 1:50.000 v1.0.
- 56 698 Ivy-Ochs, S., 2015. Variaciones glaciares en los Alpes europeos al final de la última glaciación. *Cuad.*
57 699 *Investig. Geogr.* 41, 295–315. <https://doi.org/10.18172/cig.2750>
- 58
59 700 Ivy-Ochs, S., Kerschner, H., Maisch, M., Christl, M., Kubik, P.W., Schlüchter, C., 2009. Latest Pleistocene
60 701 and Holocene glacier variations in the European Alps. *Quat. Sci. Rev.* 28, 2137–2149.
702 <https://doi.org/10.1016/j.quascirev.2009.03.009>

- 1
2 703 Joly, F., 1997. Glossaire de géomorphologie. Base de données sémiologiques pour la cartographie,
3 704 Masson/Arm. ed. Paris.
- 4
5 705 Jomelli, V., Chapron, E., Favier, V., Rinterknecht, V., Braucher, R., Tournier, N., Gascoïn, S., Marti, R.,
6 706 Galop, D., Binet, S., Deschamps, C., Tissoux, H., Aumaitre, G., Bourlès, D.L., Keddadouche, K., 2020.
7 707 Glacier fluctuations during the Late Glacial and Holocene on the Ariège valley, northern slope of the
8 708 Pyrenees and reconstructed climatic conditions. *Mediterr. Geosci. Rev.* [https://doi.org/10.1007/s42990-](https://doi.org/10.1007/s42990-020-00018-5)
9 709 020-00018-5
- 10 710 Korschinek, G., Bergmaier, A., Faestermann, T., Gerstmann, U.C., Knie, K., Rugel, G., Wallner, A.,
11 711 Dillmann, I., Dollinger, G., von Gostomski, C.L., Kossert, K., Maiti, M., Poutivtsev, M., Rimmert, A.,
12 712 2010. A new value for the half-life of ^{10}Be by Heavy-Ion Elastic Recoil Detection and liquid
13 713 scintillation counting. *Nucl. Instruments Methods Phys. Res. Sect. B Beam Interact. with Mater. Atoms*
14 714 268, 187–191. <https://doi.org/10.1016/j.nimb.2009.09.020>
- 15
16 715 Li, Y., 2018. Determining topographic shielding from digital elevation models for cosmogenic nuclide
17 716 analysis: a GIS model for discrete sample sites. *J. Mt. Sci.* 15, 939–947.
18 717 <https://doi.org/10.1007/s11629-018-4895-4>
- 19
20 718 Lifton, N., Sato, T., Dunai, T., 2014. Scaling in situ cosmogenic nuclide production rates using analytical
21 719 approximations to atmospheric cosmic-ray fluxes. *Earth Planet. Sci. Lett.* 386, 149–160.
22 720 <https://doi.org/10.1016/j.epsl.2013.10.052>
- 23
24 721 Lopes, L., Oliva, M., Fernandes, M., Pereira, P., Palma, P., Ruiz-Fernández, J., 2018. Spatial distribution of
25 722 morphometric parameters of glacial cirques in the Central Pyrenees (Aran and Boí valleys). *J. Mt. Sci.*
26 723 15. <https://doi.org/10.1007/s11629-018-4873-x>
- 27 724 López-Moreno, J.I., Alonso-González, E., Monserrat, O., Del Río, L.M., Otero, J., Lapazaran, J., Luzi, G.,
28 725 Dematteis, N., Serreta, A., Rico, I., Serrano, E., Bartolomé, M., Moreno, A., Buisan, S., Revuelto, J.,
29 726 2019. Ground-based remote-sensing techniques for diagnosis of the current state and recent evolution
30 727 of the Monte Perdido Glacier, Spanish Pyrenees. *J. Glaciol.* 65, 85–100.
31 728 <https://doi.org/10.1017/jog.2018.96>
- 32
33 729 Mangerud, J., Aarseth, I., Hughes, A.L.C., Lohne, Ø.S., Skår, K., Sønstegaard, E., Inge, J., 2016. A major re-
34 730 growth of the Scandinavian Ice Sheet in western Norway during Allerød-Younger Dryas. *Quat. Sci.*
35 731 *Rev.* 132, 175–205. <https://doi.org/10.1016/j.quascirev.2015.11.013>
- 36
37 732 Mangerud, J., Goehring, B.M., Lohne, Ø.S., Svendsen, J.I., Gyllencreutz, R., 2013. Collapse of marine-based
38 733 outlet glaciers from the Scandinavian Ice Sheet. *Quat. Sci. Rev.* 67, 8–16.
39 734 <https://doi.org/10.1016/j.quascirev.2013.01.024>
- 40 735 Martin, L.C.P., Blard, P.-H., Balco, G., Lavé, J., Delunel, R., Lifton, N., Laurent, V., 2017. The CREp
41 736 program and the ICE-D production rate calibration database: A fully parameterizable and updated
42 737 online tool to compute cosmic-ray exposure ages. *Quat. Geochronol.* 38, 25–49.
43 738 <https://doi.org/10.1016/J.QUAGEO.2016.11.006>
- 44
45 739 Martrat, B., Grimalt, J.O., Shackleton, N.J., De Abreu, L., Hutterli, M.A., Stocker, T.F., 2007. Four climate
46 740 cycles of recurring deep and surface water destabilizations on the Iberian margin. *Science* (80-). 317,
47 741 502–507. <https://doi.org/10.1126/science.1139994>
- 48
49 742 Merchel, S., Arnold, M., Aumaitre, G., Benedetti, L., Bourlès, D.L., Braucher, R., Alfimov, V., Freeman,
50 743 S.P.H.T., Steier, P., Wallner, A., 2008. Nuclear Instruments and Methods in Physics Research B
51 744 Towards more precise ^{10}Be and ^{36}Cl data from measurements at the 10 Å 14 level : Influence of
52 745 sample preparation Be / B e. *Nucl. Inst. Methods Phys. Res. B* 266, 4921–4926.
53 746 <https://doi.org/10.1016/j.nimb.2008.07.031>
- 54 747 Merchel, S., Herpers, U., 1999. An Update on Radiochemical Separation Techniques for the Determination
55 748 of Long-Lived Radionuclides via Accelerator Mass Spectrometry. *Radiochim. Acta* 84, 215–219.
56 749 <https://doi.org/10.1524/ract.1999.84.4.215>
- 57
58 750 Moreno, A., Stoll, H., Jiménez-Sánchez, M., Cacho, I., Valero-Garcés, B., Ito, E., Edwards, R.L., 2010. A
59 751 speleothem record of glacial (25–11.6 kyr BP) rapid climatic changes from northern Iberian Peninsula.
60 752 *Glob. Planet. Change* 71, 218–231. <https://doi.org/10.1016/j.gloplacha.2009.10.002>

- 1
2 753 Obase, T., Abe-Ouchi, A., 2019. Abrupt Bølling-Allerød Warming Simulated under Gradual Forcing of the
3 754 Last Deglaciation. *Geophys. Res. Lett.* 46, 11397–11405. <https://doi.org/10.1029/2019GL084675>
- 4
5 755 Oliva, M., Fernandes, M., Palacios, D., Fernández-Fernández, J.M., Schimmelpfennig, I., Team, A.S.T.E.R.,
6 756 Antoniades, D., 2021a. Rapid deglaciation during the Bølling-Allerød Interstadial in the Central
7 757 Pyrenees and associated glacial and periglacial landforms. *Geomorphology* 107735.
8 758 <https://doi.org/10.1016/j.geomorph.2021.107735>
- 9 759 Oliva, M., Gómez Ortiz, A., Palacios, D., Salvador-Franch, F., Salvà-Catarineu, M., 2014. Environmental
10 760 evolution in Sierra Nevada (South Spain) since the Last Glaciation, based on multi-proxy records.
11 761 *Quat. Int.* 353, 195–209. <https://doi.org/10.1016/j.quaint.2014.02.009>
12
- 13 762 Oliva, M., Palacios, D., Fernández-Fernández, J.M., 2021b. Iberia, land of glaciers. Elsevier.
- 14 763 Oliva, M., Palacios, D., Fernández-Fernández, J.M., Rodríguez-Rodríguez, L., García-Ruiz, J.M., Andrés,
15 764 N., Carrasco, R.M., Pedraza, J., Pérez-Alberti, A., Valcárcel, M., Hughes, P., 2019. Late Quaternary
16 765 glacial phases in the Iberian Peninsula. *Earth-Science Rev.* 192, 564–600.
17 766 <https://doi.org/10.1016/j.earscirev.2019.03.015>
- 19 767 Oliva, M., Serrano, E., Gómez-Ortiz, A., González-Amuchastegui, M.J., Nieuwendam, A., Palacios, D.,
20 768 Pérez-Alberti, A., Pellitero, R., Ruiz-Fernández, J., Valcárcel, M., Vieira, G., Antoniades, D., 2016.
21 769 Spatial and temporal variability of periglaciation of the Iberian Peninsula. *Quat. Sci. Rev.* 137, 176–
22 770 199. <https://doi.org/10.1016/j.quascirev.2016.02.017>
23
- 24 771 Osmaston, H., 2005. Estimates of glacier equilibrium line altitudes by the Area×Altitude, the Area×Altitude
25 772 Balance Ratio and the Area×Altitude Balance Index methods and their validation. *Quat. Int.* 138–139,
26 773 22–31. <https://doi.org/10.1016/j.quaint.2005.02.004>
- 27
28 774 Palacios, D., Andrés, N., Marcos, J., Vázquez-Selem, L., 2012a. Maximum glacial advance and deglaciation
29 775 of the Pinar Valley (Sierra de Gredos, Central Spain) and its significance in the Mediterranean context.
30 776 *Geomorphology* 177–178, 51–61. <https://doi.org/10.1016/j.geomorph.2012.07.013>
- 31 777 Palacios, D., de Andrés, N., de Marcos, J., Vázquez-Selem, L., 2012b. Glacial landforms and their
32 778 paleoclimatic significance in Sierra de Guadarrama, Central Iberian Peninsula. *Geomorphology* 139–
33 779 140, 67–78. <https://doi.org/10.1016/j.geomorph.2011.10.003>
34
- 35 780 Palacios, D., de Andrés, N., Gómez-Ortiz, A., García-Ruiz, J.M., 2017a. Evidence of glacial activity during
36 781 the Oldest Dryas in the mountains of Spain. *Geol. Soc. London, Spec. Publ.* 433, 87–110.
37 782 <https://doi.org/10.1144/SP433.10>
- 38
39 783 Palacios, D., de Andrés, N., López-Moreno, J.I., García-Ruiz, J.M., 2015a. Late Pleistocene deglaciation in
40 784 the upper Gállego Valley, central Pyrenees. *Quat. Res. (United States)* 83, 397–414.
41 785 <https://doi.org/10.1016/j.yqres.2015.01.010>
- 42 786 Palacios, D., García-Ruiz, J.M., 2015. Foreword: Deglaciation in Europe. New insights and questions. *Cuad.*
43 787 *Investig. Geogr.* 41, 257–259. <https://doi.org/10.18172/cig.2808>
44
- 45 788 Palacios, D., García-Ruiz, J.M., Andrés, N., Schimmelpfennig, I., Campos, N., Léanni, L., Aumaître, G.,
46 789 Bourlès, D.L., Keddadouche, K., 2017b. Deglaciation in the central Pyrenees during the Pleistocene–
47 790 Holocene transition: Timing and geomorphological significance. *Quat. Sci. Rev.* 162, 111–127.
48 791 <https://doi.org/10.1016/j.quascirev.2017.03.007>
- 49
50 792 Palacios, D., Gómez-Ortiz, A., Andrés, N., Salvador-Franch, F., Oliva, M., 2016. Timing and new
51 793 geomorphologic evidence of the last deglaciation stages in Sierra Nevada (southern Spain). *Quat. Sci.*
52 794 *Rev.* 150, 110–129. <https://doi.org/10.1016/j.quascirev.2016.08.012>
- 53 795 Palacios, D., Gómez-Ortiz, A., Andrés, N., Vázquez-Selem, L., Salvador-Franch, F., Oliva, M., 2015b.
54 796 Maximum extent of Late Pleistocene glaciers and last deglaciation of La Cerdanya mountains,
55 797 Southeastern Pyrenees. *Geomorphology* 231, 116–129. <https://doi.org/10.1016/j.geomorph.2014.10.037>
56
- 57 798 Palacios, D., Hughes, P., García-Ruiz, J.M., Andrés, N., 2021. European Glacial Landscapes. Elsevier.
- 58 799 Pallàs, R., Rodés, Á., Braucher, R., Bourlès, D., Delmas, M., Calvet, M., Gunnell, Y., 2010. Small, isolated
59 800 glacial catchments as priority targets for cosmogenic surface exposure dating of Pleistocene climate
60 801 fluctuations, southeastern Pyrenees. *Geology* 38, 891–894. <https://doi.org/10.1130/G31164.1>

- 1
2 802 Pallàs, R., Rodés, Á., Braucher, R., Carcaillet, J., Ortuño, M., Bordonau, J., Bourlès, D., Vilaplana, J.M.,
3 803 Masana, E., Santanach, P., 2006. Late Pleistocene and Holocene glaciation in the Pyrenees: a critical
4 804 review and new evidence from ^{10}Be exposure ages, south-central Pyrenees. *Quat. Sci. Rev.* 25, 2937–
5 805 2963. <https://doi.org/10.1016/j.quascirev.2006.04.004>
- 6
7 806 Paterson, W.S.B., 1994. *The Physics of Glaciers*, 3rd Editio. ed. Elsevier, London.
8 807 <https://doi.org/10.1016/C2009-0-14802-X>
- 9 808 Pellitero, R., Fernández-Fernández, J.M., Campos, N., Serrano, E., Pisabarro, A., 2019. Late Pleistocene
10 809 climate of the northern Iberian Peninsula: New insights from palaeoglaciers at Fuentes Carrionas
11 810 (Cantabrian Mountains). *J. Quat. Sci.* 34, 342–354. <https://doi.org/10.1002/jqs.3106>
- 12
13 811 Pellitero, R., Rea, B.R., Spagnolo, M., Bakke, J., Hughes, P., Ivy-Ochs, S., Lukas, S., Ribolini, A., 2015. A
14 812 GIS tool for automatic calculation of glacier equilibrium-line altitudes. *Comput. Geosci.* 82, 55–62.
15 813 <https://doi.org/10.1016/j.cageo.2015.05.005>
- 16
17 814 Pellitero, R., Rea, B.R., Spagnolo, M., Bakke, J., Ivy-Ochs, S., Frew, C.R., Hughes, P., Ribolini, A., Lukas,
18 815 S., Renssen, H., 2016. GlaRe, a GIS tool to reconstruct the 3D surface of palaeoglaciers. *Comput.*
19 816 *Geosci.* 94, 77–85. <https://doi.org/10.1016/j.cageo.2016.06.008>
- 20 817 Quesada, C., Oliveira, J., 2019. *The Geology of Iberia: A Geodynamic Approach: The Variscan Cycle*.
- 21
22 818 Rasmussen, S.O., Bigler, M., Blockley, S.P., Blunier, T., Buchardt, S.L., Clausen, H.B., Cvijanovic, I., Dahl-
23 819 Jensen, D., Johnsen, S., Fischer, H., Gkinis, V., Guillevic, M., Hoek, W.Z., Lowe, J.J., Pedro, J.B.,
24 820 Popp, T., Seierstad, I.K., Steffensen, J.P., Svensson, A.M., Vallelonga, P., Vinther, B.M., Walker,
25 821 M.J.C., Wheatley, J.J., Winstrup, M., 2014. A stratigraphic framework for abrupt climatic changes
26 822 during the Last Glacial period based on three synchronized Greenland ice-core records: Refining and
27 823 extending the INTIMATE event stratigraphy. *Quat. Sci. Rev.* 106, 14–28.
28 824 <https://doi.org/10.1016/j.quascirev.2014.09.007>
- 29
30 825 Rea, B.R., 2009. Defining modern day Area-Altitude Balance Ratios (AABRs) and their use in glacier-
31 826 climate reconstructions. *Quat. Sci. Rev.* 28, 237–248. <https://doi.org/10.1016/j.quascirev.2008.10.011>
- 32 827 Rea, B.R., Pellitero, R., Spagnolo, M., Hughes, P., Ivy-Ochs, S., Renssen, H., Ribolini, A., Bakke, J., Lukas,
33 828 S., Braithwaite, R.J., 2020. Atmospheric circulation over Europe during the Younger Dryas. *Sci. Adv.*
34 829 6.
- 35
36 830 Reixach, T., Delmas, M., Calvet, M., 2021. Climatic conditions between 19 and 12 ka in the eastern
37 831 Pyrenees, and wider implications for atmospheric circulation patterns in Europe. *Quat. Sci. Rev.* 260.
38 832 <https://doi.org/10.1016/j.quascirev.2021.106923>
- 39
40 833 René, P., 2011. Régression des glaciers pyrénéens et transformation du paysage depuis le Petit Âge
41 834 Glaciaire. *Sud-Ouest Eur.* 5–19. <https://doi.org/10.4000/soe.639>
- 42 835 Renssen, H., Goosse, H., Roche, M., Sepp, H., 2018. The global hydroclimate response during the Younger
43 836 Dryas event. <https://doi.org/10.1016/j.quascirev.2018.05.033>
- 44
45 837 Renssen, H., Isarin, R.F.B., 2001. The two major warming phases of the last deglaciation at 14.7 and 11.5 ka
46 838 cal BP in Europe. *Glob. Planet. Change* 30, 117–153.
- 47 839 Rodríguez-Rodríguez, L., Jiménez-Sánchez, M., Domínguez-Cuesta, M.J., Rinterknecht, V., Pallàs, R., 2017.
48 840 Timing of last deglaciation in the Cantabrian Mountains (Iberian Peninsula; North Atlantic Region)
49 841 based on in situ-produced ^{10}Be exposure dating. *Quat. Sci. Rev.* 171, 166–181.
50 842 <https://doi.org/10.1016/j.quascirev.2017.07.012>
- 51
52 843 Rodríguez-Rodríguez, L., Jiménez-Sánchez, M., Domínguez-Cuesta, M.J., Rinterknecht, V., Pallàs, R.,
53 844 Bourlès, D., 2016. Chronology of glaciations in the Cantabrian Mountains (NW Iberia) during the Last
54 845 Glacial Cycle based on in situ-produced ^{10}Be . *Quat. Sci. Rev.* 138, 31–48.
55 846 <https://doi.org/10.1016/j.quascirev.2016.02.027>
- 56
57 847 Schilling, D.H., Hollin, J.T., 1981. Numerical reconstructions of valley glaciers and small ice caps, in:
58 848 Denton, G.H., Hughes, T.J. (Eds.), *The Last Great Ice Sheets*. Wiley, New York, pp. 207–220.
- 59 849 Serrano, E., Gómez-Lende, M., Pellitero, R., González-Trueba, J.J., 2015. Deglaciación en la Cordillera
60 850 Cantábrica: Modelo y evolución. *Cuad. Investig. Geogr.* 41, 389–408.
851 <https://doi.org/10.18172/cig.2716>

- 1
2 852 Serrano, E., González-Trueba, J.J., Pellitero, R., Gómez-Lende, M., 2016. Quaternary glacial history of the
3 853 Cantabrian Mountains of northern Spain: a new synthesis. *Geol. Soc. London, Spec. Publ.* 433, 55–85.
4 854 <https://doi.org/10.1144/sp433.8>
- 5
6 855 Small, D., Fabel, D., 2016. Was Scotland deglaciated during the Younger Dryas ? *Quat. Sci. Rev.* 145, 259–
7 856 263. <https://doi.org/10.1016/j.quascirev.2016.05.031>
- 8 857 Stange, K.M., van Balen, R.T., Kasse, C., Vandenberghe, J., Carcaillet, J., 2014. Linking morphology across
9 858 the glaciofluvial interface: A ^{10}Be supported chronology of glacier advances and terrace formation in
10 859 the Garonne River, northern Pyrenees, France. *Geomorphology* 207, 71–95.
11 860 <https://doi.org/10.1016/j.geomorph.2013.10.028>
- 12
13 861 Styllas, M.N., Schimmelpfennig, I., Benedetti, L., Ghilardi, M., Aumaître, G., Bourlès, D., Keddadouche, K.,
14 862 2018. Late-glacial and Holocene history of the northeast Mediterranean mountains - New insights from
15 863 in situ-produced ^{36}Cl -based cosmic ray exposure dating of paleo-glacier deposits on Mount Olympus,
16 864 Greece. *Quat. Sci. Rev.* 193, 244–265. <https://doi.org/10.1016/j.quascirev.2018.06.020>
- 17
18 865 Tomkins, M.D., Dortch, J.M., Hughes, P., Huck, J.J., Stimson, A.G., Delmas, M., Calvet, M., Pallàs, R.,
19 866 2018. Rapid age assessment of glacial landforms in the Pyrenees using Schmidt hammer exposure
20 867 dating (SHED). *Quat. Res.* 90, 26–37. <https://doi.org/10.1017/qua.2018.12>
- 21 868 Uppala, S.M., Kållberg, P.W., Simmons, A.J., Andrae, U., da Costa Bechtold, V., Fiorino, M., Gibson, J.K.,
22 869 Haseler, J., Hernandez, A., Kelly, M.A., Li, X., Onogi, K., Saarinen, S., Sokka, N., Allan, R.P.,
23 870 Andersson, E., Arpe, K., Balmaseda, M.A., Beljaars, A.C.M., van de Berg, L., Bidlot, J., Bormann, N.,
24 871 Caires, S., Chevallier, F., Dethof, A., Dragosavac, M., Fisher, M., Fuentes, M., Hagemann, S., Hólm,
25 872 E., Hoskins, B.J., Isaksen, L., Janssen, P.A.E.M., Jenne, R., McNally, A.P., Mahfouf, J.F., Morcrette,
26 873 J.J., Rayner, N.A., Saunders, R.W., Simon, P., Sterl, A., Trenberth, K.E., Untch, A., Vasiljevic, D.,
27 874 Viterbo, P., Woollen, J., 2005. The ERA-40 re-analysis. *Q. J. R. Meteorol. Soc.* 131, 2961–3012.
28 875 <https://doi.org/10.1256/qj.04.176>
- 29
30 876 Ward, G.K., Wilson, S.R., 1978. Procedures for Comparing and Combining Radiocarbon Age
31 877 Determinations: a Critique. *Archaeometry* 20, 19–31. [https://doi.org/10.1111/j.1475-](https://doi.org/10.1111/j.1475-4754.1978.tb00208.x)
32 878 [4754.1978.tb00208.x](https://doi.org/10.1111/j.1475-4754.1978.tb00208.x)
- 33
34 879 Zasadni, J., Piotr, K., Bro, E., Ivy-ochs, S., Andrzej, Ś., Christl, M., Balá, L., 2020. Latest Pleistocene glacier
35 880 advances and post-Younger Dryas rock glacier stabilization in the Mt. Kriváň group, High Tatra
36 881 Mountains, Slovakia. *Geomorphology* 358. <https://doi.org/10.1016/j.geomorph.2020.107093>
37
38 882
39 883
40
41
42
43
44
45
46
47
48
49
50
51
52
53
54
55
56
57
58
59
60

1
2 884 **List of figures**

3
4 885 Figure 1. Geographical setting of the Ruda Valley. (A) Location in Europe. (B) Location in the Pyrenees with
5 886 the distribution of the studies mentioned in the discussion (green stars). (C) Limits and topography of the valley
6 887 with the distribution and view direction of the photos in Figure 2.

7
8 888 Figure 2. Examples of the main geomorphological landforms of glacial origin in the Ruda Valley, together
9 889 with the location and typology of the dated samples: (A) terminal moraine damming a paleolake at 2080 m;
10 890 (B) N-S perspective of the Saboredo Cirque floor showing several lakes distributed in staggered overdeepened
11 891 basins; (C) polished bedrock surface including striations that reveal the former glacial flow; and (D) *roches*
12 892 *moutonnées* located in the forested valley bottom of the valley at 1860 m.

14 893 Figure 3. (A) Geomorphological map of the study area, with the location of the CRE samples; and (B)
15 894 enlargement of the highest parts of the cirque including the location of the ^{10}Be ages.

17 895 Figure 4. Examples of sampled moraines and polished bedrock surfaces, together with CRE ages (ka).

19 896 Figure 5. Reconstruction of the glacial extent during the different time stages: (A) Extensive glaciers occupying
20 897 the entire Upper Garonne Basin during the ILGM based on the reconstruction of [Fernandes et al. \(2017\)](#); (B)
21 898 Glacial extent during the mid B-A at ~13.5 ka in the Ruda Valley; (C) Glacier flowing from the Saboredo
22 899 Cirque during the transition between the late B-A and the early YD at ~13 ka; and (D) Small glaciers confined
23 900 within the highest hollows next to the Sendrosa (D) and Saboredo (E) peaks during the early YD at ~12.7/12.6
25 901 ka.

26 902 Figure 6. Schematic evolution of the glacial phases recorded in the Ruda Valley during the last glacial cycle:
27 903 (A) extensive and thick glaciers inundated the valley and only few nunataks protruded the ice during the ILGM;
29 904 (B) warm temperatures in the early B-A favoured glacial recession, and subsequently the lowest areas of the
30 905 valley as well as some rock outcrops of the cirque became exposed; (C) glacial advances/stillstands formed
31 906 moraines during the B-A and at the transition to the YD; (D) small glaciers persisted during the early YD in
32 907 the highest north-facing cirques; and (E) subsequent temperature increases favoured complete deglaciation and
34 908 triggered paraglacial dynamics, which promoted the formation of rock glaciers in the recently deglaciated ice-
35 909 free cirques.

36 910 Figure 7. Normalized probability distribution functions (PDF) of surface exposure ages vs. temperature
38 911 evolution from the OD to the early Holocene based on the $\delta^{18}\text{O}$ record from the NGRIP ice core from
39 912 Greenland and the $\delta^{18}\text{O}$ record from the speleothem of the Ostolo cave in north Iberia (time periods are defined
40 913 after [Rasmussen et al. \(2014\)](#)). The plots of the units result from the sum of the individual PDF of the samples
41 914 belonging to them; cold (warm) phases are represented by the blue (red) bands.

43 915
44

45 916
46

47 917
48

48 918
49

50 919
51

52 920
53

54 921
55

55 922
56

57 923
58

59
60

List of tables

Table 1. Geographic location of samples, topographic shielding factor and sample thickness.

Sample name	Landform	Latitude (DD)	Longitude (DD)	Elevation (m a.s.l.) ^a	Topographic shielding factor	Thickness (cm)	Lithology	Size of the boulders largest axis (m)
<i>Valley polished surfaces</i>								
ARAN-40	Polished surface	42.6416	0.9713	1862	0.9630	3.7	Granodiorite	
ARAN-39	Polished surface	42.6393	0.9701	1900	0.9640	5.0	Granodiorite	
<i>Valley external moraines</i>								
ARAN-38	Moraine boulder	42.6296	0.9624	2079	0.9759	4.2	Granite	3.5
ARAN-37	Moraine boulder	42.6299	0.9620	2075	0.9752	3.0	Granite	3
<i>Valley internal moraines</i>								
ARAN-28	Polished surface	42.6263	0.9593	2188	1.0000	3.5	Granite	
ARAN-27	Moraine boulder	42.6257	0.9599	2184	0.9852	5.0	Granite	4
<i>Cirque polished surfaces</i>								
ARAN-36	Polished surface	42.6111	0.9681	2360	0.9806	3.5	Granite	
ARAN-35	Polished surface	42.6152	0.9630	2316	0.9875	3.2	Granite	
ARAN-34	Polished surface	42.6224	0.9596	2266	0.9901	5.0	Granite	
ARAN-31	Polished surface	42.6274	0.9536	2378	1.0000	3.0	Granite	
<i>Cirque moraines</i>								
ARAN-33	Moraine boulder	42.6275	0.9487	2470	0.9841	3.0	Granite	5
ARAN-32	Moraine boulder	42.6277	0.9480	2467	0.9789	4.0	Granite	6

^a Elevations are derived from the 5 m Digital Elevation Model of the Spanish "Instituto Geográfico Nacional" and are subjected to a vertical accuracy of ± 5 m.

Table 2. AMS analytical data and calculated exposure ages. $^{10}\text{Be}/^{9}\text{Be}$ ratios were inferred from measurements at the ASTER AMS facility. Chemistry blank correction was done by subtracting the number of ^{10}Be atoms in the blank from that in the sample. Individual ages are shown with their full uncertainties (including analytical AMS uncertainty and production rate uncertainty) and analytical uncertainty only within brackets. Arithmetic mean ages are given with their full uncertainties (including standard deviation and production rate uncertainty) and standard deviations only in brackets.

^{10}Be samples analytical AMS data								
Sample name	Quartz weight (g)	Mass of carrier (^9Be mg)	ASTER AMS cathode number	$^{10}\text{Be}/^9\text{Be}$ (10^{-14})	Blank correction (%)	$[^{10}\text{Be}]$ (10^4 atoms g^{-1})	Age (ka)	Mean age (ka)
<i>Valley polished surfaces</i>								
ARAN-40	20.44	0.46	CHBL	16.34 ± 0.56	2.11	23.85 ± 0.83	15.0 ± 0.9 (0.5)	14.4 ± 1.2 (0.8)
ARAN-39	21.32	0.45	CHBK	15.92 ± 0.49	2.18	22.15 ± 0.70	13.8 ± 0.8 (0.4)	
<i>Valley external moraines</i>								
ARAN-38	21.11	0.46	CHBJ	17.56 ± 0.54	1.95	24.99 ± 0.79	13.3 ± 0.8 (0.4)	13.5 ± 0.9 (0.2)
ARAN-37	21.38	0.46	CHBI	18.08 ± 0.87	1.09	25.74 ± 1.25	13.7 ± 1.0 (0.6)	
<i>Valley internal moraines</i>								
ARAN-28	20.97	0.46	CHBB	18.79 ± 0.62	1.05	27.13 ± 0.91	13.0 ± 0.8 (0.4)	13.0 ± 0.8 (0.1)
ARAN-27	20.89	0.45	CHBA	18.64 ± 0.58	1.85	26.61 ± 0.84	13.1 ± 0.8 (0.4)	
<i>Cirque polished surfaces</i>								
ARAN-36	21.51	0.46	CHBH	21.24 ± 0.65	1.62	29.53 ± 0.92	12.7 ± 0.8 (0.4)	12.7 ± 0.8 (0.0)
ARAN-35	21.43	0.47	CHBG	20.18 ± 0.62	1.65	29.05 ± 0.91	12.8 ± 0.8 (0.4)	
ARAN-34	20.85	0.46	CHBF	21.13 ± 0.66	1.63	30.35 ± 0.96	14.0 ± 0.8 (0.4)	
ARAN-31	21.40	0.44	CHBC	26.54 ± 0.72	1.35	35.74 ± 0.98	14.8 ± 0.9 (0.4)	
<i>Cirque moraines</i>								
ARAN-33	20.26	0.45	CHBE	20.30 ± 0.68	1.70	29.92 ± 1.02	11.8 ± 0.7 (0.4)	12.6 ± 1.3 (1.0)
ARAN-32	21.63	0.45	CHBD	24.19 ± 1.26	0.85	33.15 ± 1.75	13.3 ± 1.0 (0.7)	
Chemistry blank details								
Blank name	Processed with	mass of carrier (^9Be mg)	ASTER AMS cathode number	$^{10}\text{Be}/^9\text{Be}$ (10^{-14})	$[^{10}\text{Be}]$ (10^4 atoms)			
BK-1	ARAN-27, 31, 33, 34, 35, 36, 38, 39, 40	0.46	CHAT	0.34 ± 0.04	10.30 ± 1.24	-	-	
BK-2	ARAN-32	0.46	CHBM	0.20 ± 0.03	6.13 ± 0.80	-	-	
BK-3	ARAN-28, 37	0.46	IGHI	0.20 ± 0.03	5.98 ± 0.93	-	-	

Table 3. Exposure ages according to erosion and snow cover corrections.

Sample name	Exposure ages (arithmetic mean, in ka)			
	No correction	Erosion correction	Snow correction	Erosion + snow correction
<i>Valley - polished surfaces</i>	14.4 ± 1.2	14.6 ± 1.2	15.5 ± 1.3	15.7 ± 1.3
ARAN-40	$15.0 \pm 0.9 (0.5)$	$15.2 \pm 0.9 (0.5)$	$16.1 \pm 1.0 (0.5)$	$16.4 \pm 1.0 (0.6)$
ARAN-39	$13.8 \pm 0.8 (0.4)$	$14.0 \pm 0.8 (0.4)$	$14.8 \pm 0.9 (0.4)$	$15.0 \pm 0.9 (0.5)$
<i>Valley - external moraines</i>	13.5 ± 0.9	13.7 ± 0.9	14.5 ± 1.0	14.7 ± 1.0
ARAN-38	$13.3 \pm 0.8 (0.4)$	$13.5 \pm 0.8 (0.4)$	$14.4 \pm 0.9 (0.4)$	$14.6 \pm 0.9 (0.4)$
ARAN-37	$13.7 \pm 1.0 (0.6)$	$13.8 \pm 1.0 (0.7)$	$14.7 \pm 1.0 (0.7)$	$14.9 \pm 1.0 (0.7)$
<i>Valley - internal moraines</i>	13.0 ± 0.8	13.2 ± 0.8	14.1 ± 0.9	14.2 ± 0.9
ARAN-28	$13.0 \pm 0.8 (0.4)$	$13.1 \pm 0.8 (0.4)$	$14.0 \pm 0.9 (0.5)$	$14.2 \pm 0.9 (0.5)$
ARAN-27	$13.1 \pm 0.8 (0.4)$	$13.3 \pm 0.8 (0.4)$	$14.1 \pm 0.8 (0.4)$	$14.3 \pm 0.9 (0.4)$
<i>Cirque - polished surfaces</i>	12.7 ± 0.7	12.9 ± 0.8	13.7 ± 0.8	13.9 ± 0.8
ARAN-36	$12.7 \pm 0.8 (0.4)$	$12.9 \pm 0.8 (0.4)$	$13.7 \pm 0.8 (0.4)$	$13.9 \pm 0.8 (0.4)$
ARAN-35	$12.8 \pm 0.8 (0.4)$	$12.9 \pm 0.8 (0.4)$	$13.8 \pm 0.8 (0.4)$	$14.0 \pm 0.8 (0.4)$
ARAN-34	$14.0 \pm 0.8 (0.4)$	$14.2 \pm 0.9 (0.4)$	$15.1 \pm 0.9 (0.5)$	$15.3 \pm 0.9 (0.5)$
ARAN-31	$14.8 \pm 0.9 (0.4)$	$15.1 \pm 0.9 (0.4)$	$16.0 \pm 0.9 (0.4)$	$16.2 \pm 0.9 (0.4)$
<i>Cirque - moraines</i>	12.6 ± 1.3	12.7 ± 1.4	13.5 ± 1.4	13.7 ± 1.5
ARAN-33	$11.8 \pm 0.7 (0.4)$	$12.0 \pm 0.8 (0.4)$	$12.7 \pm 0.8 (0.4)$	$12.9 \pm 0.8 (0.4)$
ARAN-32	$13.3 \pm 1.0 (0.7)$	$13.5 \pm 1.0 (0.7)$	$14.3 \pm 1.0 (0.7)$	$14.5 \pm 1.0 (0.7)$

Table 4. Reconstructed ELAs (m a.s.l.) for the middle, late B-A and YD moraines using the AAR and AABR methods.

Phase	Glacier	AAR (0.6±0.2)	AABR (1.9±0.81)	AABR (1.75±0.71)	Average ELA
Valley external moraines (middle B-A; GI-1c)	Ruda	2481 ± 20	2449 -30/+20	2454 -30/+15	2461
Valley internal moraines (transition B-A/YD; GI-1b)	Ruda	2515 -15/+10	2498 -25/+15	2503 -25/+20	2505
Cirque moraines (early YD)	Sendrosa	2568 -10/+5	2571 -15/+5	2576 ± 10	2571

Table 5. Glacial response in the Ruda Valley during the B-A Interstitial according to the reconstructed climate in Greenland and in Iberian Peninsula.

Phase (ages in ka)	Climate trend in Greenland based on ice core records (Rasmussen et al., 2014)	Glacier response in the Ruda Valley	Climate in the Iberian Peninsula based on other independent proxies
GI-1e (14.7-14.1)	Abrupt warming (3-5°C)	Rapid recession at ~15-14 ka	Gradual warming in the northern Iberia at 15.4-13.4 cal ka BP (Moreno et al., 2010). Warming conditions in the Pyrenees at 14.7-14.0 cal ka BP (González-Sampérez et al., 2006).
GI-1d (14.1-14.0)	Short cold reversal (1-2°C)		
GI-1c (14.0-13.3)	Significant warming at the beginning (2-4°C) followed by a gradual cooling at (~2°C). Intense cold conditions at 13.7-13.6 ka	Glacier advance or stillstand with moraine formation at 13.5 ka	Colder conditions starting at 13.5 cal ka BP in northern Iberia (Moreno et al., 2010). Cold climate in the Pyrenees at 14-13.4 cal ka BP (González-Sampérez et al., 2006).
GI-1b (13.3-13.1)	Short cold reversal (1-2°C)	-	Short periods of colder and drier conditions (Moreno et al., 2010). Expansion of cold-climate forest species in the Pyrenees at 13.4-13.1 cal ka BP (González-Sampérez et al., 2006).
GI-1a (13.1-12.9)	Early warming followed by a general cooling	Glacier advance or stillstand with moraine formation at 13.0 ka	Cold and dry conditions in the Pyrenees starting at 13.1 cal ka BP (González-Sampérez et al., 2006).

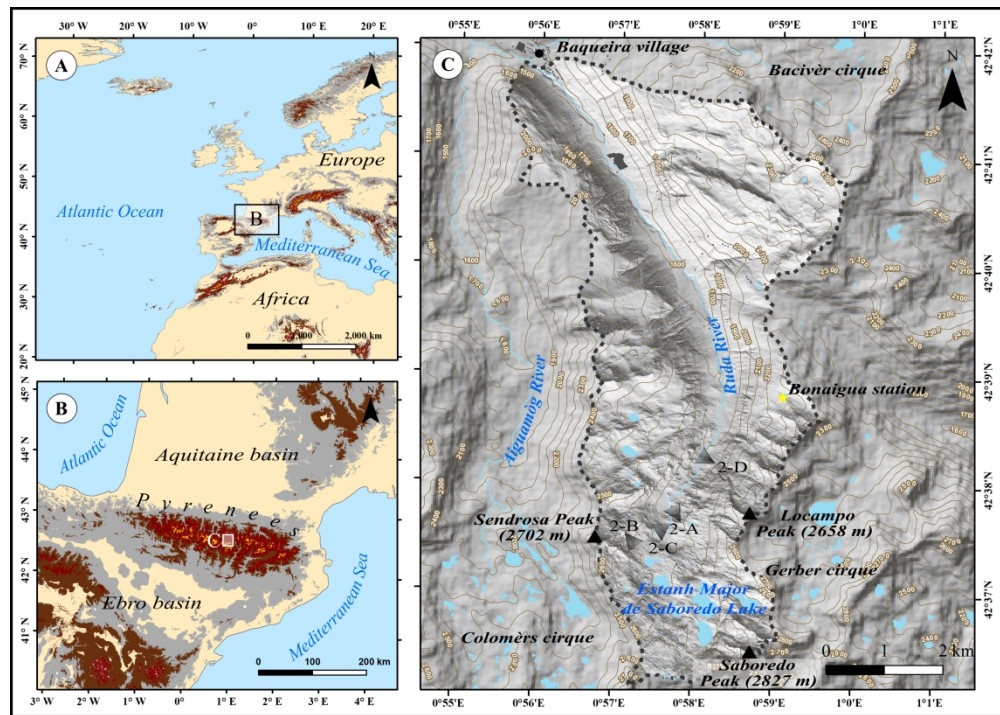


Figure 1. Geographical setting of the Ruda Valley. (A) Location in Europe. (B) Location in the Pyrenees with the distribution of the studies mentioned in the discussion (green stars). (C) Limits and topography of the valley with the distribution and view direction of the photos in Figure 2.

2476x1757mm (39 x 39 DPI)

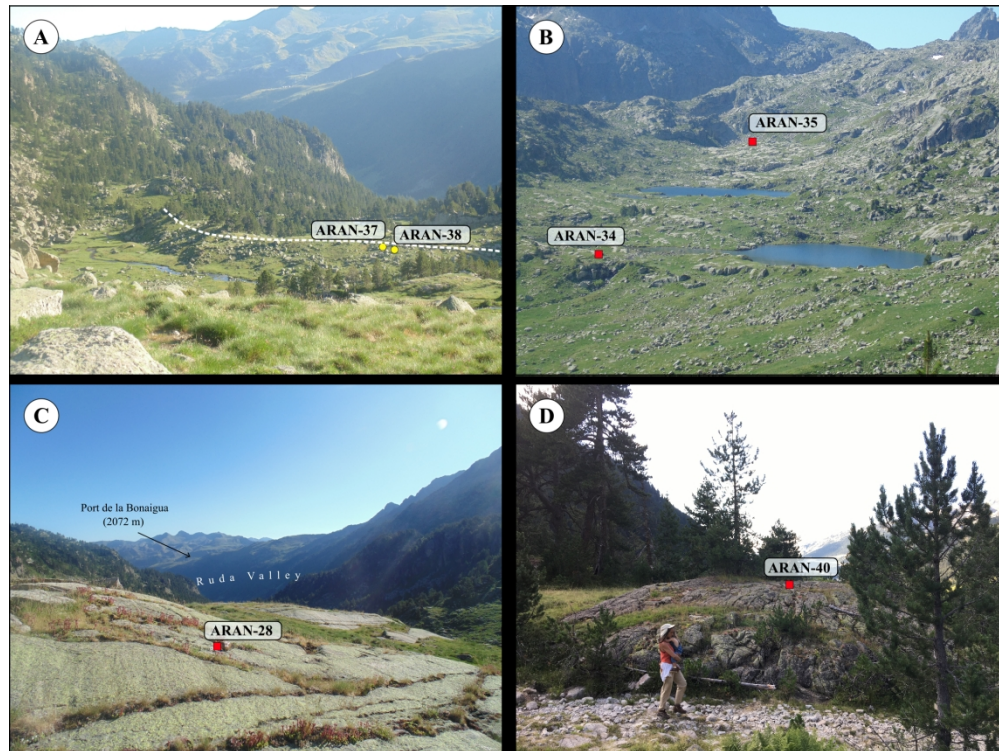
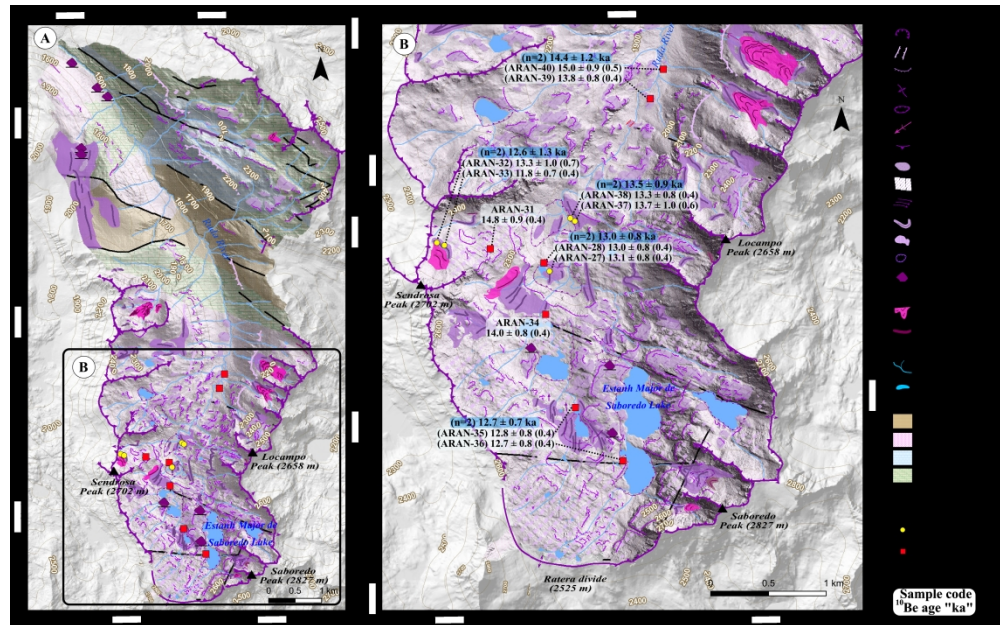


Figure 2. Examples of the main geomorphological landforms of glacial origin in the Ruda Valley, together with the location and typology of the dated samples: (A) terminal moraine damming a paleolake at 2080 m; (B) N-S perspective of the Saboredo Cirque floor showing several lakes distributed in staggered overdeepened basins; (C) polished bedrock surface including striations that reveal the former glacial flow; and (D) roches moutonnées located in the forested valley bottom of the valley at 1860 m.



3331x2073mm (39 x 39 DPI)

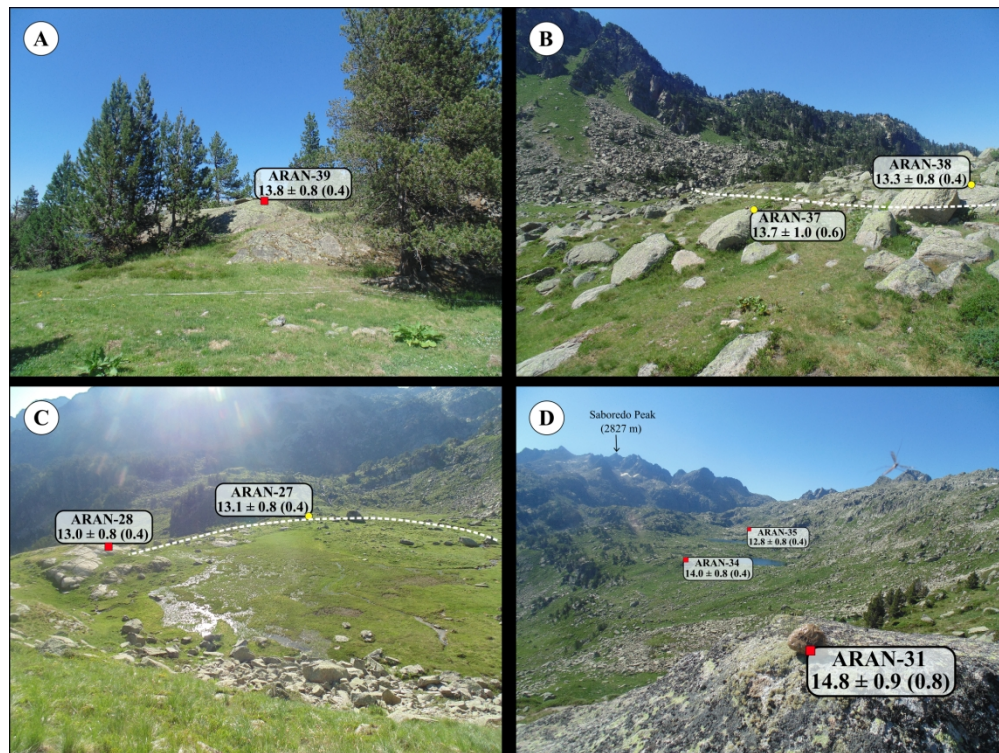


Figure 4. Examples of sampled moraines and polished bedrock surfaces, together with CRE ages (ka).

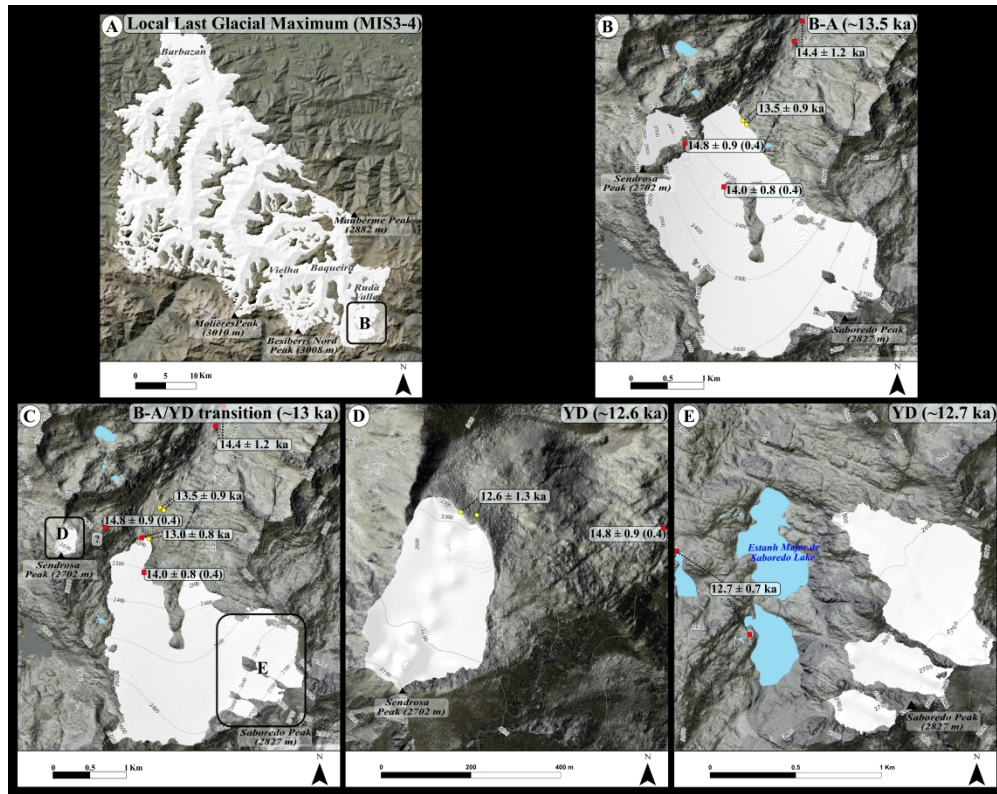


Figure 5. Reconstruction of the glacial extent during the different time stages: (A) Extensive glaciers occupying the entire Upper Garonne Basin during the ILGM based on the reconstruction of Fernandes et al. (2017); (B) Glacial extent during the mid B-A at ~ 13.5 ka in the Ruda Valley; (C) Glacier flowing from the Saboredo Cirque during the transition between the late B-A and the early YD at ~ 13 ka; and (D) Small glaciers confined within the highest hollows next to the Sendrosa (D) and Saboredo (E) peaks during the early YD at $\sim 12.7/12.6$ ka.

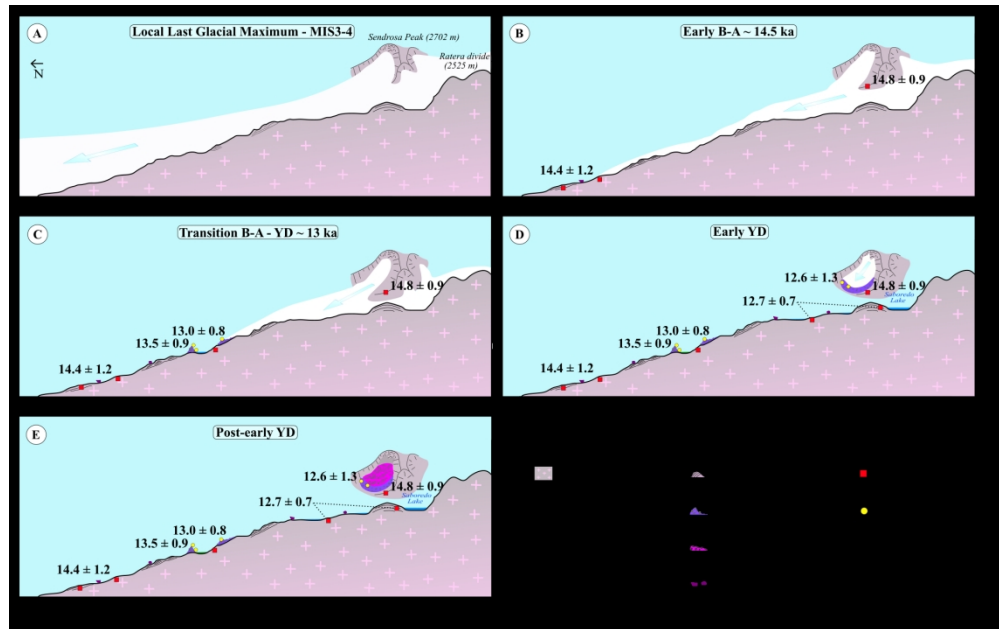


Figure 6. Schematic evolution of the glacial phases recorded in the Ruda Valley during the last glacial cycle: (A) extensive and thick glaciers inundated the valley and only few nunataks protruded the ice during the ILGM; (B) warm temperatures in the early B-A favoured glacial recession, and subsequently the lowest areas of the valley as well as some rock outcrops of the cirque became exposed; (C) glacial advances/standstills formed moraines during the B-A and at the transition to the YD; (D) small glaciers persisted during the early YD in the highest north-facing cirques; and (E) subsequent temperature increases favoured complete deglaciation and triggered paraglacial dynamics, which promoted the formation of rock glaciers in the recently deglaciated ice-free cirques.

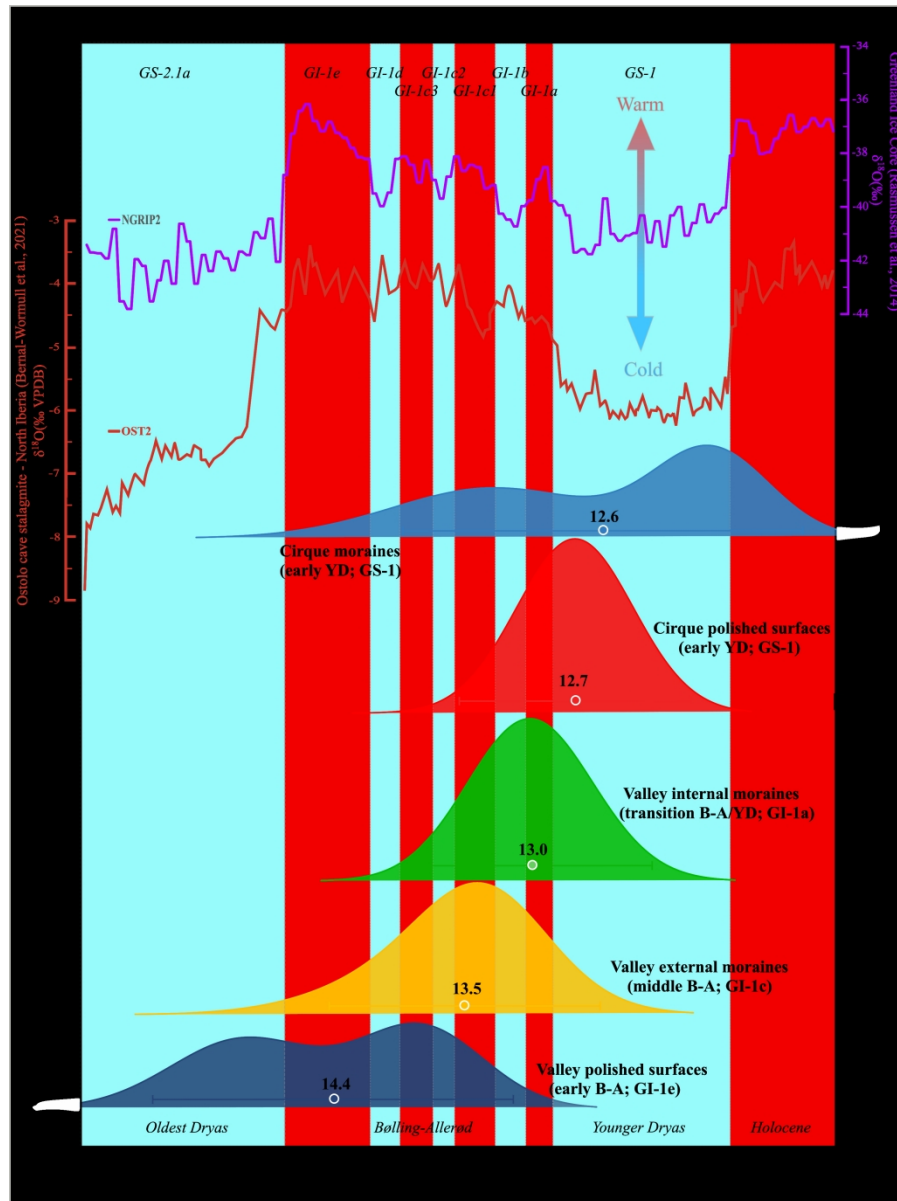


Figure 7. Normalized probability distribution functions (PDF) of surface exposure ages vs. temperature evolution from the OD to the early Holocene based on the $\delta^{18}\text{O}$ record from the NGRIP ice core from Greenland and the $\delta^{18}\text{O}$ record from the speleothem of the Ostolo cave in north Iberia (time periods are defined after Rasmussen et al. (2014)). The plots of the units result from the sum of the individual PDF of the samples belonging to them; cold (warm) phases are represented by the blue (red) bands.

670x895mm (118 x 118 DPI)